STRUCTURAL MODIFICATIONS IN OPTOMECHANICAL SYSTEMS FOR VIBRATION REDUCTION BY USING SEQUENTIAL MODEL UPDATING METHOD

A THESIS SUBMITTED TO
THE GRADUATE SCHOOL OF NATURAL AND APPLIED SCIENCES
OF
MIDDLE EAST TECHNICAL UNIVERSITY

BY

MUSTAFA SEZER CAMCI

IN PARTIAL FULFILLMENT OF THE REQUIREMENTS
FOR
THE DEGREE OF MASTER OF SCIENCE
IN
MECHANICAL ENGINEERING

JULY 2020

Approval of the thesis:

STRUCTURAL MODIFICATIONS IN OPTOMECHANICAL SYSTEMS FOR VIBRATION REDUCTION BY USING SEQUENTIAL MODEL UPDATING METHOD

submitted by **MUSTAFA SEZER CAMCI** in partial fulfillment of the requirements for the degree of **Master of Science** i**n Mechanical Engineering, Middle East Technical University** by,

Prof. Dr. Halil Kalıpçılar
Dean, Graduate School of **Natural and Applied Sciences** _____

Prof. Dr. M. A. Sahir Arıkan
Head of the Department, **Mechanical Engineering, METU** _____

Prof. Dr. H. Nevzat Özgüven
Supervisor, **Mechanical Engineering, METU** _____

Examining Committee Members:

Prof. Dr. Ender Ciğeroğlu
Mechanical Engineering, METU _____

Prof. Dr. H. Nevzat Özgüven
Mechanical Engineering, METU _____

Doç. Dr. Yiğit Yazıcıoğlu
Mechanical Engineering, METU _____

Doç. Dr. Bülent Özer
Mechanical Engineering, METU _____

Doç. Dr. Can Ulaş Doğruer
Mechanical Engineering, Hacettepe University _____

Date: 21.07.2020

I hereby declare that all information in this document has been obtained and presented in accordance with academic rules and ethical conduct. I also declare that, as required by these rules and conduct, I have fully cited and referenced all material and results that are not original to this work.

Name, Last name : Mustafa Sezer Camcı

Signature :

ABSTRACT

STRUCTURAL MODIFICATIONS IN OPTOMECHANICAL SYSTEMS FOR VIBRATION REDUCTION BY USING SEQUENTIAL MODEL UPDATING METHOD

Camcı, Mustafa Sezer
Master of Science, Mechanical Engineering
Supervisor : Prof. Dr. H. Nevzat Özgüven

July 2020, 124 pages

It is required to have high image performance in optomechanical systems working under excessive vibrations. If optical elements in an optomechanical system cannot be stabilized sufficiently, image problems (blurring, jitter, etc.) can arise due to excessive vibrations. The motivation of this thesis is to increase the optical performance of an optomechanical system which is exposed to high vibration levels coming from the platform. In order to eliminate high vibrations affecting the optical element of an optomechanical system, design modifications can be made, which requires a reliable mathematical model of the system. In this thesis, a new approach, which is named Sequential Model Updating Method, is developed and used for modeling and updating the FE model of an optomechanical system simultaneously, since the methods in the literature are found to be inadequate for systems composed of not only substructures, but also several moving parts. In this method, modelling and model updating are carried out sequentially. Initially, one component is modeled and updated by adjusting some parameters of the component. Afterwards, a new subsystem is added to the system, and the resulting model is updated by changing

some parameters of the newly added subassembly only, using the experimental results for that subsystem. The procedure is repeated until the FE model of the complete system is obtained. Using the updated FE model, structural modifications on a selected part can be carried out to eliminate the undesired vibrations. The application of the method developed for model updating, and the structural modification of a selected part to minimize vibrations of the optical element are shown on a problematic optomechanical system. The results obtained show the performance of the method developed.

Keywords: Model Updating of Complex Systems, Structural Modifications, Design Optimization, Optomechanical System Performance, Finite Element

ÖZ

OPTOMEKANİK SİSTEMLERDEKİ TİTREŞİM ETKİLERİNİ AZALTMAK İÇİN SIRALI MODEL GÜNCELLEME YÖNTEMİ KULLANARAK YAPISAL DEĞİŞİMLER

Camcı, Mustafa Sezer
Yüksek Lisans, Makina Mühendisliği
Tez Yöneticisi: Prof. Dr. H. Nevzat Özgüven

Temmuz 2020, 124 sayfa

Optomekanik sistemlerin, yüksek titreşim seviyeleri altında çalışırken yüksek görüntü performansına sahip olmaları gerekmektedir. Eğer bir optomekanik sistemdeki optik elemanlar yeterince stabilize edilemezse, yüksek titreşim seviyeleri nedeniyle görüntü problemleri (bulanıklaşma, titreme vs.) ortaya çıkabilir. Bu tezde, takılı olduğu platformdan gelen titreşim etkilerine maruz kalan optomekanik bir sistemin optik performansının iyileştirilmesi amaçlanmıştır. Optik elemana etki eden titreşim seviyelerini azaltabilmek için optomekanik sistem üzerinde tasarım değişiklikleri yapmak gerekmektedir ve bu nedenle sistemin doğrulanmış bir matematiksel modeline ihtiyaç duyulmaktadır. Bu tezde, optomekanik sistemin sonlu elemanlar modelini oluşturmak ve aynı anda güncellemek için, Sıralı Model Güncelleme Yöntemi adlı yeni bir yaklaşım geliştirilip kullanılmıştır. Literatürde bulunan model güncelleme yöntemleri, birçok hareketli parçadan oluşan bu karmaşık sistemin matematiksel modelini güncellemek için yetersizdir. Bu yöntemde, modelleme ve model güncelleme sırayla gerçekleştirilmektedir. İlk olarak bir parçanın sonlu elemanlar modeli oluşturulur ve parçanın parametreleri ayarlanarak oluşturulan model güncellenir. Daha sonra sisteme yeni bir alt sistem

eklenir ve elde edilen model, yalnızca yeni eklenen alt sistemin bazı parametreleri değiştirilerek ve elde edilen sistemin deneysel sonuçları kullanılarak güncellenir. Bu prosedür, tüm sistemin sonlu elemanlar modeli oluşturulup, deneysel modeli ile doğrulanana kadar tekrar edilir. Optomekanik sistemin doğrulanmış matematiksel modeli kullanılarak, istenmeyen titreşimleri azaltmak için sistemin seçilen bir parçası üzerinde tasarım değişiklikleri yapılabilir. Model güncelleme için geliştirilen yeni yöntemin uygulaması ve optik elemanın titreşimini en aza indirmek için, seçilen bir parçanın yapısal modifikasyonu, optomekanik bir sistem üzerinde gösterilmiştir. Elde edilen sonuçlar geliştirilen yöntemin performansını göstermektedir.

Anahtar Kelimeler: Karmaşık Sistemlerin Model Güncellemesi, Yapısal Değişimler, Optomekanik Sistem Performansı, Tasarım Optimizasyonu, Sonlu Elemanlar

To My Family…

ACKNOWLEDGMENTS

I would like to express my deepest and sincere gratitude to my supervisor, Prof. Dr. H. Nevzat ÖZGÜVEN for his boundless help, excellent supervision and leading guidance from beginning to end of thesis work.

Also, I would like to thank Dr. Tolga DURSUN, Dr. Murat AYKAN, İsa Gazi YÜKSEL and Erdem Rahmi ŞENÖZ for their technical support, intelligence and helpful advice.

I am grateful to my parents and my brother for their love, wonderful support and endless patience for educating and preparing me for my future. I am very much thankful to my wife for her love, understanding and continuing support to complete this thesis work.

Also, thanks to the Scientific and Technological Research Council of Turkey (TÜBİTAK) for giving the financial support throughout this work, and to ASELSAN Inc., for using its facility, computational and testing capabilities and precious knowledge.

TABLE OF CONTENTS

LIST OF TABLES

TABLES

LIST OF FIGURES

FIGURES

LIST OF ABBREVIATIONS

ABBREVIATIONS

FE	Finite element
FEM	Finite element model
ROCP	Reduced order characteristic polynomial
NNUM	Neural network updating method
RFMB	Residual flexibility mixed-boundary
PSD	Power spectral density
MMC	Metal-matrix-composite
IMU	Inertial measurement unit
RMS	Root-mean-square
APSD	Acceleration PSD
FRF	Frequency response function
DOF	Degree of freedom
DOE	Design of experiments
MOGA	Multi-Objective Genetic Algorithm

LIST OF SYMBOLS

SYMBOLS

δ	Deflection
F	Force
L	Contact length
ν	Poisson's ratio
E	Modulus of elasticity
R	Radius of cylinder
k	Contact stiffness
k_{eqv}	Equivalent contact stiffness

CHAPTER 1

INTRODUCTION

1.1 Definition of the Problem and the Objective

Optomechanics can be defined as an engineering discipline, which is interested in protecting and positioning of optical elements properly to fulfill system performance needs related to optics and increase efficiency.

Optomechanical systems basically consist of optical elements like lenses, cameras, mirrors, and mechanical parts. These components must be positioned accurately and stabilized by mechanical parts like optical mounts, gimbals and mechanisms under any external disturbances like vibration, shock, thermal effects, etc. Therefore, the design and analysis of mechanical parts and mechanisms play an important role in the optical performance of optomechanical systems.

In today's technology, optomechanical systems have to meet strict requirements in terms of field of view, sensitivity, shape, and size while being resistant to all kinds of environmental loads. This makes the development and design of optomechanical devices a challenging task. Optomechanical engineers need to come up with solutions for these challenges, using their knowledge about the principles of mechanical engineering.

Environmental loads coming from platforms like excessive vibrations may affect the system performance by causing performance degradation and failure of optical components. Due to vibration effects, optical elements could move with respect to each other. These motions may result in defocusing, i.e., image blurring and may cause short-term phase variations of optical arrays, i.e., jitter.

In this thesis, studies are focused on increasing the image performance of an optomechanical system, which is integrated on an armored vehicle. System performance is sufficient when the vehicle is not moving, but it is observed that the performance of the system decreases severely while the vehicle is in motion. It shows that this is a vibration-induced problem, which affects the optical elements in the mechanism.

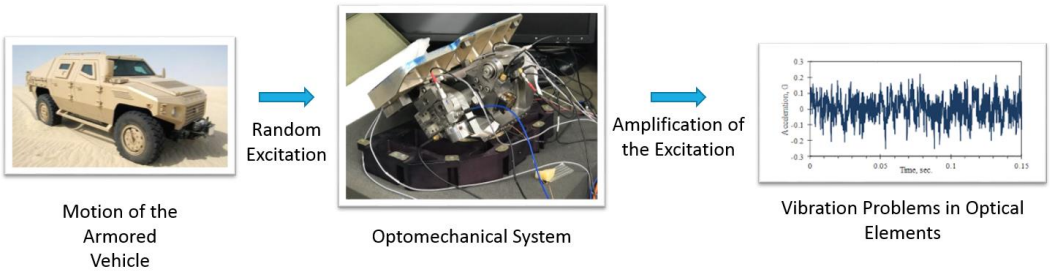

Figure 1.1. Diagram of the Problem

The main motivation in this thesis was to solve the vibration-induced image problem of the optomechanical system. High excitation level coming from the vehicle to the optical elements is required to be eliminated. In order to make structural modifications in the mechanism that carries, positions and stabilizes the optical elements, it is necessary to have a reliable mathematical model of the whole optomechanical system, which is responsible for transferring and amplifying the

excitations coming from the vehicle. The classical approaches in modeling and then updating the finite element model (FEM) of the optomechanical system did not work because of not having a single structural system, but instead several structures connected with moving connections. Therefore, the main objective of this thesis is to develop a new approach in modeling and updating structural systems consist of several structural elements with moving connections. It is also aimed to apply the proposed approach to the existing optomechanical system in order to make structural modifications to solve the vibration-induced image problem of the optomechanical system.

1.2 Literature Survey

In order to obtain reliable mathematical models of the mechanical systems, there are a variety of model updating techniques developed. Baruch and Bar Itzhack [1] developed a direct model updating method, which updates the FE eigenvectors and stiffness matrix by minimizing the difference between measured and FE eigenvectors. In this study, they assumed the analytical mass matrix is correct, but the stiffness matrix and measured modes have errors. Baruch [2] presented a new method in which the analytical stiffness matrix and eigenvectors are updated with minimization of the difference between the analytical and updated stiffness matrices by using Lagrange multipliers and assuming that the mass matrix is correct. Bucher and Braun [3] proposed a direct method, which uses the partially known modal test results. In this method, Eigen-frequencies and Eigen-vectors of actual structures can be obtained by using a partial set of Eigen-solutions obtained from the experiments. Friswell et al. [4] employed a direct method to update the analytical stiffness and damping matrices simultaneously by using measured modal data. In this study, the mass matrix is assumed to be correct. Lin and Zhu [5] studied model updating of damped structures. In this approach, frequency response functions (FRFs) are used to identify the analytical mass, stiffness and also the damping matrices of the system. For the proportional and non-proportional damping coefficients of the systems, a

complex updating method by using the FRF data is developed. Li [6] proposed a new approach for model updating of FE models by using only the experimentally measured natural frequencies or eigenvalues with reduced order characteristic polynomial (ROCP). In this study, the emphasis is put on the identification of joint stiffness. The proposed method is also verified by using simulated data. Kwon and Lin [7] developed a robust model updating method to update FE models by applying Taguchi method. The difference between the measured and analytical data is optimized in this method. This technique is also known to be good for noisy vibration data, because in the calculations, signal to noise ratio is maximized by updating the parameters.

The number and complexity of large mechanical assemblies increase rapidly as the technological developments continue, and professionals need to come up with new model updating methods suitable for the increasing demand. There are a few model updating techniques proposed and used to build accurate dynamic models of complex mechanical systems. Giagopoulos and Natsiavas [8] studied on hybrid (numerical and experimental) modeling of large order mechanical assemblies. Various numerical methods are used to develop mathematical models of some of the substructures of a complex mechanical system, and dynamic modeling of the rest of the components are formed by using proper experimental techniques. Sadeghi et al. [9] presented a new approach for model updating of complex assembled structures by using parametric FE models of the joints existing in the real system and modal testing results of the system and its substructures. Eigen-sensitivity method and genetic algorithm are also utilized for model updating procedures in this study. Grafe [10] investigated several FRF based model updating methods and determined important points about the usages. The convergence of the predictor-collector method is emphasized on large design parameter modifications. Belotti et al. [11] developed a new methodology to use for model updating of dynamic models of flexible-link mechanisms. The FE model of the system, rigid-body motion formulation and elastic deformation characteristics of the links are utilized in the

method. The nonlinear parts of the dynamic model are linearized in the studies. Goller et al. [12] employed a stochastic model updating technique to complex, large-scale aerospace structures. The application of the Bayesian updating procedure is shown by using numerical examples. Also, strategies to decrease the computational efforts and costs are illustrated. Inman [13] presented a new method to update the dynamic models of complex structures which are modified due to environmental changes, repair and replacement of parts with a considerable decrease in computational time and effort. Updated parameters of the system are found with high accuracy by using the neural network updating method (NNUM), which utilizes frequency domain data. Cao et al. [14] proposed a new approach for model updating of complex assemblies based on Residual flexibility mixed-boundary (RFMB) substructure method. In this study, a complex system is divided into several substructures, and the order of each substructure is reduced by employing the RFMB method. Model updating of these reduced substructures are carried out after assembling. By utilizing this method, dynamic models of large systems that have complex designs could be updated in four steps. Arailopoulos and Giagopoulos [15] presented several model updating methods to define linear and nonlinear components of complex dynamic assemblies. Time responses and FRFs of the parts are utilized with FE analysis software to reduce computational effort. Single and multi-objective structural identification methods with suitable substructuring techniques are applied on complex systems to predict the parameters of the dynamic model. Soleimanian et al. [16] studied damping properties of complex assemblies while updating the dynamic models by using a substructure-joint based approach. Damping properties of the system are identified with a direct method by using previously found accurate mass and stiffness matrices of the components, joints and whole assembly with the Eigen-sensitivity approach.

1.3 Scope of Thesis

The outline of this thesis is given below:

In Chapter 2, vibration measurements are carried out on the base vehicle with the optomechanical system in order to investigate the excitation experienced by the system. Measured time-domain vibration data is post-processed, and analyzed in frequency-domain by making random vibration analysis. Frequency range, magnitude and energy level of the excitation are obtained and investigated by using Power-spectral-density (PSD) functions.

In Chapter 3, modeling of the optomechanical system by using Finite Element (FE) method, and updating of the FE model are explained. A new model updating method is developed in order to have a reliable dynamic model of this complex structure, which is called by Sequential Model Updating Method. FE model of the system is formed, and correlated with the experimental model of the actual system by using the new approach. Modal tests are done to create the experimental model of the system. Model updating on the parameters like density, modulus of elasticity, Poisson's ratio, stiffness values of the bearings and joint definitions of the bolts etc. are carried out. FRFs and natural frequencies obtained from the FE model are verified with the ones calculated with modal identification techniques from the experimental data.

In Chapter 4, structural modifications are carried out on the system in order to increase the image performance of the optomechanical system by reducing the vibrations of the optical element. The natural frequencies of the system are increased to avoid having resonances at frequencies where there are high excitations coming from the base vehicle. Topology optimization method is used to make the best design modification. The necessary inputs like design domain, excluded regions, objective function and response constraint are defined to the optimization algorithm to get the optimal part. Also, the material of the optimized part is changed with a type of metal-

matrix-composite (MMC) to have further improvements. Natural frequencies of the system and vibration responses of the optical element are compared to see the results of the studies.

In Chapter 5, summary and conclusions obtained from the studies are given.

CHAPTER 2

ANALYSIS OF THE EXCITATION COMING FROM THE VEHICLE

2.1 Data Collection from the Vehicle

Military devices are generally exposed to high level of environmental loads like noise, shock and vibration. Among these loads vibration usually affects service life of the devices. Mechanical and electronic parts fail from excessive strains due to cyclic stresses i.e. fatigue. Apart from this, vibration has critical importance on optomechanical military devices because it affects both service life and operation performance of these sensitive devices critically. Image performance of the optomechanical devices decreases significantly, when high excitations affect the optical elements resulting in blurring and jitter. Therefore, measuring and analyzing the vibration coming to such critical devices from the vehicle is required in designing or improving an existing design of these devices.

Optomechanical devices are generally mounted on platforms like aircrafts, tanks, ships and helicopters and these vehicles create various excitations due to their engines, rotors, cooling/heating systems etc., which have different types of frequency characters. In addition, these vehicles are subjected to harsh environmental vibration effects while operating on rough roads, seas and in severe winds. Optomechanical devices are exposed to these excessive random vibrations transferred from the platforms and characteristics of these vibration effects must be measured and analyzed. Therefore, random vibration measurements and analyses are commonly used and required in military applications.

In real time applications, military devices experience random vibrations in time domain occurring in all frequencies simultaneously. They experience non-deterministic excitations which cannot be estimated precisely. Therefore, real-time data acquisition is required to analyze the statistical approximation of the excitation spectrum.

The optomechanical system that will be investigated in this thesis experiences performance decrease in image processing when the vehicle is in motion. It shows that there is a vibration-induced problem caused by the platform. As a result, random vibration measurement is done in this configuration to see what type of excitation is lowering the performance of the optomechanical device.

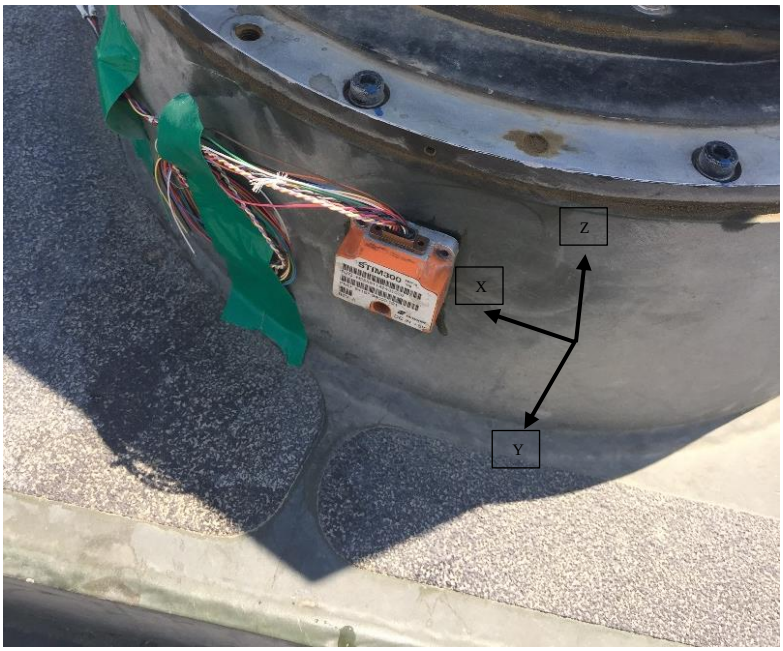

Figure 2.1. Position of the Sensor (IMU)

Vibration measurement is carried out at the integration point of the optomechanical system with the vehicle while it is moving at its normal operation speed on rough terrain shown in Figure 2.1. STIM300 Inertial Measurement Unit (IMU) is used to record the data in time-domain with a sampling rate of 1000 Hz in three directions. The IMU is put onto the mounting point with instant adhesive to have reliable data even at higher frequencies. Data is taken as acceleration (g units) for approximately 25 seconds, which is quite enough for post-processing analysis. For pre-processing of the time-domain data, MATLAB® software is used and time-domain results are shown in Figure 2.2, Figure 2.3 and Figure 2.4.

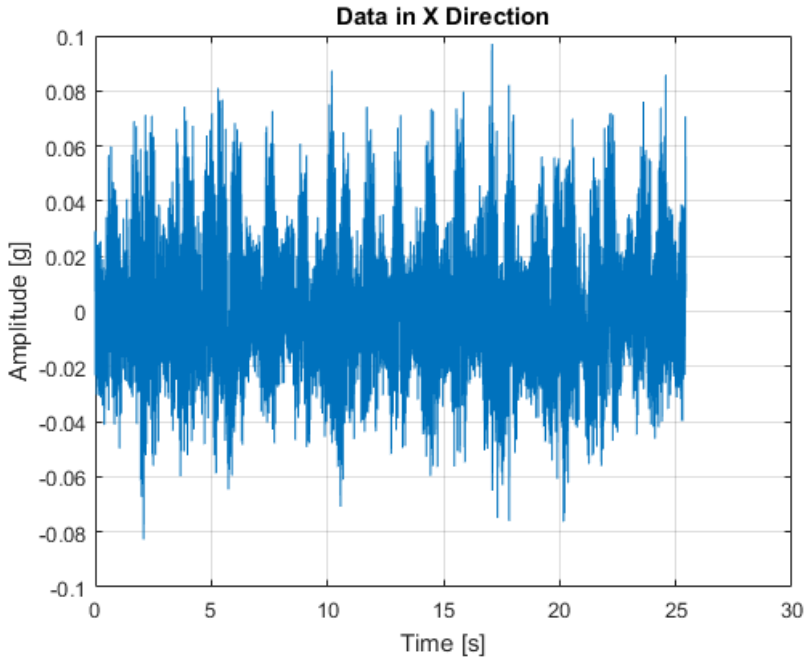

Figure 2.2. Recorded Time Domain Data in X Direction

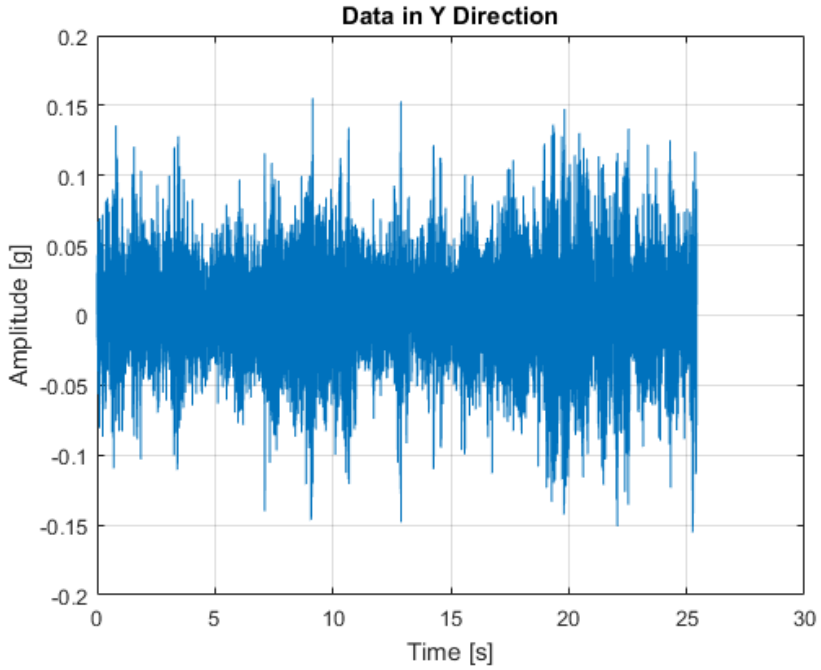

Figure 2.3. Recorded Time Domain Data in Y Direction

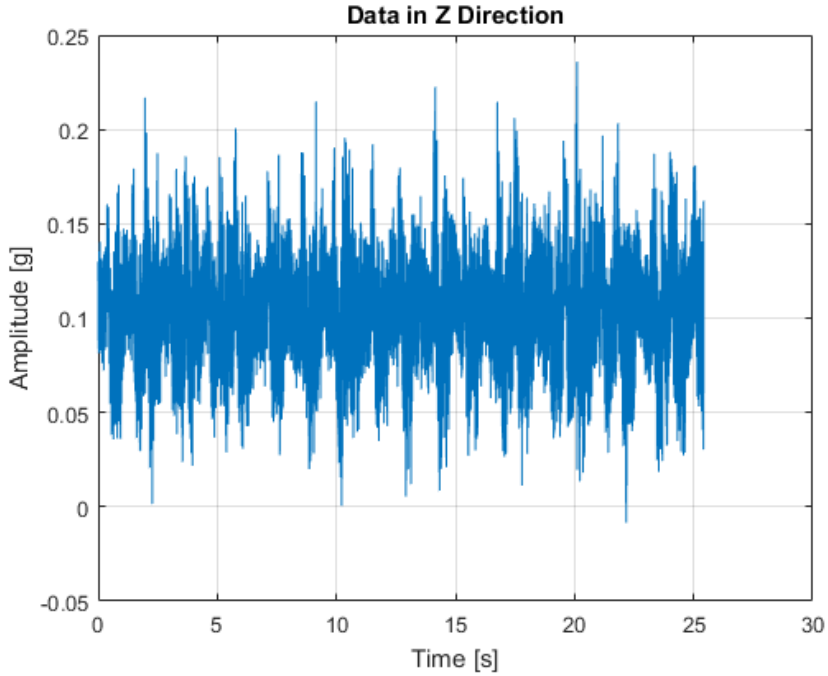

Figure 2.4. Recorded Time Domain Data in Z Direction

It can be seen that the acceleration amplitudes in Z direction are higher than those in other directions, and minimum amplitudes are observed in X direction. In order to understand the energy level of the excitation and distribution of this energy in frequency spectrum, random vibration analysis is carried out.

2.2 Analysis of Data

Random vibrations data in time-domain does not give sufficient information about the characteristics of the excitation; therefore, it is necessary to analyze and post-process the data in frequency-domain. The effects of the random vibration excitation, which consists of the excitations that have different frequency contents, could be predicted by conducting random vibration analysis. Characteristics of the random vibrations, like frequency range, magnitude and energy level are calculated and shown by using Power Spectral Densities (PSDs). PSDs are frequency domain representations of the excitations that occur in time domain. Effects of random vibration on dynamical characteristics of the systems can be studied properly by using PSDs.

"Power-spectral-density (PSD) analysis is a type of frequency-domain analysis in which a structure is subjected to a probabilistic spectrum of harmonic loading to obtain probabilistic distributions for dynamic response measures. A root-mean-square (RMS) formulation translates the PSD curve for each response quantity into a single, most likely value. Because PSD curves represent the continuous probability density function of each response measure, most of the integrated area will occur near the resonant frequencies of the structure. For accuracy, it is important to capture response at frequency steps near the natural modes of the structure." [17]

In this study, for post-processing and PSD analysis, MATLAB® software is used. Data is taken as acceleration in time-domain and acceleration PSDs (APSDs) are calculated by using open source codes. [18]

In the analysis, mean removal is achieved by subtracting static error from the time-domain signal. By this way, the time series signal is centered and more accurate PSD estimation was obtained. In addition, Hanning window is used to avoid spectral leakage and to have good frequency resolution. The PSDs are calculated using 49 segments and 512 samples. As a result, each segment is 0.5 seconds and PSD graphs have approximately 2 Hz resolution.

PSD graphs in Figure 2.5 are plotted in log-log form to have logarithmic scale on both axes. Y axis shows the amplitude of PSD in g^2/Hz units and X axis indicates frequency in Hz units.

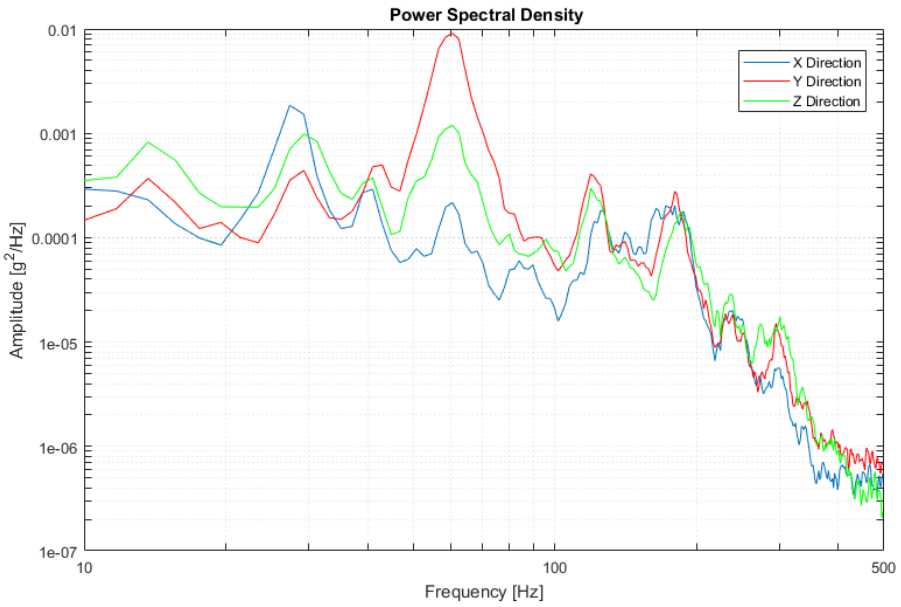

Figure 2.5. Calculated PSDs in All Directions

It is observed that in all axes there are high amplitude excitations up to 300 Hz, so in this study our aim will be to shift the natural frequencies of the optomechanical system above 300 Hz to avoid having resonance at frequencies where there are high excitations. In this way, high amplitude resonance peaks on the optical elements will be lowered.

CHAPTER 3

FINITE ELEMENT MODEL OF THE OPTOMECHANICAL SYSTEM AND UPDATING OF THE MODEL BY USING SEQUENTIAL MODEL UPDATING METHOD

3.1 Modeling of Complete Optomechanical System by Using Finite Element Method

In order to shift any resonance of the optomechanical system outside the frequency range where there are high excitations, structural modifications are required on the critical parts of the mechanism. Design optimization methods can be used to make optimal structural modifications on the parts. However, in order to make structural modifications in the system, it is required to have a reliable dynamic model of the system which will give reliable estimates for the dynamic response of the structure. Having a reliable dynamic model is very important for engineers to understand vibration behavior of the systems under any environmental load.

The dynamic model of the system could be formed by using analytical formulations, which are generally suitable for simple systems only, or by using Finite Element (FE) method. The optomechanical system studied in this thesis is a complex structure with moving parts, and it can be modeled using FE method. However, FE models may not represent real life systems accurately if they are not updated and corrected by using experimental data taken from the actual structure. Therefore, model updating on FE model is required in order to obtain a reliable spatial dynamic model of the system. "Model updating can be defined as the adjustment of an existing analytical model which represents the structure under study, using experimental data, so that it more accurately reflects the dynamic behavior of that structure." [19]

3.1.1 Experimental Modal Analysis of the Optomechanical System

Firstly, the complete system's experimental modal test and analysis are carried out in order to create an experimental model of the actual system. The optomechanical system is tested on a soft foam to simulate free-free boundary conditions.

To measure the vibration spectra, a modal hammer with a force sensor and accelerometers are used. The accelerometers, which are used in the tests, have dynamic range of 50g and frequency range of 10-500 Hz. The models of the accelerometers used in the measurements are Endevco 65-100 and Brüel&Kjaer 4507B. They are bonded to system's mechanical parts by using instant adhesives shown in Figure 3.1. This mounting type prevents dynamic effects coming from the bonding of accelerometers even at high frequencies. To excite the system, modal hammer (B&K 8206) with a white plastic tip is used. Force data is recorded simultaneously with the force transducer, which is integrated in the modal hammer. All the accelerometers and the modal hammer are connected to a data acquisition system (Dewesoft Sirius-HD-STGS) to record synchronous experimental data.

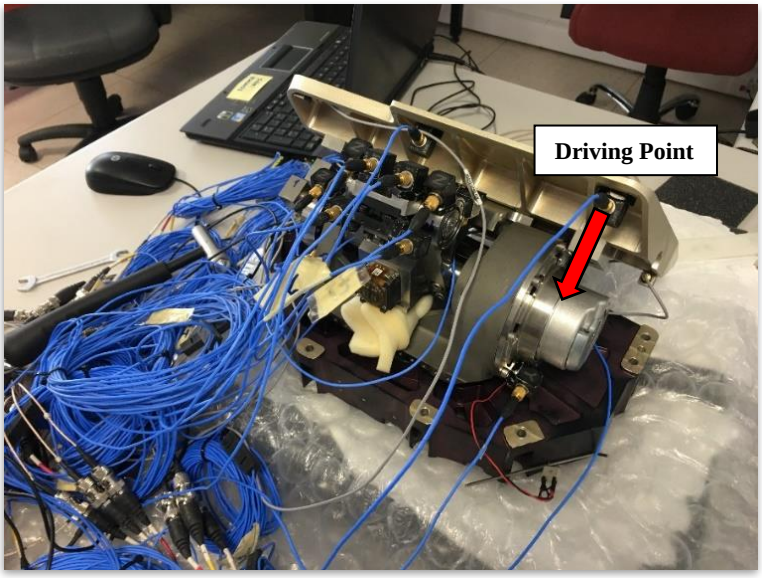

Figure 3.1. Modal Test Configuration of Complete Optomechanical System

There are two methods when doing multiple point modal tests by using impulse hammer; roving hammer or roving accelerator. Roving hammer method is used in this study, because it is easy to change the direction and location of the hammer impact point, and the mass distribution of the system is not affected when roving hammer method is used. In the modal tests of the system, the coordinates and directions of each impact and measurement point are specified before the measurement according to preliminary FE analysis. Preliminary FE analysis results were also used to find the best excitation points in order to obtain accurate mode shapes and Frequency Response Functions (FRFs). The measurements are carried out by exciting the system at different impact points in different directions and the response of the structure is measured by using multiple accelerometers synchronoulsy. Measurements were repeated 15 times for each impact point to obtain the best coherence parameters and thus the best FRFs, which will give a reliable dynamic model of the optomechanical system.

Data analyses are carried out after the data acquisition step. Experimental model of the optomechanical system is constructed by using measurement and force excitations points as shown in Figure 3.2. FRFs are calculated seperately at each impact point, and modal parameters (natural frequencies, damping ratios and modal constants, and thus mode shapes of the system) are extracted from these functions by using LMS Test Lab software's Polymax algorithm, which is a modal identification algorithm. It is based on least-squares complex frequency-domain method, and by using this algorithm highly accurate modal parameters can be obtained with high computational efficiency.

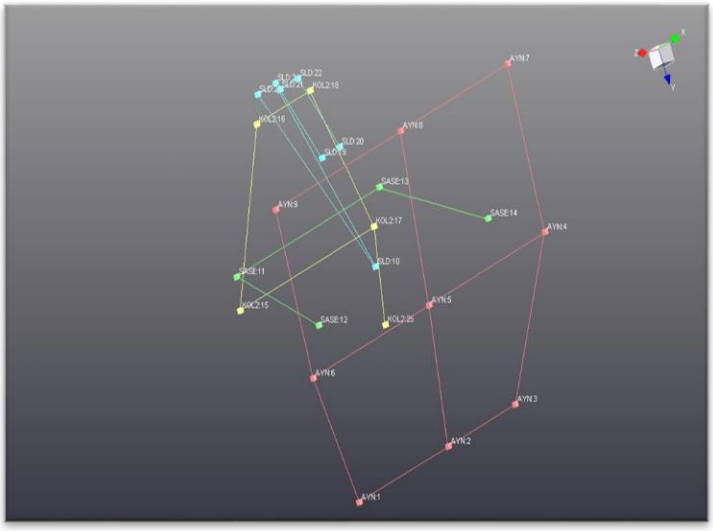

Figure 3.2. Construction of the Complete Optomechanical System in Modal Analysis Software

A typical measured direct FRF of the driving point on the optical element (direction and location are shown with an arrow in Figure 3.1), and the natural frequencies and corresponding damping ratios identified are shown in Figure 3.3 and Table 3.1, respectively.

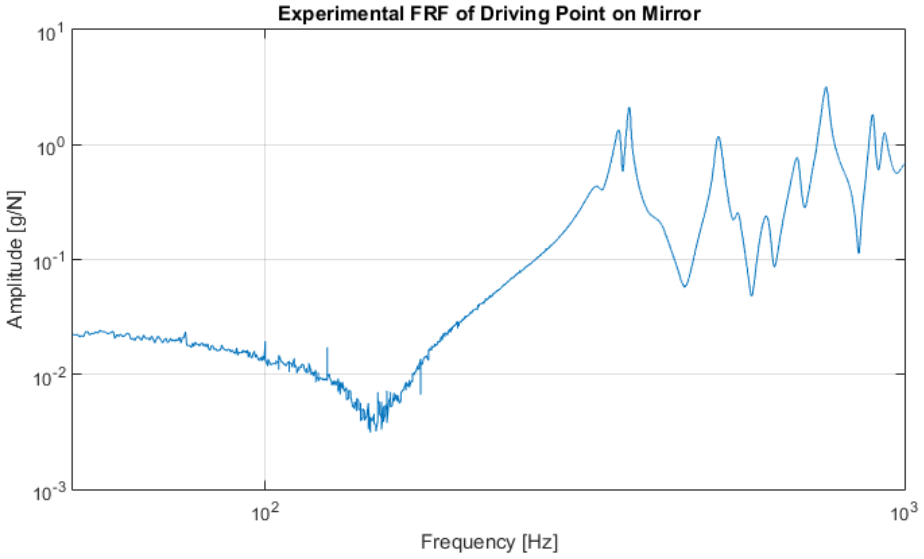

Figure 3.3. Experimental FRF of Driving Point on Optical Element

Table 3.1 Modal Parameters Obtained from Experimental Modal Analysis

Mode	Natural Frequency [Hz]	Damping Ratio [%]
1.	357	1.23
2.	370.4	0.58
3.	511.3	1.00
4.	613.7	1.95
5.	685.2	0.87
6.	704.4	1.34
7.	757.7	0.89
8.	820.3	2.76
9.	888.4	1.07
10.	927.4	1.12
11.	987.5	3.40

3.1.2 Modal Analysis of the Optomechanical System by Using Finite Element Method

The mathematical model of the optomechanical system by using FE method is created after the experimental modal analysis. Mechanical design of the system is done on a CAD software of PTC Creo, and the FE model of the system is created by using ANSYS Workbench program, which can be connected to this CAD program easily. All the parts and assemblies are imported directly to FEM analysis from the CAD software. All the analysis are done on ANSYS software, and FRFs, natural frequencies and mode shapes are obtained after completing of the FE model of the system.

The optomechanical system studied in this thesis has many mechanical parts and components, therefore it has high number of elements in the FE model. While

modelling, some features like holes, rounds and chamfers, which do not affect the dynamical characteristics of the system significantly, are simplified to increase the speed of the analysis and to reduce the total degree of freedom (DOF). Material properties of the all parts are defined to the library of the ANSYS software. Densities are verified by measuring mass and volume of the parts. Modulus of elasticity and Poisson's ratio values are taken from the literature.

In order to have a realistic comparison of experimental and theoretical values, and have reliable results, the masses of accelerometers are also considered in the FE model of the system (shown in Figure 3.4). Joint definitions of the bolted connections existing in the system are defined as rigid in all directions, at this point, since there is no information about their behavior. Bearing stiffness values are taken from the producer firm's provided information. Since the system is tested in free-free conditions, the same boundary conditions are used in the FE model. The direct FRF of the driving point on the optical element (direction and location are shown with an arrow in Figure 3.4) and natural frequencies obtained from the FE model are given in Figure 3.5 and Table 3.2, respectively.

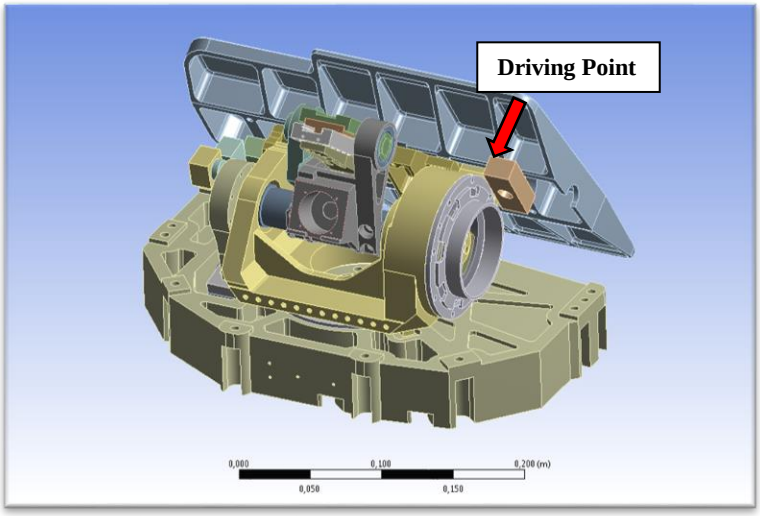

Figure 3.4. FE Model of the Optomechanical System

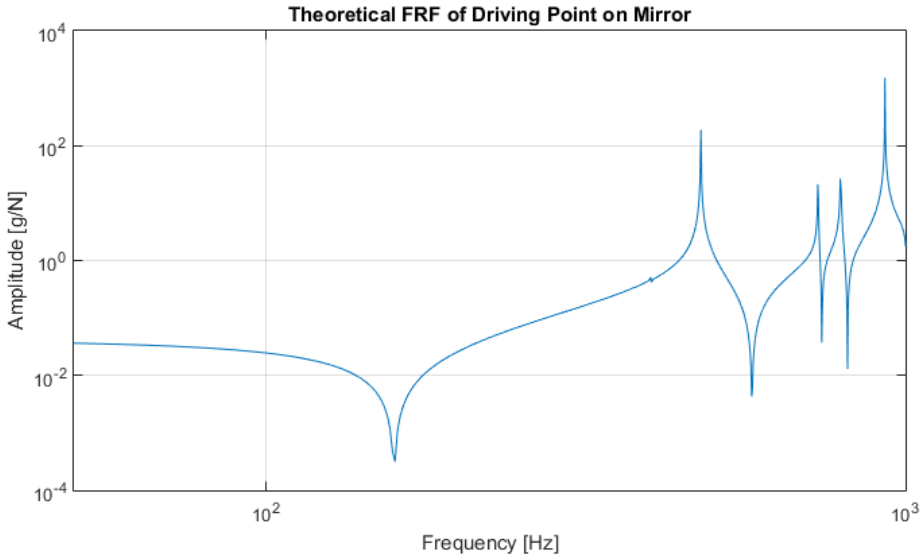

Figure 3.5. Theoretical FRF of Driving Point on Optical Element

Table 3.2 Natural Frequencies Obtained from FE Model

Mode	Natural Frequency [Hz]
1.	399.6
2.	478.3
3.	729
4.	792.4
5.	794.6
6.	929.6

3.1.3 Comparison of the Experimental and Finite Element Model Results of the Optomechanical System

The FRFs measured experimentally (Figure 3.3) are compared with those obtained from the FE model (Figure 3.5), in Figure 3.6. Also, the natural frequencies measured experimentally (Table 3.1) are compared with those obtained from the FE model

(Table 3.2), in Table 3.3 and Figure 3.7. It can be observed that the FRFs are not in good agreement, , and similarly the differences in natural frequencies are very high.

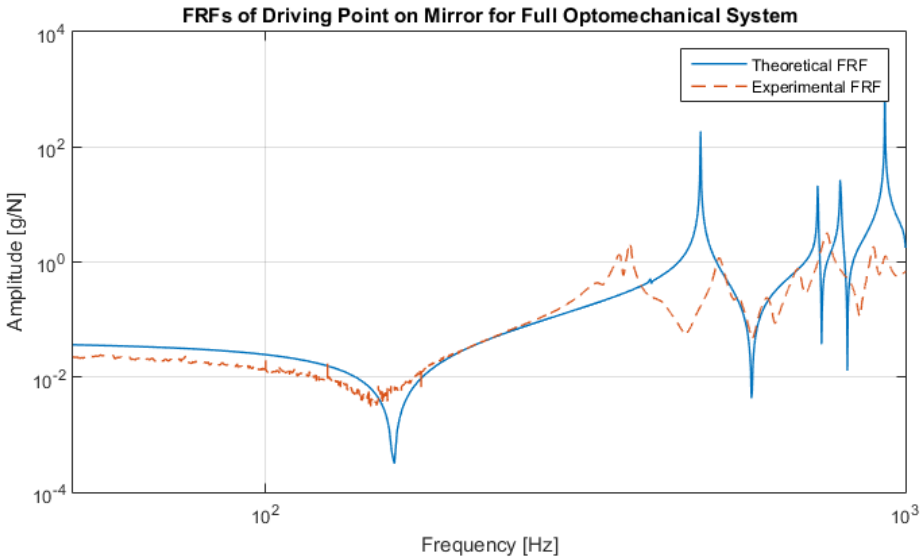

Figure 3.6. Comparison of Experimentally Measured and Theoretically Calculated FRF of Driving Point for Complete Optomechanical System

Table 3.3 Comparison of Natural Frequencies

Mode	Natural Frequency (FE Model) [Hz]	Natural Frequency (Experimental) [Hz]	% Error
1.	399.6	357.0	11.9
2.	478.3	370.4	29.1
3.	729.0	511.3	42.6
4.	792.4	613.7	29.1
5.	794.6	685.2	16.0
6.	929.6	704.4	32.0

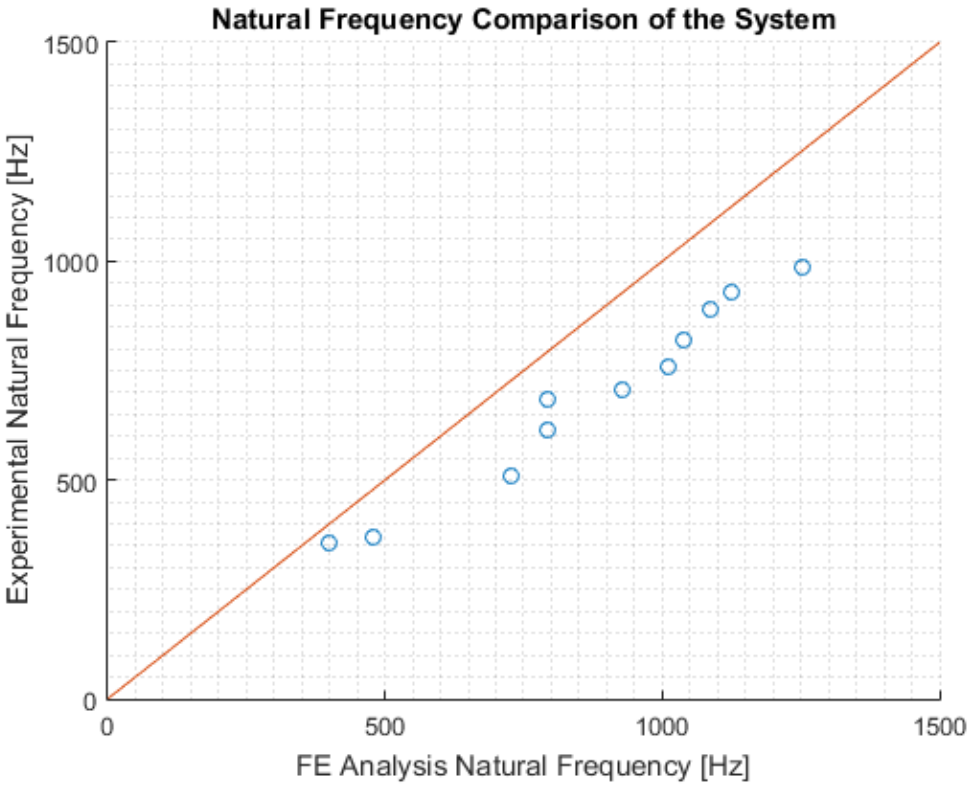

Figure 3.7. Comparison of Natural Frequencies

From the comparison of the experimental and FE analysis results, it can be observed that the experimental and FE models do not match with each other. Since the optomechanical system has many components, and there are many parameters affecting the system's response in FE analysis such as bolt models, joint models, material differences (density, modulus of elasticity, Poisson's ratio) and modeling of mechanical elements like bearings and linear motion guide, these parameters cannot be defined accurately to obtain an updated FE model. Moreover, the model updating methods existing in literature could not be applied to this system because there are many parameters, and updating of these parameters all together will cause uncertainites in the system and increase computational time and effort.

3.2 Introduction of the Sequential Model Updating Method

In today's technology, engineers have to meet strict requirements in terms of endurance, shape, size and sensitivity etc. while being resistant to all kinds of external loads. This makes development and design of devices a challenge. Engineers put so much effort to have accurate mathematical models, so that they can be used to make structural modifications by using design optimizations. However, if these models do not represent the actual systems accurately, optimizations could lead them to make wrong decisions. At this stage, model updating is very crucial and is required to have reliable mathematical models.

Model updating is a developing technology and it aims to improve and verify numerical models of the systems with their real ones by correlating numerical results with dynamic response of real test models. To minimize the differences and incompatibilities between mathematical and test models, global (density, Young's Modulus, Poisson's Ratio etc.) or local (thickness, beam cross-section, joint stiffness) parameters are required to be updated.

In literature, several model-updating methods are proposed to optimize the FE model of a structure to compromise with experimental data; but these methods could not be applied here to this complex system effectively, since the system is composed of a mechanism which has many components, bolted joints, bearings and a linear motion guide. There are high number of variables (bolted joint types, bearing stiffnesses and damping values and linear motion guide model) to update, to have an accurate FE model.

Correlating high number of variables with the test model all together increases computational complexity because of too many numerical iterations. More

importantly, it is required to have accuracy in all subsections of the FE model of the optomechanical system to make successful structural modifications; however, with the model updating of the complete system by using classical model updating methods, it is not possible to specify which particular variable is required to be modified in order to match the total response of the model with that of the real model. Therefore, it is necessary to have a new approach to update the FE model of this complex system.

Therefore, a new approach is developed in this thesis, which is called Sequential Model Updating Method. In this method, model updating is carried out in several steps, starting with the updating the model of a single structure, and then add a component at a time and updating the model of the resulting assembly, rather than updating the complete model in one step. In other words, the FE model of the system is formed sequentially by updating and verifying the model of each subsystem with experimental data at each step. The diagram, which explains the approach used in Sequential Model Updating Method is shown in Figure 3.8.

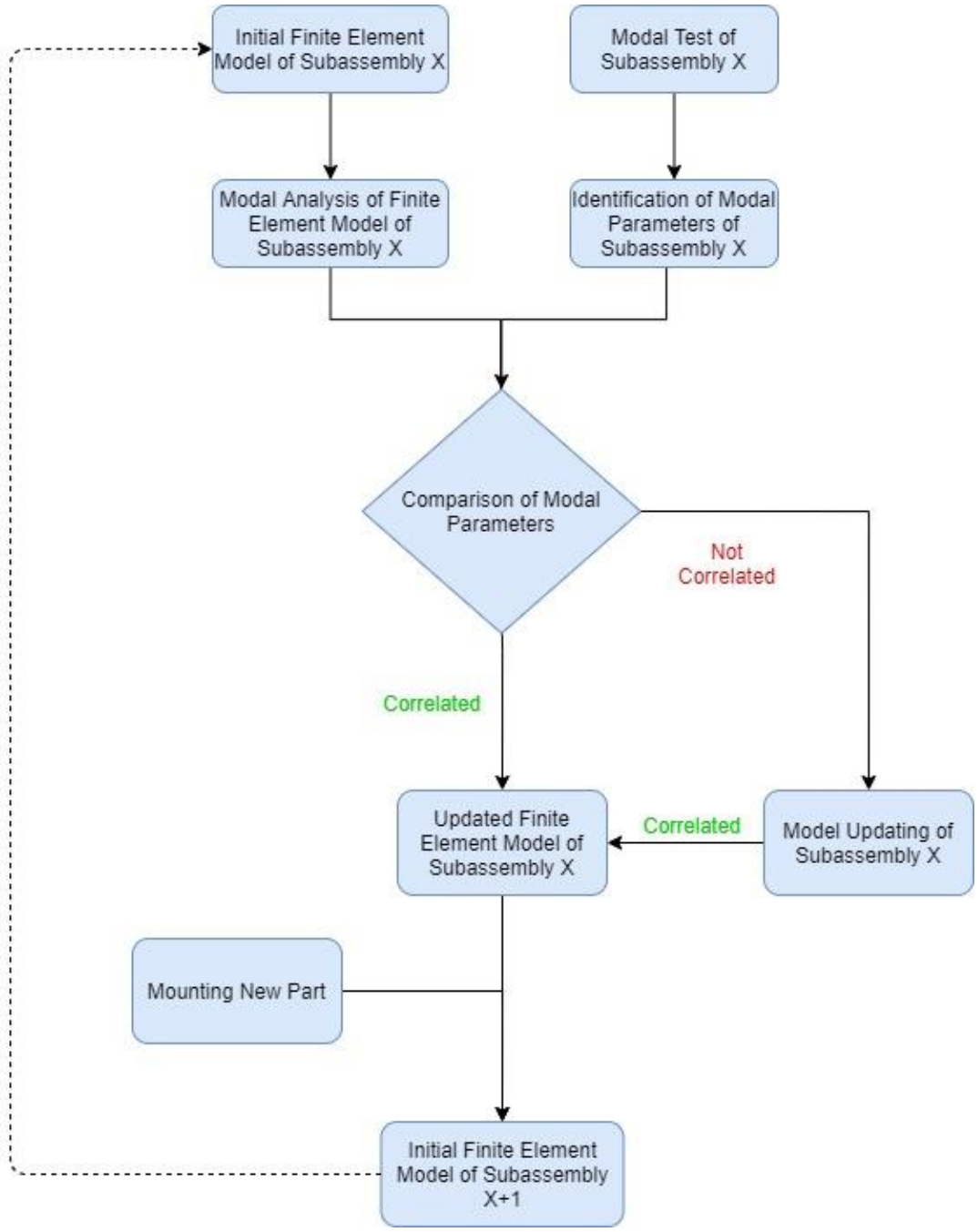

Figure 3.8. Diagram of Sequential Model Updating Method

In this method, studies start with the initial FE model of a particular subassembly at each step. FRFs and natural frequencies are found by making modal analysis on this initial model. Modal tests are also carried out on the real subassembly to form the

test model and find modal parameters experimentally. Then, the modal parameters found from initial FE model and the test model are compared to check the initial FE model's compatibility with real system.

If a good correlation is not obtained, then the initial FE model is updated by using the experimental results. At each subassembly, the global and local parameters of the system are updated iteratively without using any routine exists in the literature, as there are usually a few parameters to be updated. After updating and obtaining a reliable FE model for the subassembly, another part or small assembly is mounted and a new subassembly is obtained. The procedure is repeated until the complete system is assembled and modeled, thus obtaining the updated FE model of the whole system.

In this thesis, model updating procedure is started with the lowest level of the optomechanical system, which is the part called optical element. The new method is applied until the complete optomechanical system is assembled and modeled in FE. All the parts, bolted joints, bearings and linear motion guide existing in the optomechanical system is updated and defined accurately in the FE model by using the method proposed.

3.3 Updating Finite Element Model of Optical Element

In this section, finite element model updating of the optical element is explained.

3.3.1 Initial Finite Element Model of the Optical Element

Initial finite element model is created in this section. Firstly, the CAD model of the optical element is exported to ANSYS software. In finite element analyses, the number of nodes and element types are very important since they directly affect the

solution time. For this reason, in modeling, some features like holes, rounds and chamfers, which do not affect the dynamical characteristics of the system significantly, are simplified to increase the speed of the analyses, and to reduce the number of total DOF.

The material of the optical element is aluminum alloy, and its material properties are defined to ANSYS Library. The density is verified by measuring the mass and volume of the optical element. Modulus of elasticity and Poisson's ratio values are taken from the literature. The damping ratio of the optical element is not defined at this stage; it will be determined in the model updating process according to experimental results. The material properties of the optical element used in the analyses are shown in Table 3.4.

Table 3.4 Material Properties of Optical Element Used in Initial FE Model

Density	2770 kg/m^3
Modulus of Elasticity	71 GPa
Poisson's Ratio	0.33

The masses of the accelerometers are also considered in the FE model, at the locations where they are expected to be placed, since they will be used in the modal tests, and their mass affects the modal test results.

Since the system is tested in free-free conditions, the same boundary conditions are used in the FE model. The meshing of the part is done after these procedures. FE model has 73176 nodes and 40156 tetrahedral elements (shown in Figure 3.9).

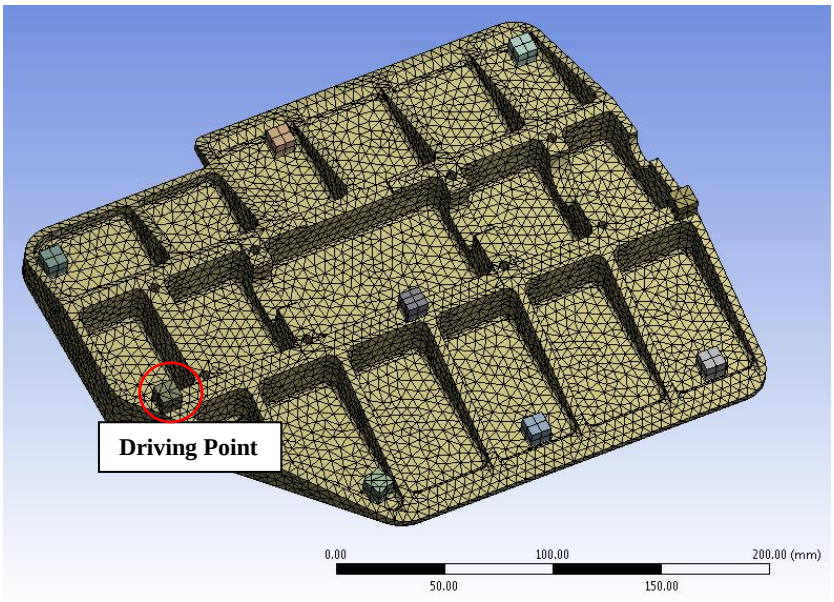

Figure 3.9. FE Model of the Optical Element Used in the Analyses

The direct FRF of the driving point (location is shown in Figure 3.9 and direction is perpendicular to the surface) and natural frequencies of the optical element obtained from initial FE model are shown in Figure 3.10 and Table 3.5, respectively.

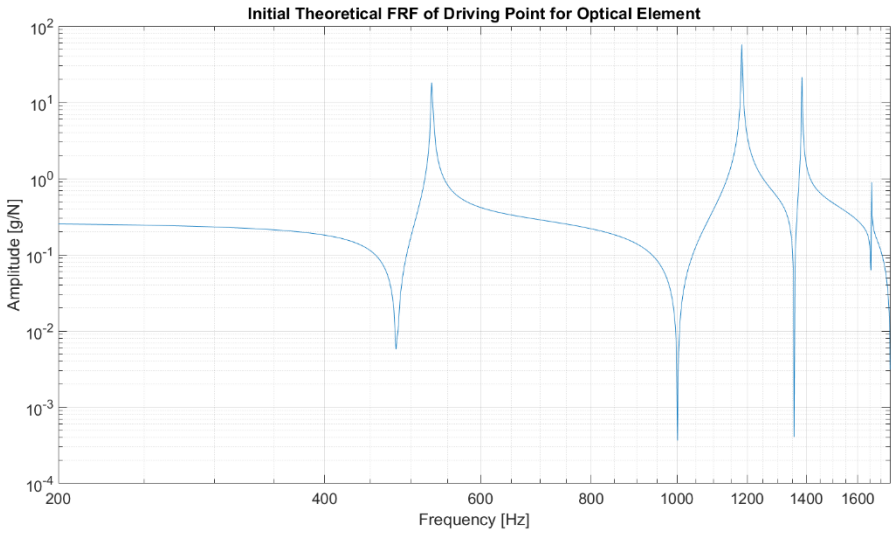

Figure 3.10. FRF of the Driving Point for Optical Element Obtained from the Initial FE Model

Table 3.5 Natural Frequencies of the Optical Element Obtained from Initial FE Model

Mode	Natural Frequency [Hz]
1.	528.67
2.	1183.5
3.	1384
4.	1657.5
5.	2002.2

3.3.2 Modal Test of the Optical Element

For the modal tests of the optical element, nine accelerometers are used to measure vibration spectra with a dynamic range of 50g. The accelerometer models are Endevco 65-100 and Brüel&Kjaer 4507B. They are bonded by using instant adhesives (shown in Figure 3.11). This mounting type prevents dynamic effects coming from the bonding of accelerometers even at high frequencies. The accelerometers are placed according to best excitation points observed in initial FE model. Modal hammer of B&K 8206 model with a white plastic tip is used to excite the system. Tests are done on a soft foam to simulate free-free boundary conditions. The measurements are carried out by exciting the system with a single impact point (called driving point), and the response of the structure is measured by using multiple accelerometers synchronously. In the modal tests, 15 repetitions are done at the driving point. The test setup and measurement locations of the accelerometers are shown in Figure 3.11.

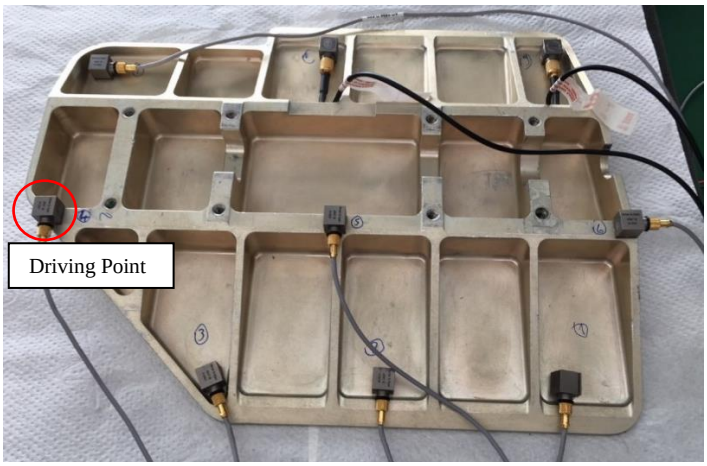

Figure 3.11. Modal Test Setup of the Optical Element

For all the measurement points, FRFs are obtained from measured forces and accelerations, and modal parameters are extracted from these functions by using LMS Test Lab software's Polymax algorithm. A typical measured direct FRF of the driving point on the optical element (location is shown in Figure 3.11 and direction is perpendicular to the surface), and natural frequencies and corresponding damping ratios identified are shown in Figure 3.12 and Table 3.6, respectively.

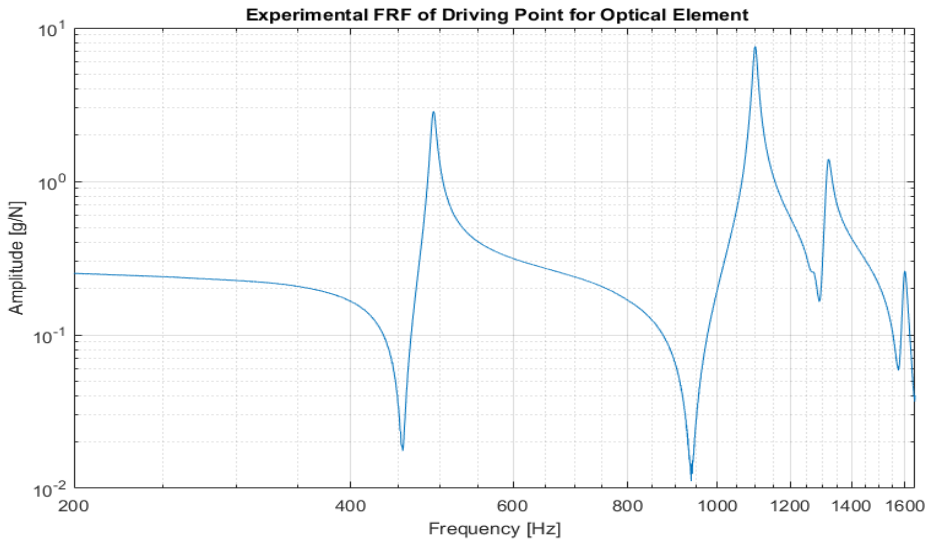

Figure 3.12. Experimental FRF of Driving Point on Optical Element

Table 3.6 Modal Parameters of the Optical Element Obtained from Experimental Modal Analysis

Mode	Natural Frequency [Hz]	Damping Ratio [%]
1.	503.0	0.55
2.	1123.6	0.39
3.	1291.0	0.49
4.	1591.8	0.56
5.	1903.8	0.58

The FRFs obtained from the initial FE model (Figure 3.10) are compared with those measured experimentally (Figure 3.12), in Figure 3.13. Also, the natural frequencies found from initial FE model (Table 3.5) are compared with those measured experimentally (Table 3.6), in Table 3.7 and Figure 3.14. It can be observed that the FRFs are not in good agreement, and similarly the differences in natural frequencies are very high. Therefore, the FE model of the optical element needs to be updated according to experimental results.

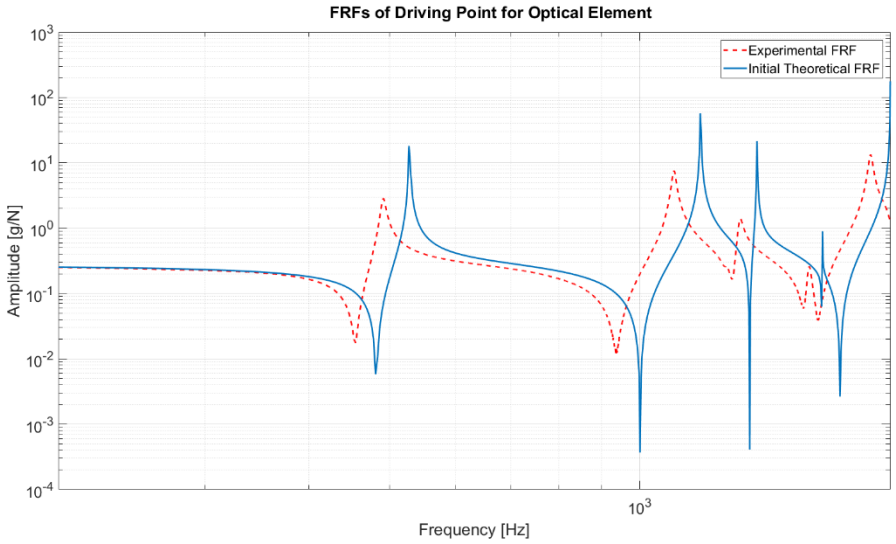

Figure 3.13. Comparison of Theoretically Calculated and Experimentally Measured FRFs of Driving Point for Optical Element

Table 3.7 Comparison of Natural Frequencies of the Optical Element Calculated from Initial FE Model with Those Obtained from Experimental Modal Analysis

Mode	Natural Frequency (Initial FE Model) [Hz]	Natural Frequency (Experimental) [Hz]	% Error
1.	528.67	503.0	5.10
2.	1183.5	1123.6	5.33
3.	1384	1291.0	7.20
4.	1657.5	1591.8	4.13
5.	2002.2	1903.8	5.17

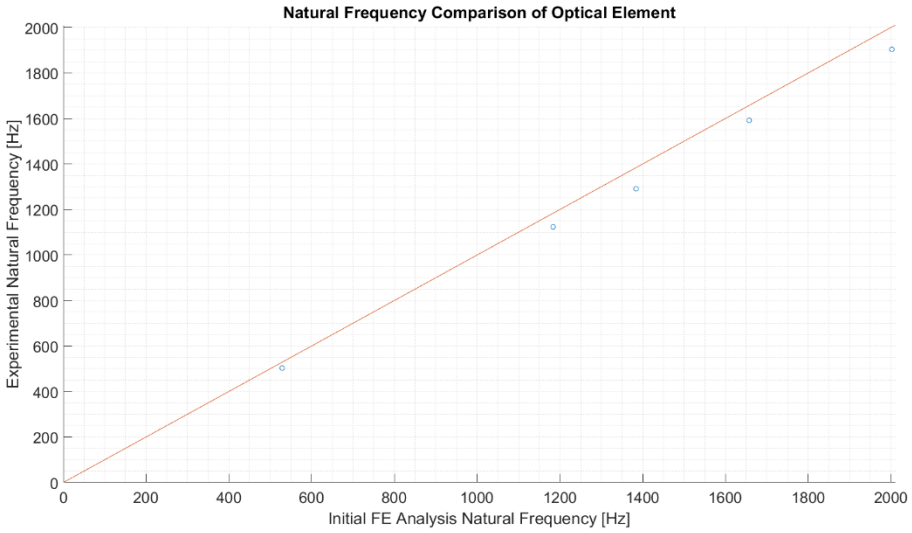

Figure 3.14. Comparison of Natural Frequencies of the Optical Element Calculated from Initial FE Model with Those Obtained from Experimental Modal Analysis

3.3.3 Updated Finite Element Model of the Optical Element

It can be observed in Table 3.7 that the initial FE model of the optical element do not match with the experimental model. Therefore, FE model is updated by improving Young's modulus, Poisson's ratio and damping ratio values of the optical element. The density of the optical element is not changed because it was already verified at

initial FE modeling stage. The damping ratio is defined according to modal test results.

Young's modulus and Poisson's ratio values are updated by using ANSYS Response Surface and Response Surface Optimization features. Firstly, parameters to be optimized (Young's modulus and Poisson's ratio in this case) and output parameters (first five natural frequencies in this case) are selected, so that Design of Experiments (DOE) are created. By using DOE, the least possible number of runs are carried out to figure out the influence of the input parameters in specified intervals. Sensitivities of the output parameters with respect to the input parameters are calculated, and response surfaces, which show the variation of the output parameters with respect to input parameters, are created. It is observed that, the effect of the Young's modulus on the natural frequencies is much higher than Poisson's ratio in this case.

By using DOE and response surface results, Response Surface Optimization, which is a goal-driven optimization feature, is conducted. It determines the candidate input parameters based on given output parameter ranges. The lower and upper bounds of both input and output parameters are specified by the user as the lowest and highest values of that parameter can take in the optimization. Targets for the output parameters are the natural frequencies measured experimentally. MOGA (Multi-Objective Genetic Algorithm) is used in the analyses, because it is a multi-goal optimization problem and there are five natural frequencies in this case as goals. The optimization is converged after 3755 evaluations. The details of the input and output parameters are given in Table 3.8.

Table 3.8 Details of the Parameters Used in the Response Surface Optimization

		Initial Value	Lower Bound	Upper Bound	Updated Value	Targets
Input Parameters	Young's Modulus [GPa]	71	68	74	69	-
	Poisson's Ratio	0.33	0.30	0.36	0.35	-
Output Parameters	1st Natural Frequency [Hz]	528.67	499	505	499	503.0
	2nd Natural Frequency [Hz]	1183.5	1118.5	1128.5	1123.3	1123.6
	3nd Natural Frequency [Hz]	1384	1285	1297	1297	1291.0
	4th Natural Frequency [Hz]	1657.5	1584	1600	1589	1591.8
	5th Natural Frequency [Hz]	2002.2	1895	1913	1910.8	1903.8

The geometry of the FE model is not changed in order not to diverge from the real structure. Since the part is tested in free-free conditions, the same boundary conditions are used in the FE model. The meshing of the part is done after these operations. The final FE model has 73176 nodes and 40156 tetrahedral elements.

The direct FRF of the driving point and natural frequencies obtained from the updated FE model of the optical element are given in Figure 3.15 and Table 3.9, respectively.

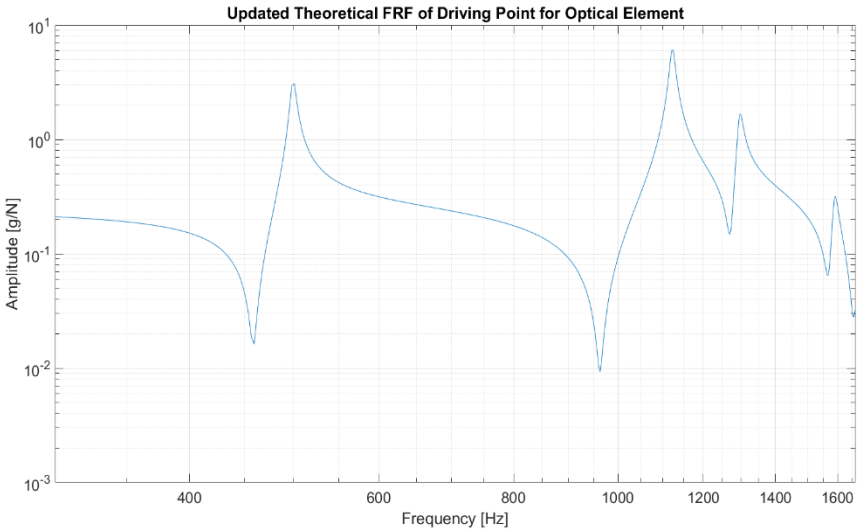

Figure 3.15. FRF of the Driving Point for Optical Element Obtained from the Updated FE Model

Table 3.9 Natural Frequencies of the Optical Element Obtained from Updated FE Model

Mode	Natural Frequency [Hz]
1.	499
2.	1123.3
3.	1297
4.	1589
5.	1910.8

The FRFs measured experimentally (Figure 3.12) are compared with those obtained from the updated FE model (Figure 3.15), in Figure 3.16. Also, the natural frequencies measured experimentally (Table 3.6) are compared with those obtained from the updated FE model (Table 3.9), in Table 3.10 and Figure 3.17. It can be observed that the FRFs are perfectly in agreement, the natural frequency results are very close to each other, and percentage errors are very low. Therefore, the model

updating process of the FE model of the optical element is completed at this point. FRFs of the driving point, found from the initial FE model, experimentally and from the updated FE model are compared in Figure 3.18 to see the improvement in the FE model of the optical element.

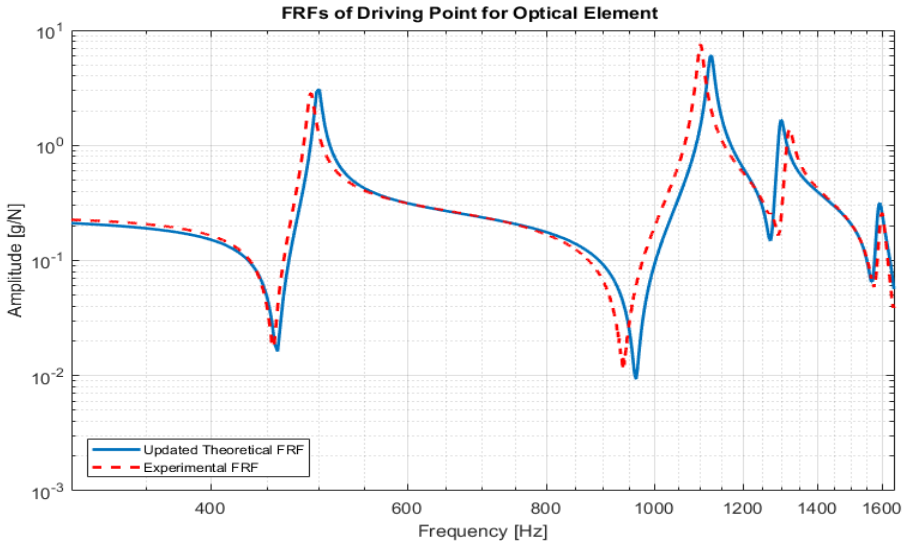

Figure 3.16. Comparison of Theoretically Calculated and Experimentally Measured FRFs of Driving Point for Optical Element

Table 3.10 Comparison of Natural Frequencies of the Optical Element Calculated from Updated FE Model with Those Obtained from Experimental Modal Analysis

Mode	Natural Frequency (Updated FE Model) [Hz]	Natural Frequency (Experimental) [Hz]	Error (%)
1.	499	503	-0.80
2.	1123.3	1123.6	-0.03
3.	1297	1291	0.46
4.	1589	1591.8	-0.18
5.	1910.8	1903.8	0.37

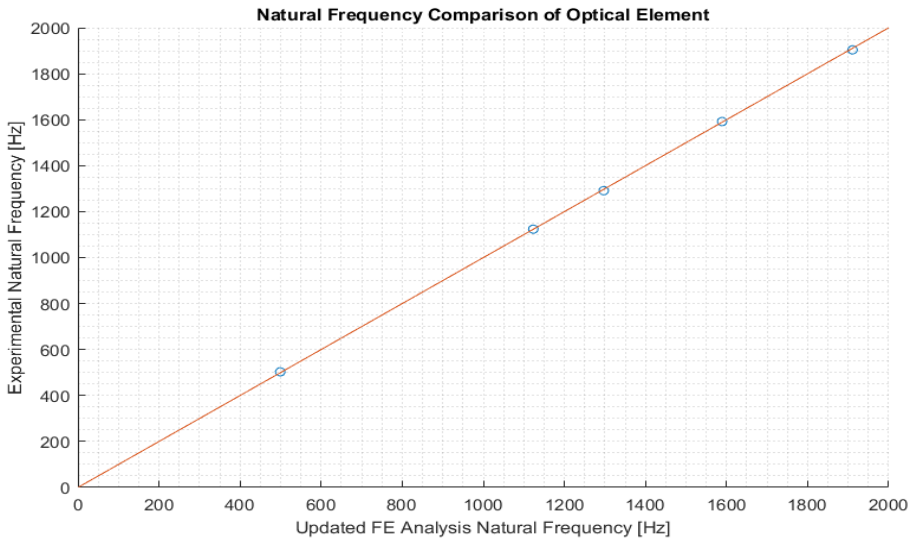

Figure 3.17. Comparison of Natural Frequencies of the Optical Element Calculated from Updated FE Model with Those Obtained from Experimental Modal Analysis

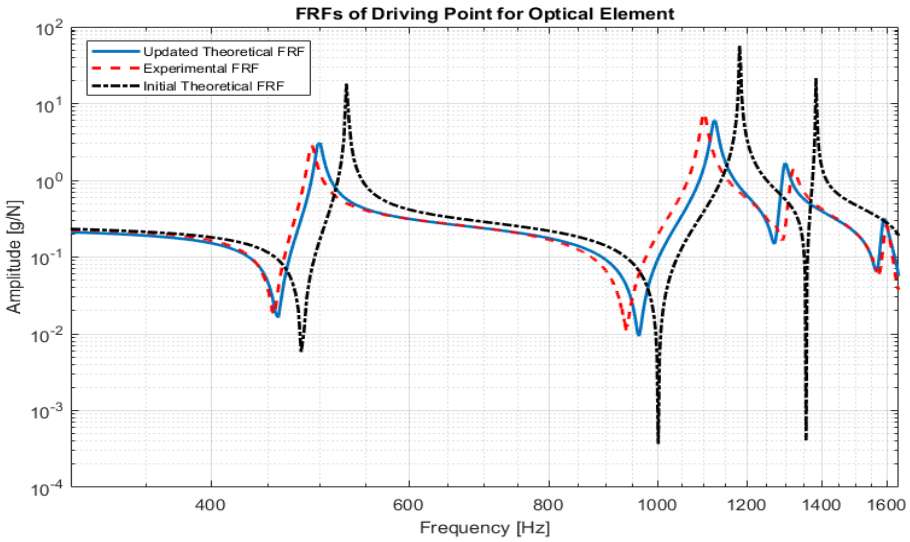

Figure 3.18. Comparison of Theoretically Calculated and Experimentally Measured FRFs of Driving Point for Optical Element

3.4 Updating Finite Element Model of Subassembly I

Holder part is mounted on the optical element, whose FE model is updated in Section 3.3, and Subassembly I is obtained. In this section, the finite element model updating of Subassembly I is explained.

3.4.1 Initial Finite Element Model of Subassembly I

Initial finite element model is created in this section. Firstly, the CAD model of Subassembly I is exported to ANSYS software. In finite element analyses, the number of nodes and element types are very important since they directly affect the solution time. For this reason, in modeling, some features like rounds and chamfers, which do not affect the dynamical characteristics of the system significantly, are simplified, as in the previous case, to increase the speed of the analyses, and to reduce the the number of total DOF.

The material of the optical element is aluminum alloy and its material properties are taken as the updated values found in Section 3.3. The material of the holder is stainless steel and its material properties are defined to ANSYS Library. The density is verified by measuring the mass and volume of the holder part. Modulus of elasticity and Poisson's ratio values are taken from the literature. The damping ratio of the holder part is not defined at this stage; it will be determined in model updating process according to experimental results. The material properties of the holder part used in the analyses are shown in Table 3.11.

Table 3.11 Material Properties of Holder Part Used in Initial FE Model

Density	7850 kg/m^3
Modulus of Elasticity	200 GPa
Poisson's Ratio	0.3

The masses of the accelerometers are also considered in the FE model, at the locations where they are expected to be placed, since they will be used in the modal tests, and their mass affects the modal test results.

Since the system is tested in free-free conditions, the same boundary conditions are used in the FE model. There are four bolted joints between the optical element and the holder parts. Initially, rigidly fixed joint model is used for these bolted joints. The meshing of the assembly is done after these procedures. FE model has 155561 nodes and 89995 tetrahedral elements (shown in Figure 3.19).

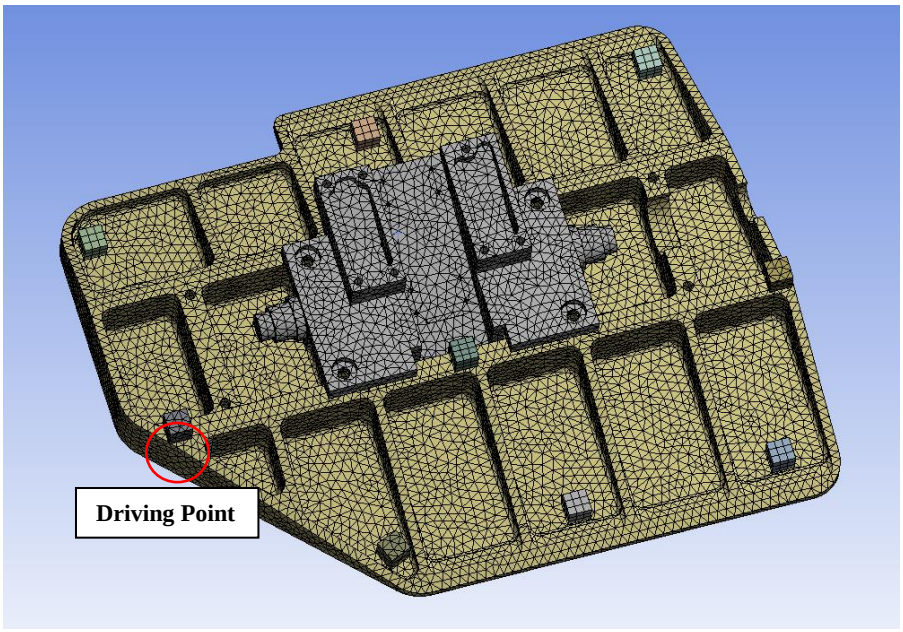

Figure 3.19. FE Model of Subassembly I Used in the Analyses

The direct FRF of the driving point (location is shown in Figure 3.19 and direction is perpendicular to the surface) and natural frequencies of Subassembly I obtained from initial FE model are shown in Figure 3.20 and Table 3.12, respectively.

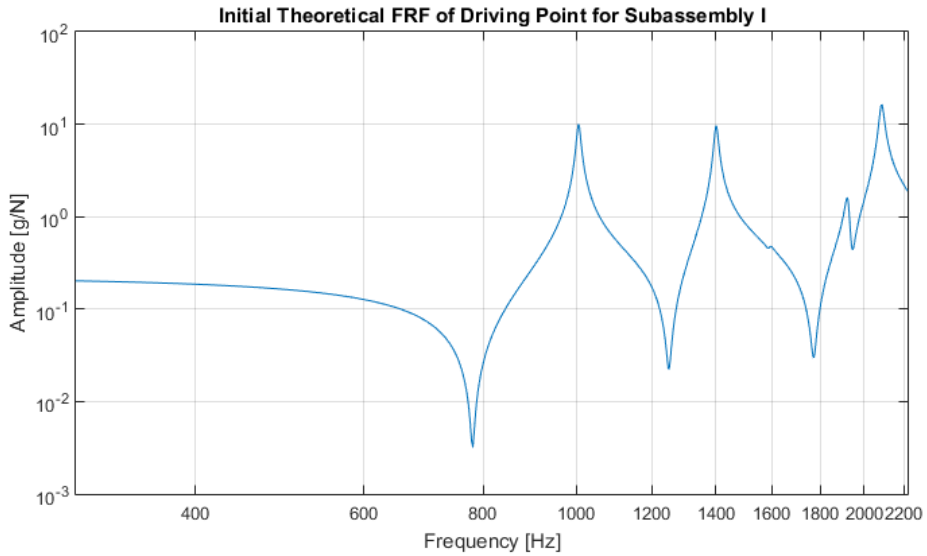

Figure 3.20. FRF of the Driving Point for Subassembly I Obtained from Initial FE Model

Table 3.12 Natural Frequencies of Subassembly I Obtained from Initial FE Model

Mode	Natural Frequency [Hz]
1.	1005.9
2.	1400.6
3.	1593.2
4.	1922.9
5.	2085.5

3.4.2 Modal Test of Subassembly I

For the modal tests of Subassembly I, nine accelerometers are used to measure vibration spectra with a dynamic range of 50g. The accelerometer models are Endevco 65-100 and Brüel&Kjaer 4507B. They are bonded by using instant adhesives (shown in Figure 3.21). This mounting type prevents dynamic effects coming from the bonding of accelerometers even at high frequencies. The accelerometers are placed according to best excitation points observed in initial FE analysis. Modal hammer of B&K 8206 model with a white plastic tip is used to excite the system. Tests are done on a soft foam to simulate free-free boundary conditions. The measurements are carried out by exciting the system with a single impact point, and the response of the structure is measured by using multiple accelerometers synchronously. In the modal tests, 15 repetitions are done at the driving point. The test setup and measurement locations of the accelerometers are shown in Figure 3.21.

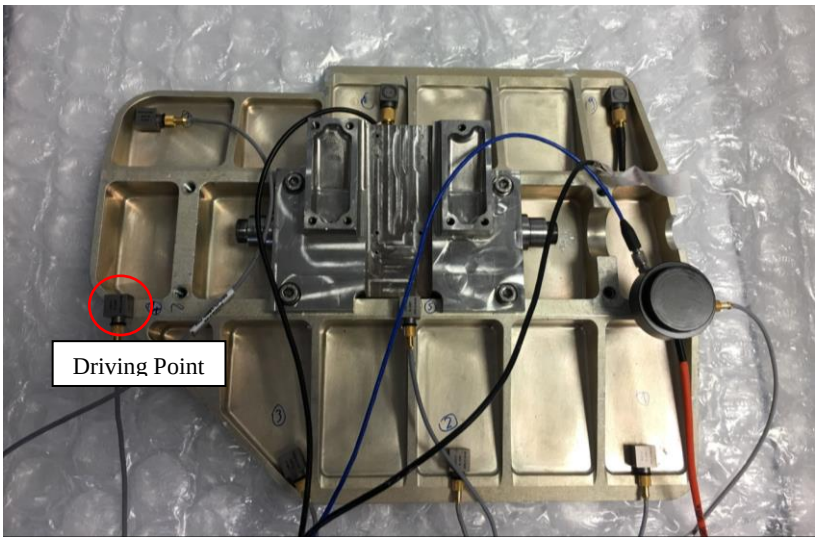

Figure 3.21. Modal Test Setup of Subassembly I

For all the measurement points, FRFs are obtained from measured forces and accelerations, and modal parameters are extracted from these functions by using LMS Test Lab software's Polymax algorithm. A typical measured direct FRF of the driving point on the optical element (location is shown in Figure 3.21 and direction is perpendicular to the surface), and natural frequencies and corresponding damping ratios identified are shown in Figure 3.22 and Table 3.13, respectively.

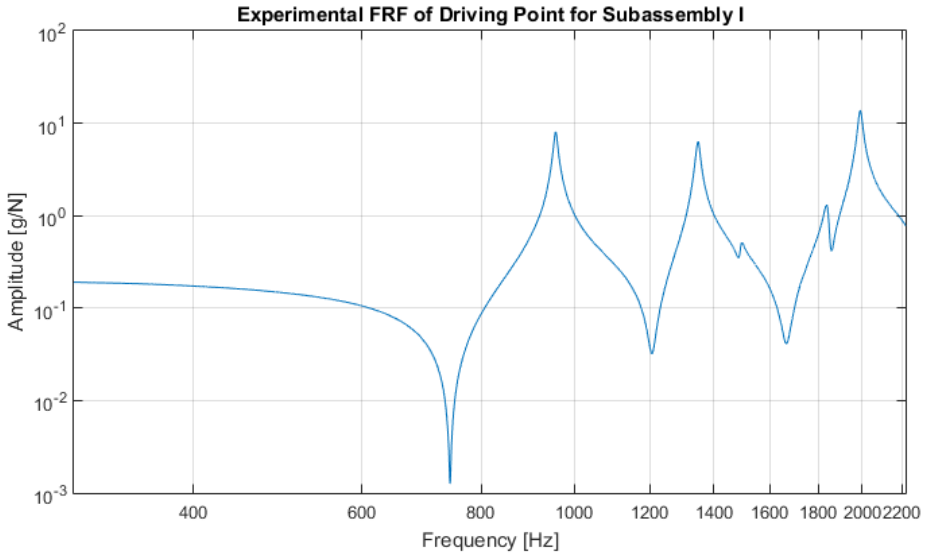

Figure 3.22. Experimental FRF of Driving Point on Subassembly I

Table 3.13 Modal Parameters of Subassembly I Obtained from Experimental Modal Analysis

Mode	Natural Frequency [Hz]	Damping Ratio [%]
1.	956.5	0.55
2.	1347.1	0.50
3.	1492.1	0.50
4.	1839.3	0.58
5.	1990.8	0.58

The FRFs obtained from the initial FE model (Figure 3.20) are compared with those measured experimentally (Figure 3.22), in Figure 3.23. Also, the natural frequencies found from initial FE model (Table 3.12) are compared with those measured experimentally (Table 3.13), in Table 3.14 and Figure 3.24. It can be observed that the FRFs are not in good agreement, and similarly the differences in natural frequencies are very high. Therefore, the FE model of Subassembly I needs to be updated according to experimental results.

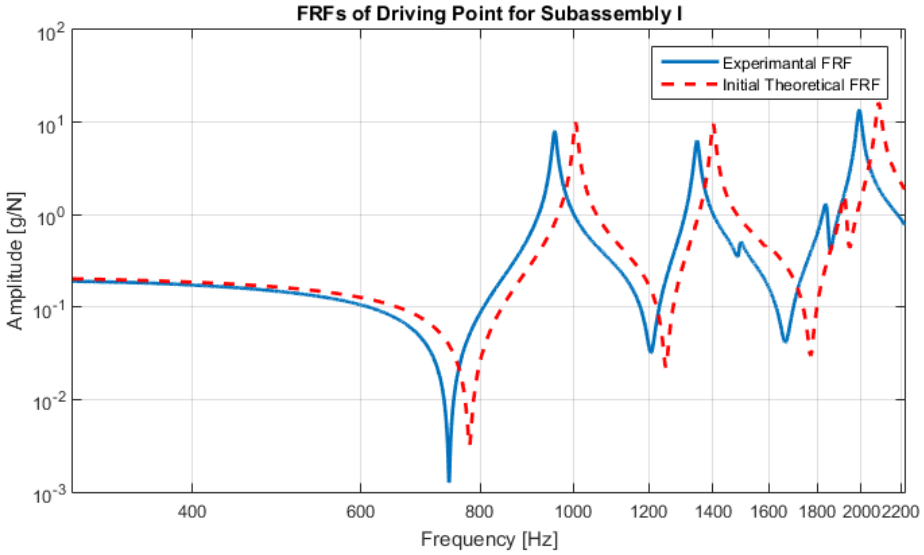

Figure 3.23. Comparison of Theoretically Calculated and Experimentally Measured FRFs of Driving Point for Subassembly I

Table 3.14 Comparison of Natural Frequencies of Subassembly I Calculated from Initial FE Model with Those Obtained from Experimental Modal Analysis

Mode	Natural Frequency (Initial FE Model) [Hz]	Natural Frequency (Experimental) [Hz]	% Error
1.	1005.9	956.5	5.16
2.	1400.6	1347.1	3.97
3.	1593.2	1492.1	6.78
4.	1922.9	1839.3	4.55
5.	2085.5	1990.8	4.76

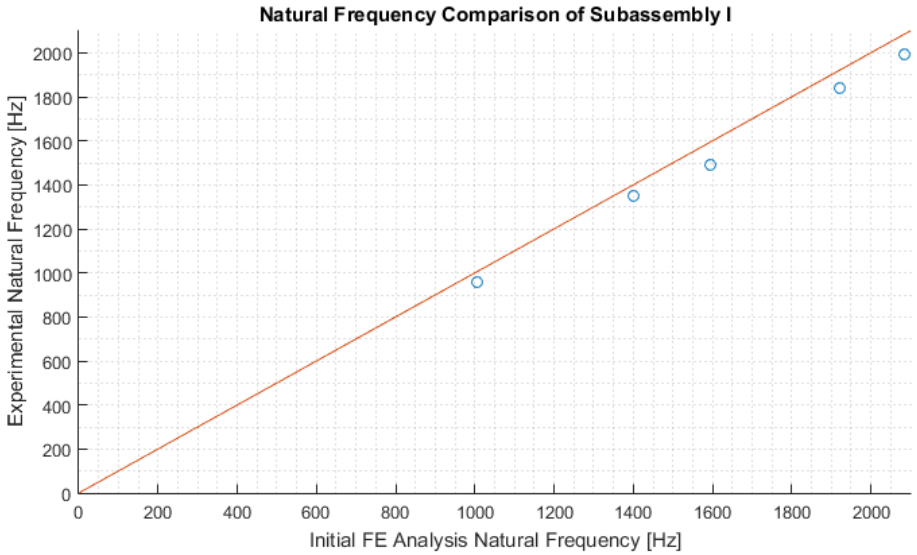

Figure 3.24. Comparison of Natural Frequencies of Subassembly I Calculated from Initial FE Model with Those Obtained from Experimental Modal Analysis

3.4.3 Updated Finite Element Model of Subassembly I

It can be observed in Table 3.14 that initial FE model of Subassembly I do not match with experimental model. Therefore, FE model is updated by improving material properties of the holder part and joint definitions of the bolted joints between optical element and holder part. Joints are defined as rigidly fixed in the initial FE model,

but they are redefined in the updated FE model as beam-rigid to simulate the bolts used in the real model. The density of the holder part is not changed because it was already verified at initial FE modeling stage. The damping ratio of the holder part is defined according to modal test results.

Young's modulus and Poisson's ratio values of the holder part and beam radii of the bolted joints between the parts are updated by using ANSYS Response Surface and Response Surface Optimization features. Firstly, parameters to be optimized (Young's modulus and Poisson's ratio and beam radii of the bolted joints in this case) and output parameters (first five natural frequencies in this case) are selected, so that Design of Experiments (DOE) are created. Sensitivities of the output parameters with respect to the input parameters are calculated, and response surfaces are created. It is observed that, the effect of the Young's modulus on the natural frequencies is much higher than Poisson's ratio, similar to previous case. Also, the resulted radii of the beams used for bolted joints are very similar to the real bolt radii used in the real model.

By using DOE and response surface results, Response Surface Optimization is conducted. It determines the candidate input parameters based on given output parameter ranges. The lower and upper bounds of both input and output parameters are specified by the user as the lowest and highest values of that parameter can take in the optimization. Targets for the output parameters are the natural frequencies measured experimentally. MOGA is used in the analyses, because it is a multi-goal optimization problem and there are five natural frequencies in this case as goals. The optimization is converged after 18783 evaluations. The details of the input and output parameters are given in Table 3.15.

Table 3.15 Details of the Parameters Used in the Response Surface Optimization

		Initial Value	Lower Bound	Upper Bound	Updated Value	Targets
Input Parameters	Young's Modulus [GPa]	200	180	220	210	-
	Poisson's Ratio	0.3	0.27	0.33	0.28	-
	Radius of 1st Beam [mm]	1.5	1	2	1.48	-
	Radius of 2nd Beam	1.5	1	2	1,53	-
	Radius of 3rd Beam	1.5	1	2	1,45	-
	Radius of 4th Beam	1.5	1	2	1,54	-
Output Parameters	1st Natural Frequency [Hz]	1005.9	946	966	948.87	956.5
	2nd Natural Frequency [Hz]	1400.6	1341	1353	1349.8	1347.1
	3rd Natural Frequency [Hz]	1593.2	1481	1503	1502.9	1492.1
	4th Natural Frequency [Hz]	1922.9	1830	1850	1838.3	1839.3
	5th Natural Frequency [Hz]	2085.5	1980	2003	2002.6	1990.8

The geometry of the FE model is not changed in order not to diverge from the real structure. Since the assembly is tested in free-free conditions, the same boundary conditions are used in the FE model. The meshing of the assembly is done after these operations. The final FE model has 155561 nodes and 89995 tetrahedral elements.

The direct FRF of the driving point and natural frequencies obtained from the updated FE model of Subassembly I are given in Figure 3.25 and Table 3.16, respectively.

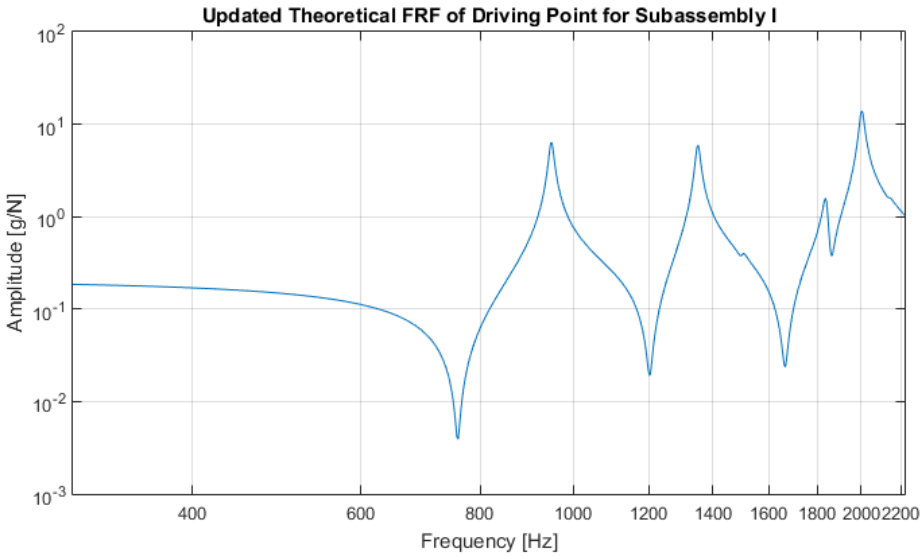

Figure 3.25. FRF of the Driving Point for Subassembly I Obtained from Updated FE Model

Table 3.16 Natural Frequencies of Subassembly I Obtained from Updated FE Model

Mode	Natural Frequency [Hz]
1.	948.87
2.	1349.8
3.	1502.9
4.	1838.3
5.	2002.6

The FRFs measured experimentally (Figure 3.22) are compared with those obtained from the updated FE model (Figure 3.25), in Figure 3.26. Also, the natural frequencies measured experimentally (Table 3.13) are compared with those obtained from the updated FE model (Table 3.16), in Table 3.17 and Figure 3.27. It can be observed that the FRFs are perfectly in agreement, the natural frequency results are

very close to each other, and percentage errors are very low. Therefore, the model updating process of the FE model of Subassembly I is completed at this point. FRFs of the driving point, found from the initial FE model, experimentally and from the updated FE model are compared in Figure 3.28 to see the improvement in the FE model of Subassembly I.

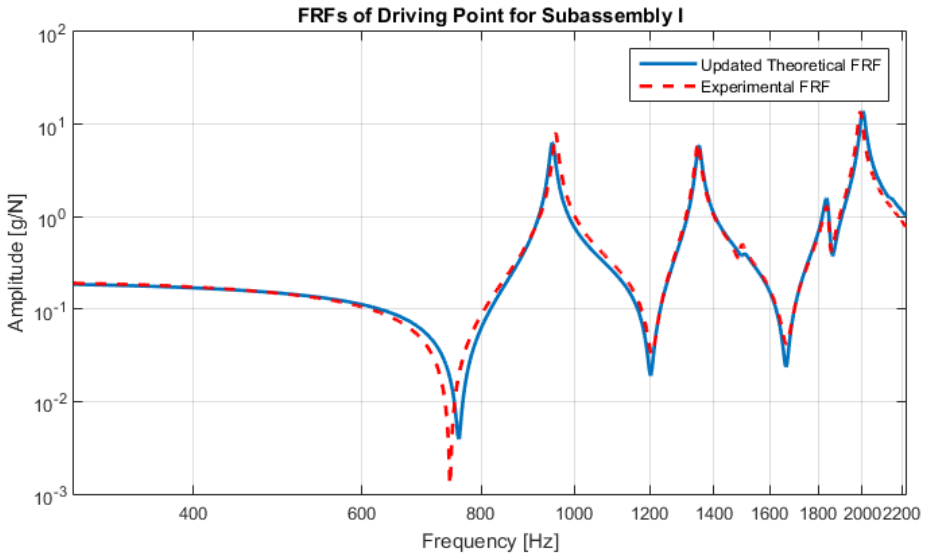

Figure 3.26. Comparison of Theoretically Calculated and Experimentally Measured FRFs of Driving Point for Subassembly I

Table 3.17 Comparison of Natural Frequencies of Subassembly I Calculated from Updated FE Model with Those Obtained from Experimental Modal Analysis

Mode	Natural Frequency (Updated FE Model) [Hz]	Natural Frequency (Experimental) [Hz]	Error (%)
1.	948.87	956.5	-0.80
2.	1349.8	1347.1	0.20
3.	1502.9	1492.1	0.72
4.	1838.3	1839.3	-0.05
5.	2002.6	1990.8	0.59

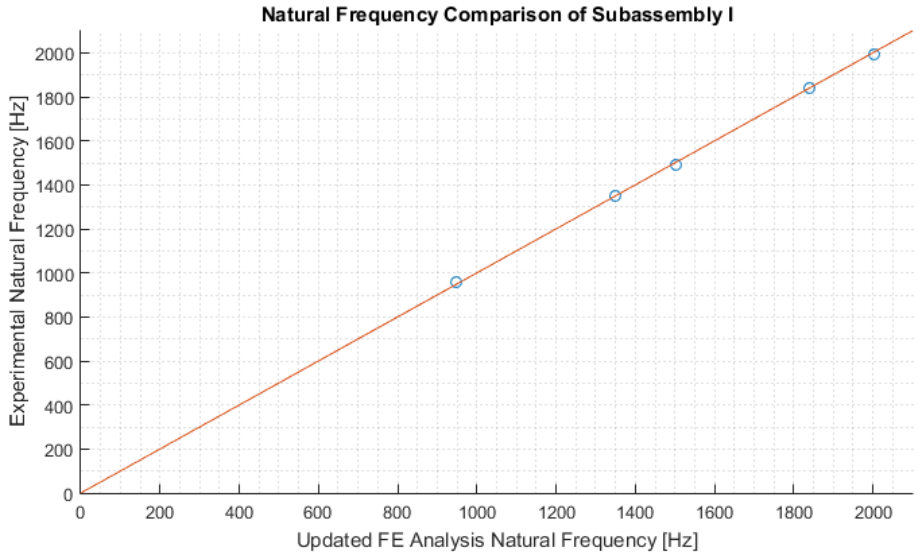

Figure 3.27. Comparison of Natural Frequencies of Subassembly I Calculated from Updated FE Model with Those Obtained from Experimental Modal Analysis

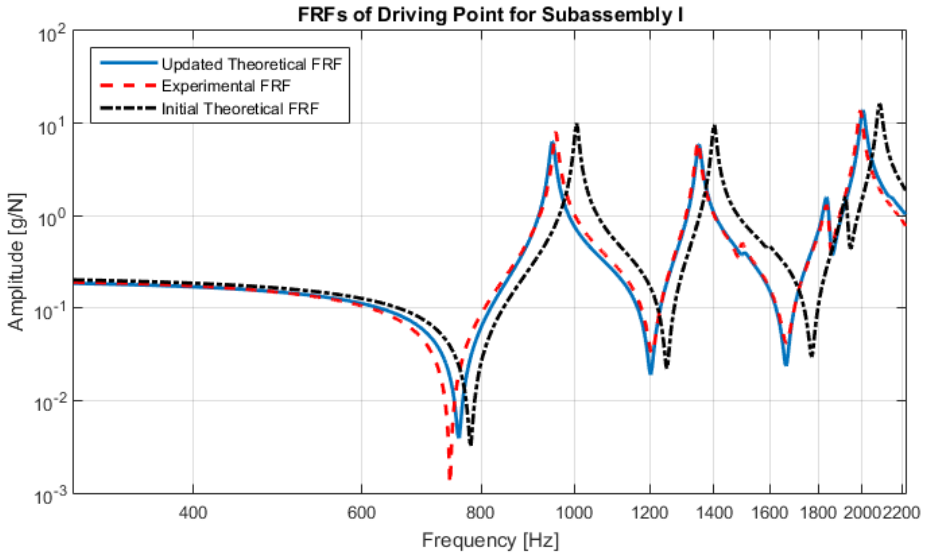

Figure 3.28. Comparison of Theoretically Calculated and Experimentally Measured FRFs of Driving Point for Subassembly I

3.5 Updating Finite Element Model of Subassembly II

Slider arm part is mounted on Subassembly I, whose FE model is updated in Section 3.4, and Subassembly II is obtained. In this section, the finite element model updating of Subassembly II is explained.

3.5.1 Initial Finite Element Model of Subassembly II

Initial finite element model is created in this section. Firstly, the CAD model of Subassembly II is exported to ANSYS software. In finite element analyses, the number of nodes and element types are very important since they directly affect the solution time. For this reason, in modeling, some features like rounds and chamfers, which do not affect the dynamical characteristics of the system significantly, are simplified, as in the previous cases, to increase the speed of the analyses, and to reduce the number of total DOF.

Material properties of the parts in Subassembly I are taken as the updated values found in Section 3.4. The material of the slider arm is stainless steel and its material properties are defined to ANSYS Library. The density is verified by measuring the mass and volume of the slider arm part. Modulus of elasticity and Poisson's ratio values are taken from the literature. The damping ratio of the slider arm part is not defined at this stage; it will be determined in model updating process according to experimental results. The material properties of slider arm part used in the analyses are shown in Table 3.18.

Table 3.18 Material Properties of Slider Arm Part Used in Initial FE Model

Density	7850 kg/m^3
Modulus of Elasticity	200 GPa
Poisson's Ratio	0.3

The masses of the accelerometers are also considered in the FE model, at the locations where they are expected to be placed, since they will be used in the modal tests, and their mass affects the modal test results.

Since the system is tested in free-free conditions, the same boundary conditions are used in the FE model. There are six bolted joints between holder and slider arm parts. Initially, rigidly fixed joint model is used for these bolted joints. The meshing of the assembly is done after these procedures. FE model has 166432 nodes and 95752 tetrahedral elements (shown in Figure 3.29).

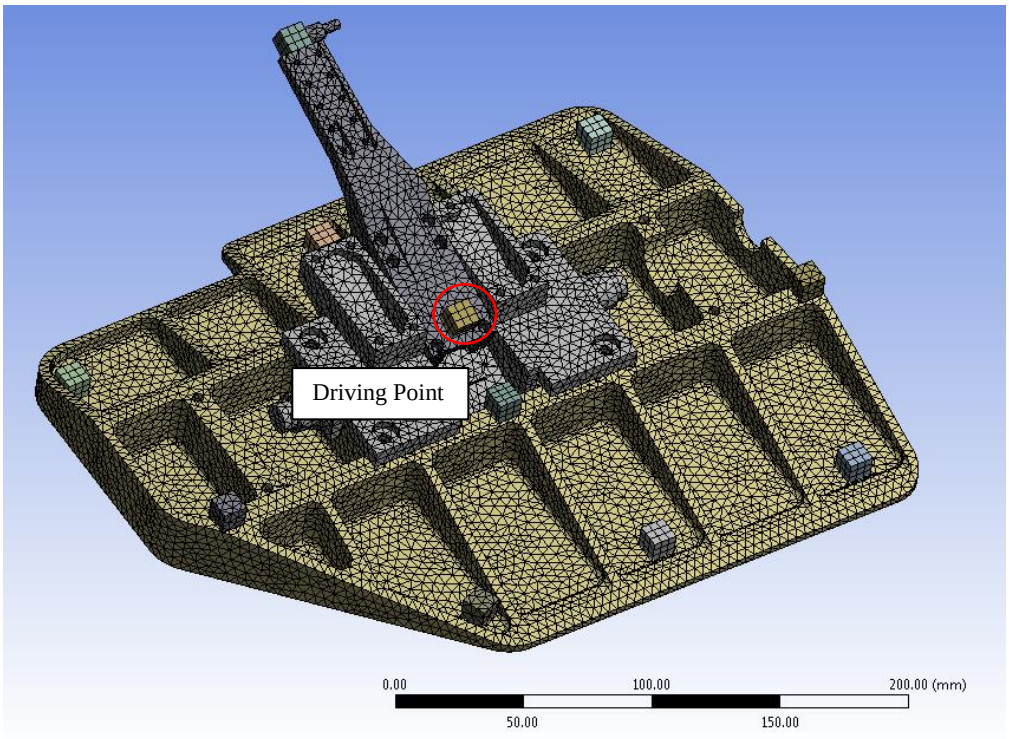

Figure 3.29. FE Model of Subassembly II Used in the Analyses

The direct FRF of the driving point (location is shown in Figure 3.29 and direction is perpendicular to the surface) and natural frequencies of Subassembly II obtained from initial FE model are shown in Figure 3.30 and Table 3.19, respectively.

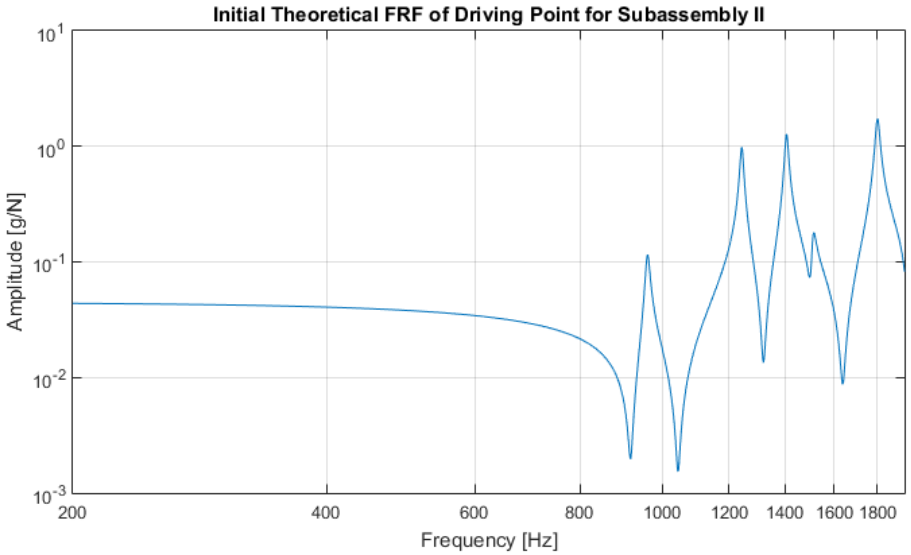

Figure 3.30. FRF of the Driving Point for Subassembly II Obtained from Initial FE Model

Table 3.19 Natural Frequencies of Subassembly II Obtained from Initial FE Model

Mode	Natural Frequency [Hz]
1.	961.16
2.	1243.7
3.	1405.2
4.	1510.4
5.	1801.7

3.5.2 Modal Test of Subassembly II

For the modal tests of Subassembly II, eleven accelerometers are used to measure vibration spectra with a dynamic range of 50g. The accelerometer models are Endevco 65-100 and Brüel&Kjaer 4507B. They are bonded by using instant adhesives (shown in Figure 3.31). This mounting type prevents dynamic effects coming from the bonding of accelerometers even at high frequencies. The accelerometers are placed according to best excitation points observed in initial FE

analysis. Modal hammer of B&K 8206 model with a white plastic tip is used to excite the system. Tests are done on a soft foam to simulate free-free boundary conditions. The measurements are carried out by exciting the system with a single impact point, and the response of the structure is measured by using multiple accelerometers synchronously. In the modal tests, 15 repetitions are done at the driving point. The test setup and measurement locations of the accelerometers are shown in Figure 3.31.

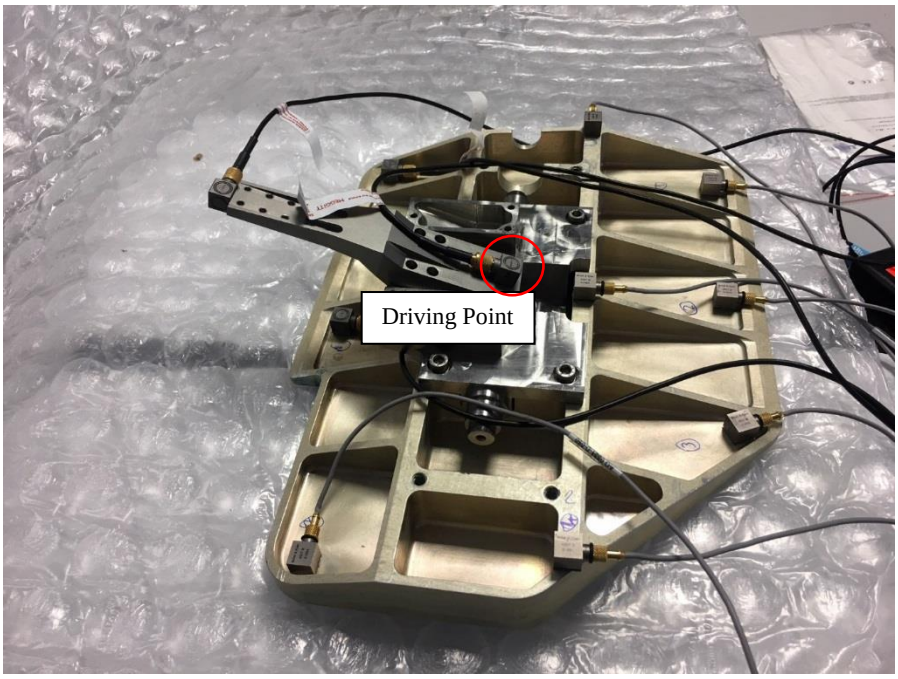

Figure 3.31. Modal Test Setup of Subassembly II

For all the measurement points, FRFs are obtained from measured forces and accelerations, and modal parameters are extracted from these functions by using LMS Test Lab software's Polymax algorithm. A typical measured direct FRF of the driving point on the slider arm part (location is shown in Figure 3.31 and direction is perpendicular to the surface), and natural frequencies and corresponding damping ratios identified are shown in Figure 3.32 and Table 3.20, respectively.

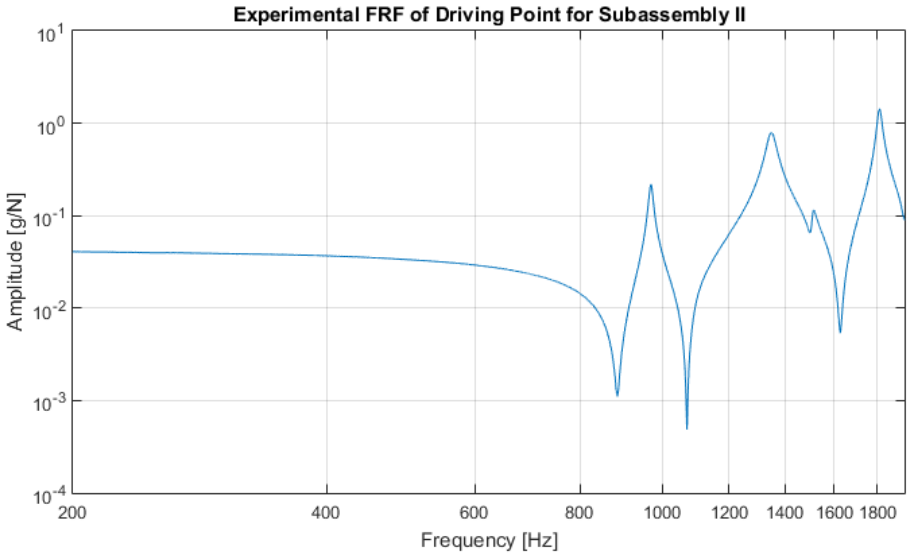

Figure 3.32. Experimental FRF of Driving Point on Subassembly II

Table 3.20 Modal Parameters of Subassembly II Obtained from Experimental Modal Analysis

Mode	Natural Frequency [Hz]	Damping Ratio [%]
1.	970.4	0.58
2.	1091.4	4.24
3.	1348.9	1.36
4.	1509.4	0.58
5.	1811.6	0.66

The FRFs obtained from the initial FE model (Figure 3.30) are compared with those measured experimentally (Figure 3.32), in Figure 3.33. Also, the natural frequencies found from initial FE model (Table 3.19) are compared with those measured experimentally (Table 3.20), in Table 3.21 and Figure 3.34. It can be observed that the FRFs are not in good agreement, and similarly the differences in natural frequencies are very high. Therefore, the FE model of Subassembly II needs to be updated according to experimental results.

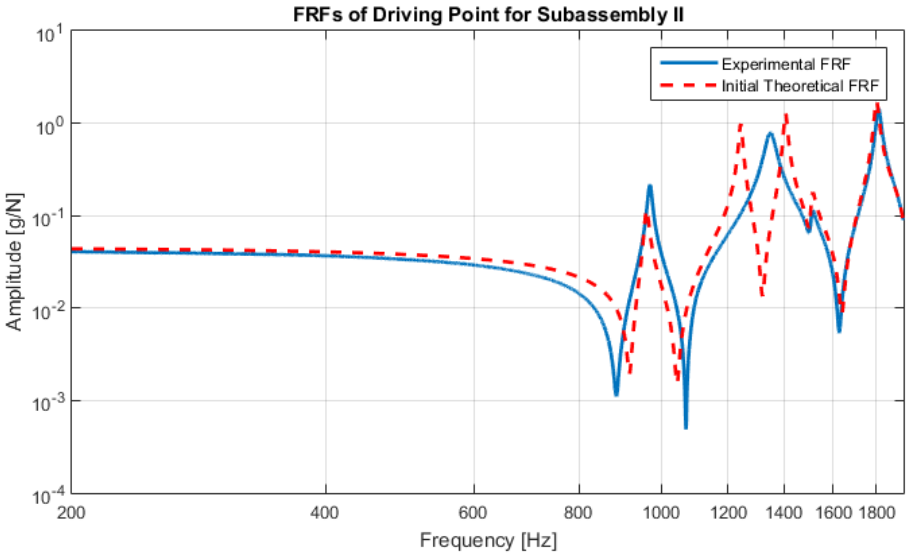

Figure 3.33. Comparison of Theoretically Calculated and Experimentally Measured FRFs of Driving Point for Subassembly II

Table 3.21 Comparison of Natural Frequencies of Subassembly II Calculated from Initial FE Model with Those Obtained from Experimental Modal Analysis

Mode	Natural Frequency (Initial FE Model) [Hz]	Natural Frequency (Experimental) [Hz]	% Error
1.	961.16	970.4	-0.95
2.	1243.7	1091.4	13.95
3.	1405.2	1348.9	4.17
4.	1510.4	1509.4	0.07
5.	1801.7	1811.6	-0.55

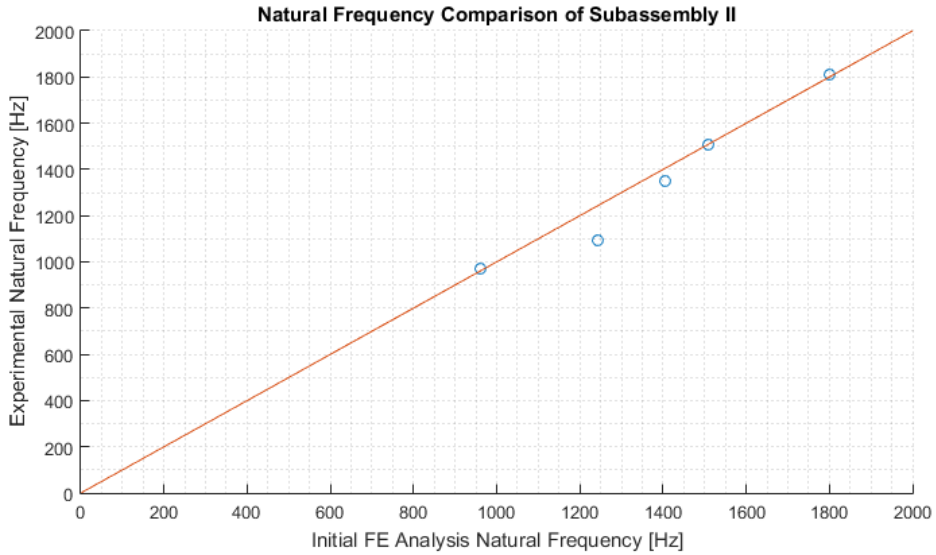

Figure 3.34. Comparison of Natural Frequencies of Subassembly II Calculated from Initial FE Model with Those Obtained from Experimental Modal Analysis

3.5.3 Updated Finite Element Model of Subassembly II

It can be observed in Table 3.21 that natural frequencies obtained from the initial FE model of Subassembly II does not match with those of the experimental model. Therefore, FE model is updated by improving joint definitions of the bolted joints between holder and slider arm parts. Joints are defined as rigidly fixed in the initial FE model, but they are redefined in updated FE model as beam-rigid to simulate the bolts used in the real model. The radii of the beams are defined identical to the real bolt radii in the real model, because this type of definition of the bolted joints in previous case gave good results. The density, modulus of elasticity and Poisson's ratio of the slider arm part are not changed. The density was already verified at initial FE modeling stage, and other material properties are not updated, since after a proper joint definition, a good correlation between FE and experimental model is obtained. The damping ratio of the slider arm part is defined according to the modal test results. The material properties (including damping ratio) of slider arm part used in the analyses are shown in Table 3.22.

Table 3.22 Material Properties of Slider Arm Part Used in Updated FE Model

Density	7850 kg/m^3
Modulus of Elasticity	200 GPa
Poisson's Ratio	0.3
Damping Ratio	0.5%

The geometry of the FE model is not changed in order not to diverge from the real structure. Since the assembly is tested in free-free conditions, the same boundary conditions are used in the FE model. The meshing of the assembly is done after these operations. The final FE model has 166432 nodes and 95752 tetrahedral elements.

The direct FRF of the driving point and natural frequencies obtained from the updated FE model of Subassembly II are given in Figure 3.35 and Table 3.23, respectively.

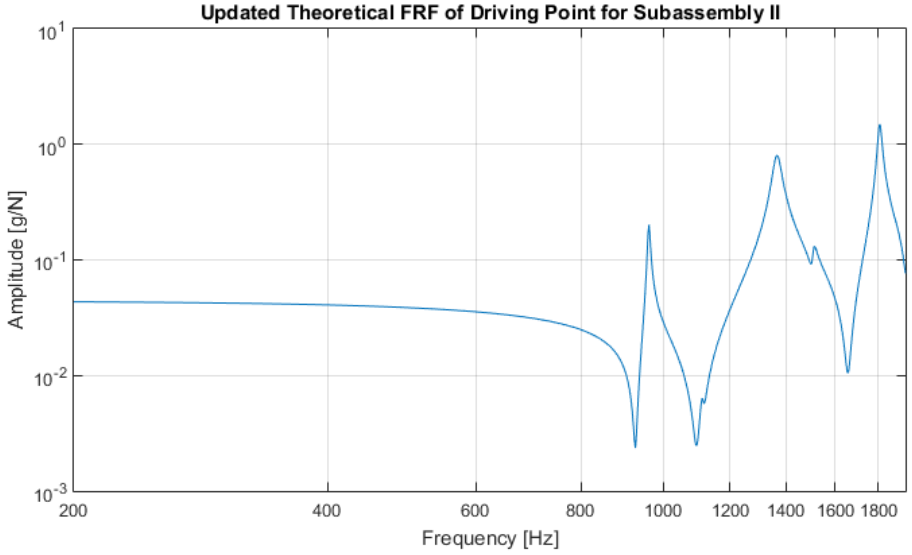

Figure 3.35. FRF of the Driving Point for Subassembly II Obtained from Updated FE Model

Table 3.23 Natural Frequencies of Subassembly II Obtained from Updated FE Model

Mode	Natural Frequency [Hz]
1.	961.91
2.	1114
3.	1365.1
4.	1508.3
5.	1807.7

The FRFs measured experimentally (Figure 3.32) are compared with those obtained from the updated FE model (Figure 3.35), in Figure 3.36. Also, the natural frequencies measured experimentally (Table 3.20) are compared with those obtained from the updated FE model (Table 3.23), in Table 3.24 and Figure 3.37. It can be observed that the FRFs are in agreement, the natural frequency results are very close to each other, and percentage errors are very low. Therefore, the model updating process of the FE model of Subassembly II is completed at this point. FRFs of the driving point, found from the initial FE model, experimentally, and from the updated FE model are compared in Figure 3.38 to see the improvement in the FE model of Subassembly II.

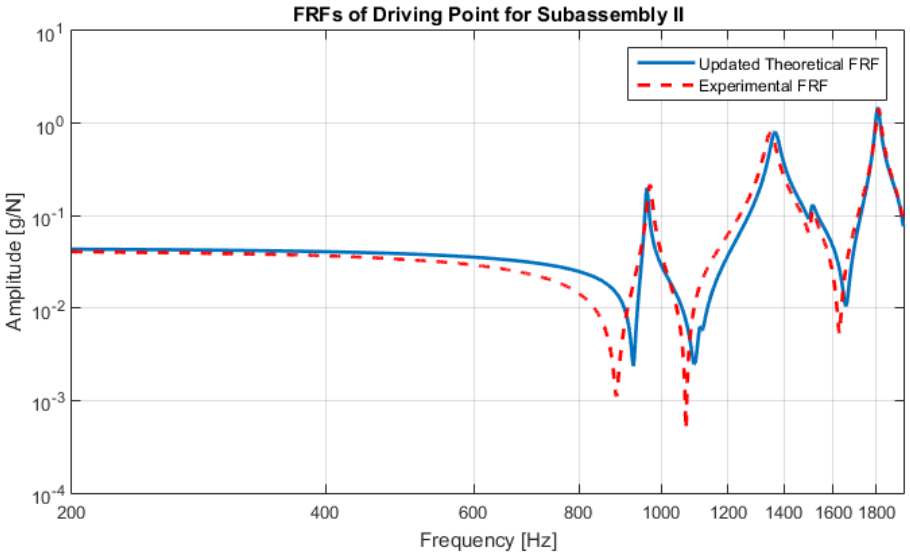

Figure 3.36. Comparison of Theoretically Calculated and Experimentally Measured FRFs of Driving Point for Subassembly II

Table 3.24 Comparison of Natural Frequencies of Subassembly II Calculated from Updated FE Model with Those Obtained from Experimental Modal Analysis

Mode	Natural Frequency (Updated FE Model) [Hz]	Natural Frequency (Experimental) [Hz]	Error (%)
1.	961.91	970.4	-0.87
2.	1114	1091.4	2.07
3.	1365.1	1348.9	1.20
4.	1508.3	1509.4	-0.07
5.	1807.7	1811.6	-0.22

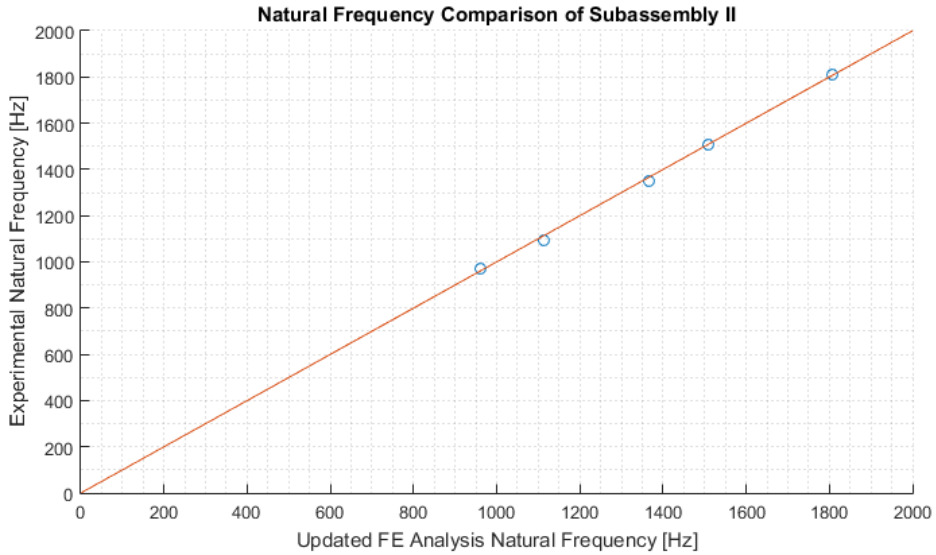

Figure 3.37. Comparison of Natural Frequencies of Subassembly II Calculated from Updated FE Model with Those Obtained from Experimental Modal Analysis

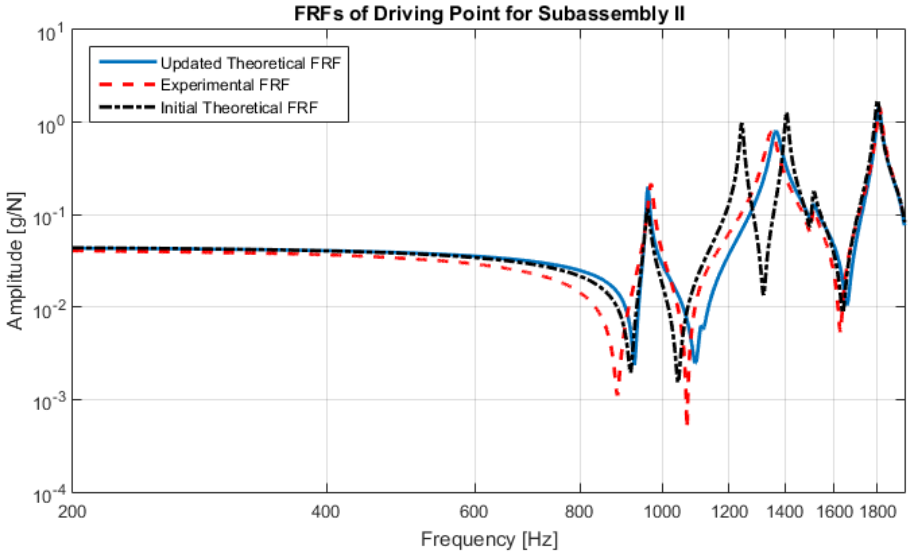

Figure 3.38. Comparison of Theoretically Calculated and Experimentally Measured FRFs of Driving Point for Subassembly II

3.6 Updating Finite Element Model of Subassembly III

Gimbal chassis and chassis side arm parts are mounted on Subassembly II, whose FE model is updated in Section 3.5, and Subassembly III is obtained. In this section, the finite element model updating of Subassembly III is explained.

3.6.1 Initial Finite Element Model of Subassembly III

Initial finite element model is created in this section. Firstly, the CAD model of Subassembly III is exported to ANSYS software. In finite element analyses, the number of nodes and element types are very important since they directly affect the solution time. For this reason, in modeling, some features like holes, rounds and chamfers, which do not affect the dynamical characteristics of the system significantly, are simplified, as in the previous cases, to increase the speed of the analyses, and to reduce the number of total DOF.

Material properties of the parts in Subassembly II are taken as the updated values found in Section 3.5. The materials of the gimbal chassis and chassis side arm are stainless steel and their material properties are defined to ANSYS Library. The densities of the two parts are verified by measuring the mass and volume of them. Modulus of elasticity and Poisson's ratio values are taken from the literature. The damping ratios of the two parts are not defined at this stage; they will be determined in model updating process according to experimental results. The material properties of the parts used in the analyses are shown in Table 3.25 and Table 3.26.

Table 3.25 Material Properties of Gimbal Chassis Part Used in Initial FE Model

Density	7550 kg/m^3
Modulus of Elasticity	200 GPa
Poisson's Ratio	0.3

Table 3.26 Material Properties of Chassis Side Arm Part Used in Initial FE Model

Density	7850 kg/m^3
Modulus of Elasticity	200 GPa
Poisson's Ratio	0.3

The masses of the accelerometers are also considered in the FE model, at the locations where they are expected to be placed, since they will be used in the modal tests, and their mass affects the modal test results.

Since the system is tested in free-free conditions, the same boundary conditions are used in the FE model. There are three bolted joints between gimbal chassis and chassis side arm parts. Initially, rigidly fixed joint model is used for these bolted joints. In addition, there exists two identical bearings between gimbal chassis and Subassembly II. The bearings are modeled with rigid joint models in all directions except rotation axes (revolute joint) in the initial FE model. The meshing of the assembly is done after these procedures. FE model has 263889 nodes and 155108 tetrahedral elements (shown in Figure 3.39).

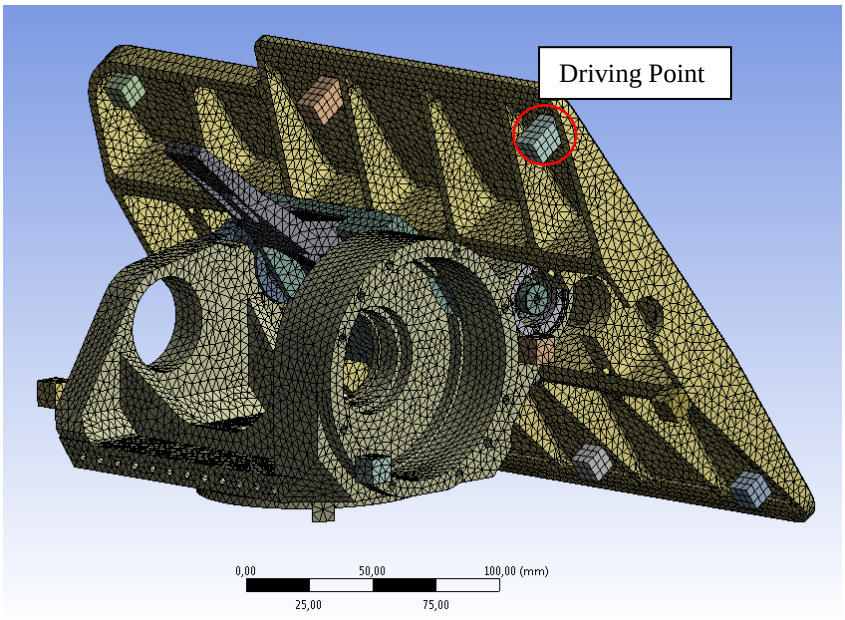

Figure 3.39. FE Model of Subassembly III Used in the Analyses

The direct FRF of the driving point (location is shown in Figure 3.39 and direction is perpendicular to the surface) and natural frequencies of Subassembly III obtained from initial FE model are shown in Figure 3.40 and Table 3.27, respectively.

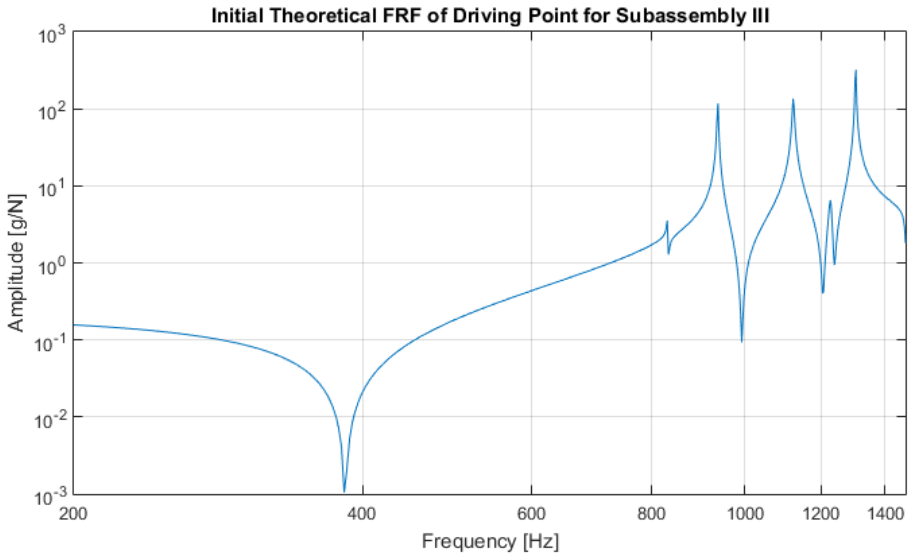

Figure 3.40. FRF of the Driving Point for Subassembly III Obtained from Initial FE Model

Table 3.27 Natural Frequencies of Subassembly III Obtained from Initial FE Model

Mode	Natural Frequency [Hz]
1.	831.09
2.	936.95
3.	1123.1
4.	1228
5.	1304
6.	1476.1
7.	1566.5

3.6.2 Modal Test of Subassembly III

For the modal tests of Subassembly III, thirteen accelerometers are used to measure vibration spectra with a dynamic range of 50g. The accelerometer models are Endevco 65-100 and Brüel&Kjaer 4507B. They are bonded by using instant adhesives (shown in Figure 3.41). This mounting type prevents dynamic effects coming from the bonding of accelerometers even at high frequencies. The accelerometers are placed according to best excitation points observed in initial FE analysis. Modal hammer of B&K 8206 model with a white plastic tip is used to excite the system. Tests are done on a soft foam to simulate free-free boundary conditions. The measurements are carried out by exciting the system at different impact points in different directions (one of them is shown in the figures), and the response of the structure is measured by using multiple accelerometers synchronously. In the modal tests, 15 repetitions are done at driving point. The test setup and measurement locations of the accelerometers are shown in Figure 3.41.

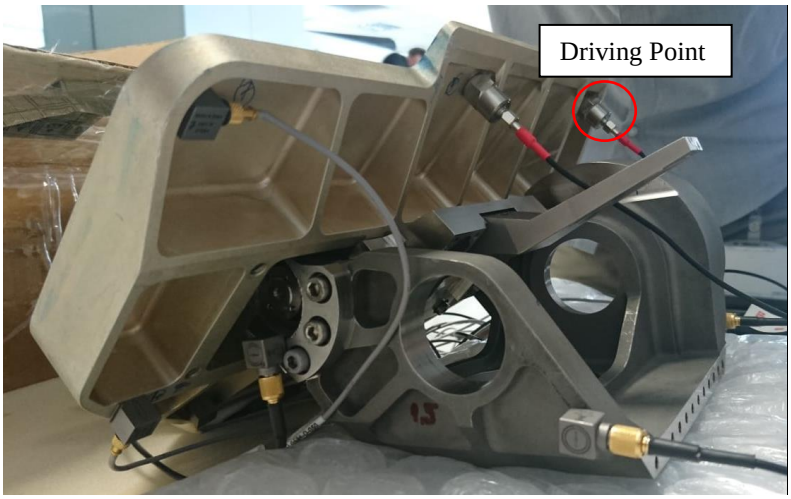

Figure 3.41. Modal Test Setup of Subassembly III

For all the measurement points, FRFs are obtained from measured forces and accelerations, and modal parameters are extracted from these functions by using LMS Test Lab software's Polymax algorithm. A typical measured direct FRF of the driving point on the optical element (location is shown in Figure 3.41 and direction is perpendicular to the surface), and natural frequencies and corresponding damping ratios identified are shown in Figure 3.42 and Table 3.28, respectively.

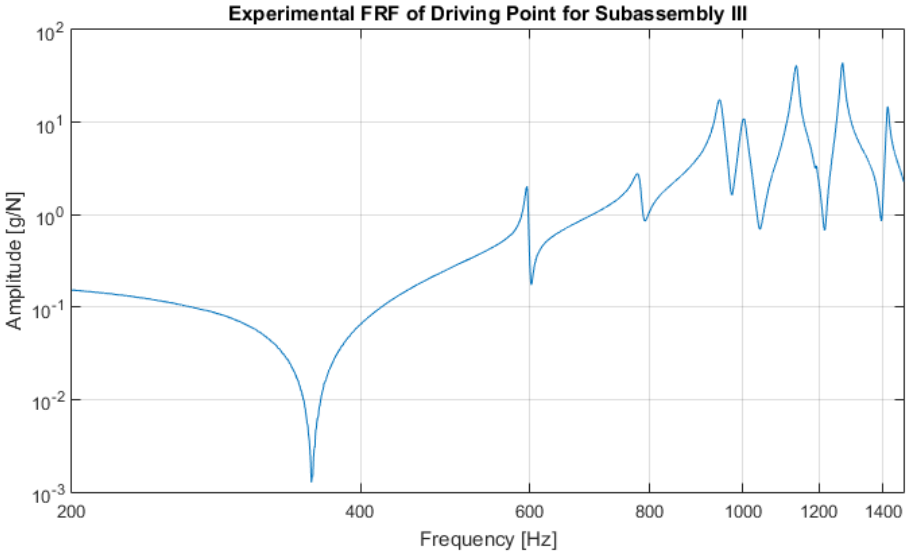

Figure 3.42. Experimental FRF of Driving Point on Subassembly III

Table 3.28 Modal Parameters of Subassembly III Obtained from Experimental Modal Analysis

Mode	Natural Frequency [Hz]	Damping Ratio [%]
1.	591.9	3.64
2.	779.8	0.77
3.	946.1	0.91
4.	1005.8	0.77
5.	1135.9	0.48
6.	1268.7	0.41
7.	1414.3	0.31

The FRFs obtained from the initial FE model (Figure 3.40) are compared with those measured experimentally (Figure 3.42), in Figure 3.43. Also, the natural frequencies found from initial FE model (Table 3.27) are compared with those measured experimentally (Table 3.28), in Table 3.29 and Figure 3.44. Mode shapes obtained from the initial FE model and experimental model are also compared in order to see whether the modes are correlated with each other or not. It can be observed that the FRFs are not in good agreement, and similarly the differences in natural frequencies are very high. Therefore, the FE model of Subassembly III needs to be updated according to experimental results.

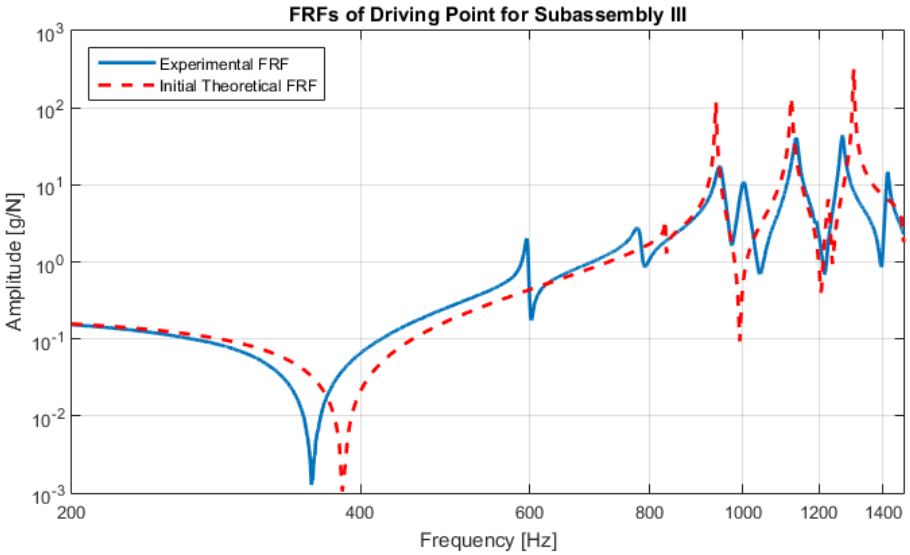

Figure 3.43. Comparison of Theoretically Calculated and Experimentally Measured FRFs of Driving Point for Subassembly III

Table 3.29 Comparison of Natural Frequencies of Subassembly III Calculated from Initial FE Model with Those Obtained from Experimental Modal Analysis

Mode	Natural Frequency (Initial FE Model) [Hz]	Natural Frequency (Experimental) [Hz]	% Error
1.	831.09	591.9	40.41
2.	936.95	779.8	20.15
3.	1123.1	946.1	18.71
4.	1228	1005.8	22.09
5.	1304	1135.9	14.80
6.	1476.1	1268.7	16.35
7.	1566.5	1414.3	10.76

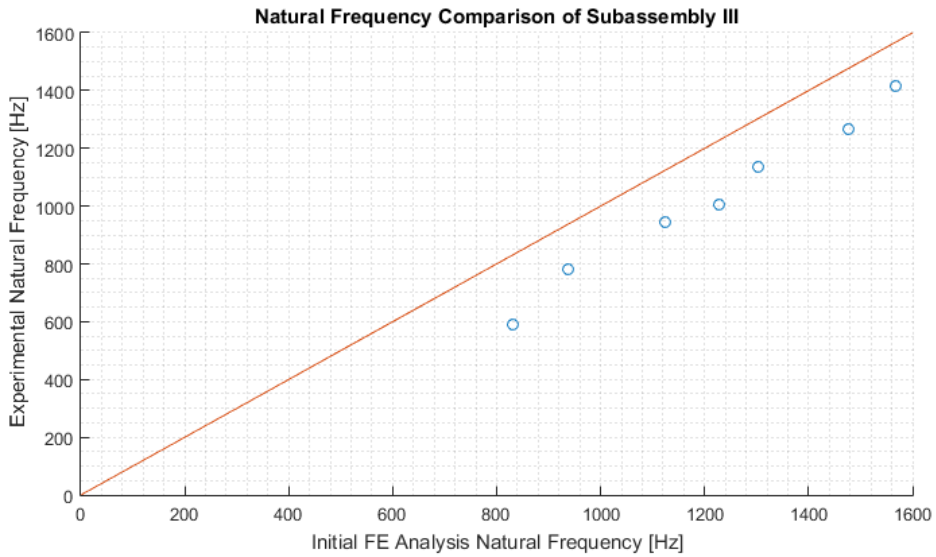

Figure 3.44. Comparison of Natural Frequencies of Subassembly III Calculated from Initial FE Model with Those Obtained from Experimental Modal Analysis

3.6.3 Updated Finite Element Model of Subassembly III

It can be observed in Table 3.29 that initial FE model of Subassembly III does not match with the experimental model. Therefore, FE model is updated by improving joint definitions of the bolted joints between gimbal chassis and chassis side arm parts, modeling of the bearings and the material properties of the gimbal chassis and chassis side arm parts. The damping ratios of the gimbal chassis and chassis side arm parts are defined according to the modal test results.

Joints are defined as rigidly fixed in the initial FE model, but they are redefined in the updated FE model as beam-rigid to simulate the bolts used in the real model. The radii of the beams are taken identical to the real bolt radii in the real model. Bearings are modelled with bushing type joint in the updated FE model, which defines matrices between selected surfaces to simulate the stiffness and damping characteristics. Stiffness values are taken from the bearing producer and defined to the stiffness matrices in the bushing type joints. The densities of the new parts are

not changed because they were already verified at the initial FE modeling stage. Young's modulus of the gimbal chassis part is updated, since it is produced by casting and has different material properties than machined steels [20]. The updated material properties of gimbal chassis and chassis side arm parts used in the analyses are shown in Table 3.30 and 3.31, respectively.

Table 3.30 Material Properties of Gimbal Chassis Part in Initial and Updated FE Models

	Initial Values	Updated Values
Density	7550 kg/m^3	7550 kg/m^3
Modulus of Elasticity	200 GPa	196 GPa
Poisson's Ratio	0.3	0.3
Damping Ratio	0%	0,6%

Table 3.31 Material Properties of Chassis Side Arm Part Used in Updated FE Model

Density	7850 kg/m^3
Modulus of Elasticity	200 GPa
Poisson's Ratio	0.3
Damping Ratio	0.5%

The geometry of the FE model is not changed in order not to diverge from the real structure. Since the assembly is tested in free-free conditions, the same boundary conditions are used in the FE model. The meshing of the assembly is done after these operations. The final FE model has 263889 nodes and 155108 tetrahedral elements.

The direct FRF of the driving point and natural frequencies obtained from the updated FE model of Subassembly III are given in Figure 3.45 and Table 3.32, respectively.

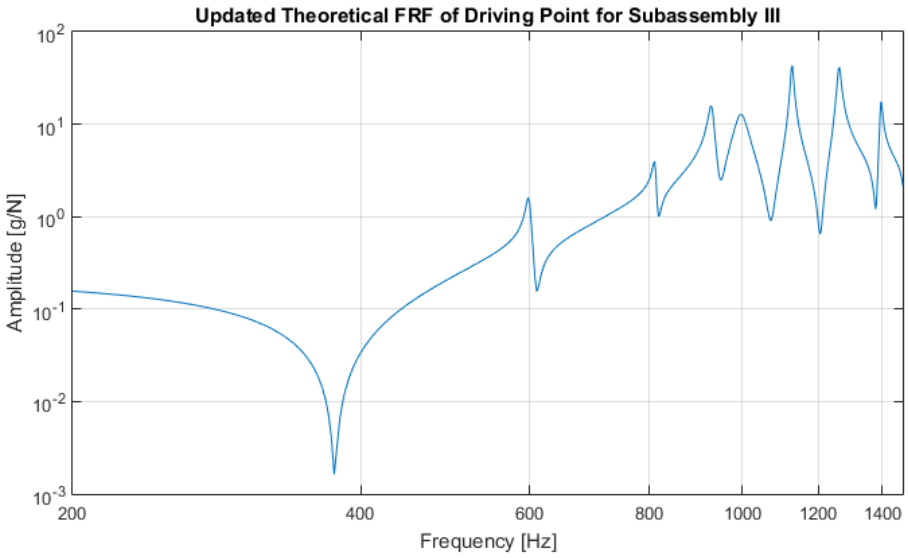

Figure 3.45. FRF of the Driving Point for Subassembly III Obtained from Updated FE Model

Table 3.32 Natural Frequencies of Subassembly III Obtained from Updated FE Model

Mode	Natural Frequency [Hz]
1.	598.91
2.	810.81
3.	928.78
4.	996.54
5.	1126.6
6.	1261.2
7.	1394.8

The FRFs measured experimentally (Figure 3.42) are compared with those obtained from the updated FE model (Figure 3.45), in Figure 3.46. Also, the natural

frequencies measured experimentally (Table 3.28) are compared with those obtained from the updated FE model (Table 3.32), in Table 3.33 and Figure 3.47. It can be observed that the FRFs are perfectly in agreement, the natural frequency results are very close to each other, and percentage errors are very low. Therefore, the model updating process of the FE model of Subassembly III is completed at this point. FRFs of the driving point, found from the initial FE model, experimentally, and from the updated FE model are compared in Figure 3.48 to see the improvement in the FE model of Subassembly III.

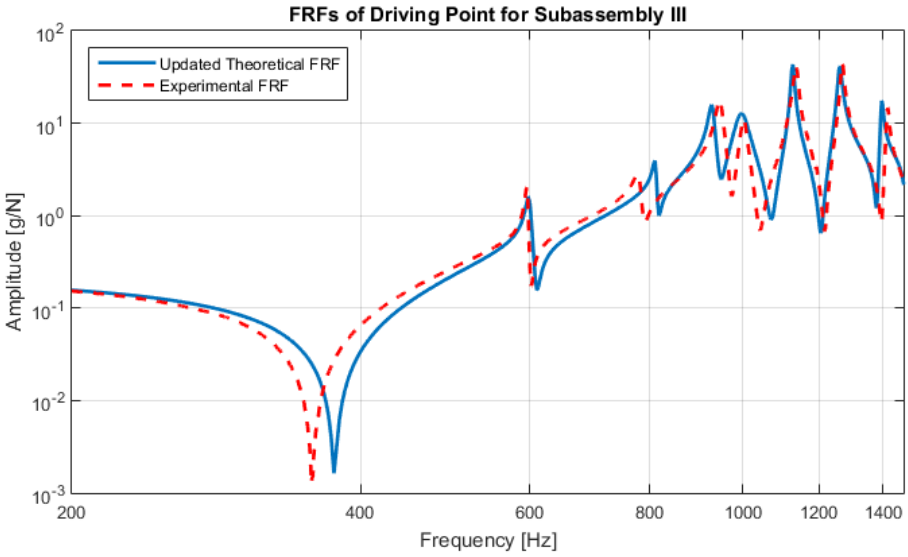

Figure 3.46. Comparison of Theoretically Calculated and Experimentally Measured FRFs of Driving Point for Subassembly III

Table 3.33 Comparison of Natural Frequencies of Subassembly III Calculated from Updated FE Model with Those Obtained from Experimental Modal Analysis

Mode	Natural Frequency (Updated FE Model) [Hz]	Natural Frequency (Experimental) [Hz]	Error (%)
1.	598.91	591.9	1.18
2.	810.81	779.8	3.98
3.	928.78	946.1	-1.83
4.	996.54	1005.8	-0.92
5.	1126.6	1135.9	-0.82

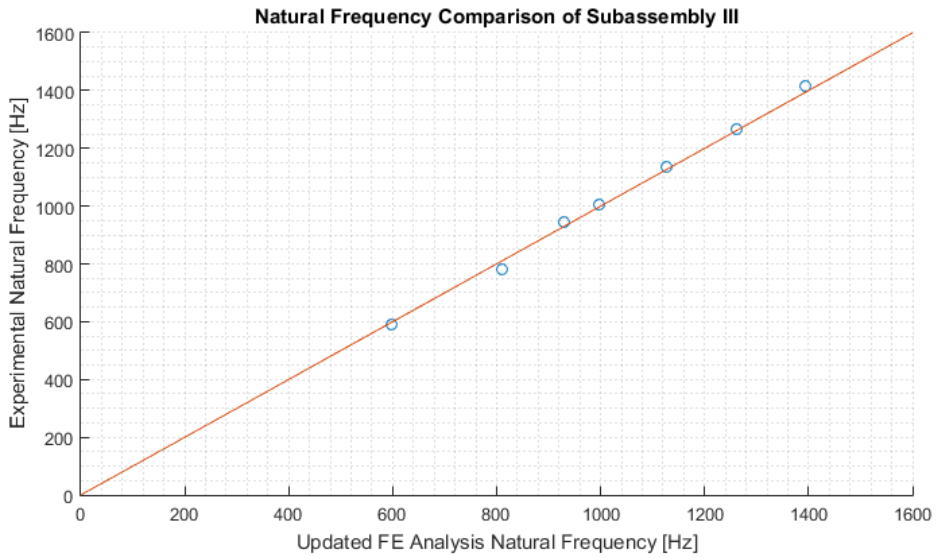

Figure 3.47. Comparison of Natural Frequencies of Subassembly III Calculated from Updated FE Model with Those Obtained from Experimental Modal Analysis

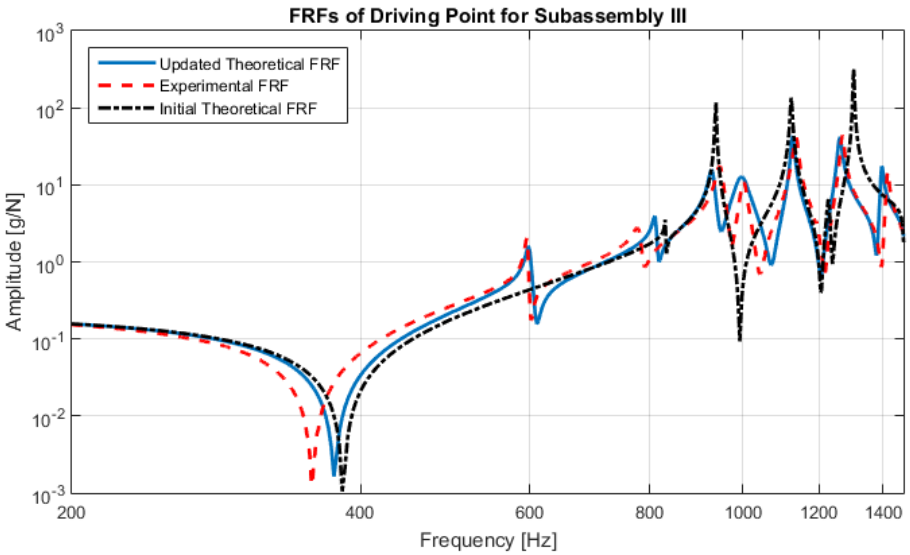

Figure 3.48. Comparison of Theoretically Calculated and Experimentally Measured FRFs of Driving Point for Subassembly III

3.7 Updating Finite Element Model of the Complete Assembly

Sensor arm and gimbal holder parts are mounted on Subassembly III, whose FE model is updated in Section 3.6, and the Complete Assembly is obtained. In this section, the finite element model updating of the Complete Assembly is explained.

3.7.1 Initial Finite Element Model of the Complete Assembly

Initial finite element model is created in this section. Firstly, the CAD model of the Complete Assembly is exported to ANSYS software. In finite element analyses, the number of nodes and element types are very important since they directly affect the solution time. For this reason, in modeling, some features like holes, rounds and chamfers, which do not affect the dynamical characteristics of the system significantly, are simplified, as in the previous cases, to increase the speed of the analyses, and to reduce the number of total DOF.

Material properties of the parts in Subassembly III are taken as the updated values found in Section 3.6. The materials of the sensor arm are stainless steel, and the material of the gimbal holder is aluminum alloy. Their material properties are defined to ANSYS Library. The densities of the parts are verified by measuring the mass and volume of them. Modulus of elasticity and Poisson's ratio values are taken from the literature. The damping ratios of the parts are not defined at this stage; they will be determined in model updating process according to experimental results. The material properties of the parts used in the analyses are shown in Table 3.34 and Table 3.35.

Table 3.34 Material Properties of Sensor Arm Parts Used in the Initial FE Model

Density	7850 kg/m^3
Modulus of Elasticity	200 GPa
Poisson's Ratio	0.3

Table 3.35 Material Properties of Gimbal Holder Part Used in the Initial FE Model

Density	2770 kg/m^3
Modulus of Elasticity	71 GPa
Poisson's Ratio	0.33

The masses of the accelerometers are also considered in the FE model, at the locations where they are expected to be placed, since they will be used in the modal tests, and their masses affect the modal test results.

Since the system is tested in free-free conditions, the same boundary conditions are used in the FE model. There are twelve bolted joints between gimbal chassis and gimbal holder parts. Initially, rigidly fixed joint model is used for these bolted joints. There exist bearings between sensor arm and Subassembly III. The bearings are modeled with rigid joint model in all directions except rotation axes (revolute joint) in the initial FE model. There is also a linear motion guide in the system between sensor arm and Subassembly III. It is modeled with a rigid joint model in all directions except its direction of motion (translational joint). The meshing of the assembly is done after these procedures. FE model has 157278 nodes and 89556 tetrahedral elements (shown in Figure 3.49).

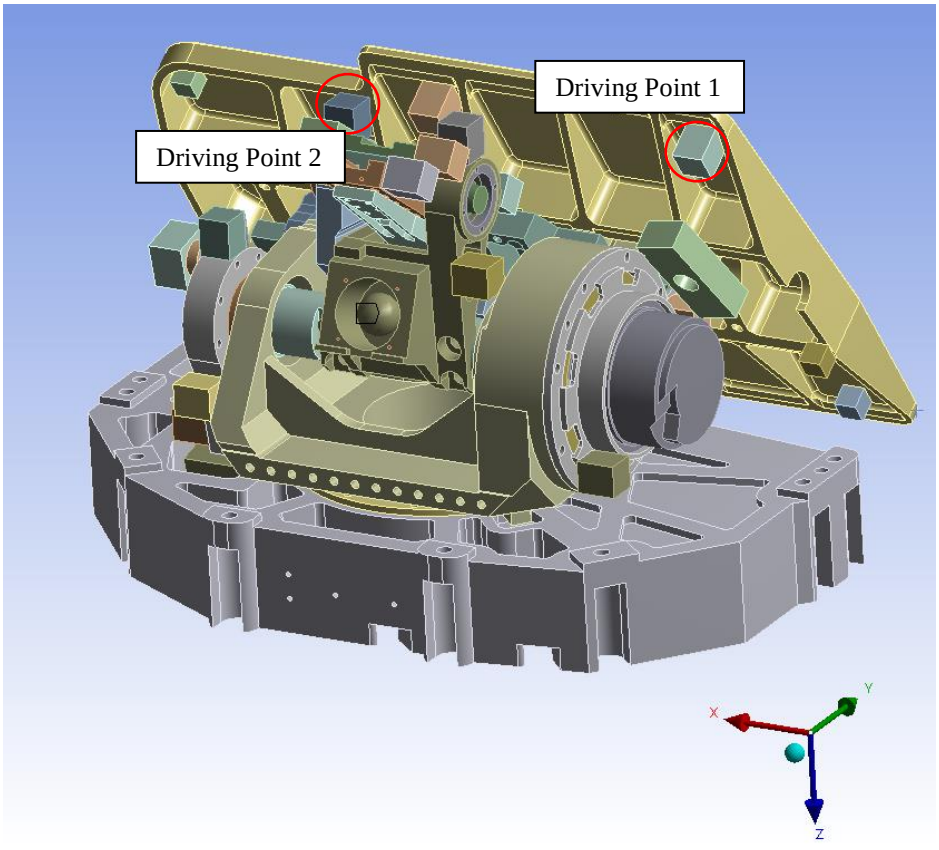

Figure 3.49. FE Model of the Complete Assembly Used in the Analyses

The direct FRF of the driving point 1 (location is shown in Figure 3.49 and direction is perpendicular to the surface) and natural frequencies of the Complete Assembly obtained from the initial FE model are shown in Figure 3.50 and Table 3.36, respectively.

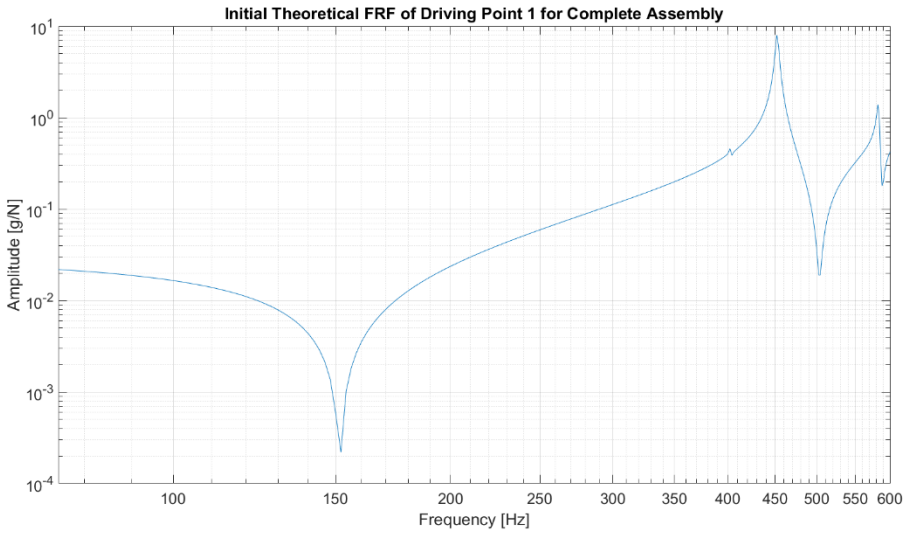

Figure 3.50. FRF Model of the Driving Point 1 for the Complete Assembly Obtained from the Initial FE Model

Table 3.36 Natural Frequencies of the Complete Assembly Obtained from Initial FE Model

Mode	Natural Frequency [Hz]
1.	402.7
2.	452.43
3.	582.98

3.7.2 Modal Test of the Complete Assembly

For the modal tests of the Complete Assembly, twenty-four accelerometers are used to measure vibration spectra with a dynamic range of 50g. The accelerometer models

are Endevco 65-100 and Brüel&Kjaer 4507B. They are bonded by using instant adhesives (shown in Figure 3.51). This mounting type prevents dynamic effects coming from the bonding of accelerometers even at high frequencies. The accelerometers are placed according to best excitation points observed in initial FE analysis. Modal hammer of B&K 8206 model with a white plastic tip is used to excite the system. Tests are done on a soft foam to simulate free-free boundary conditions. The measurements are carried out by exciting the system at different impact points in different directions (two of them are shown in the figures), and the response of the structure is measured by using multiple accelerometers synchronously. In the modal tests, 15 repetitions are done at driving point 1 and 2. The test setup and measurement locations of the accelerometers are shown in Figure 3.51.

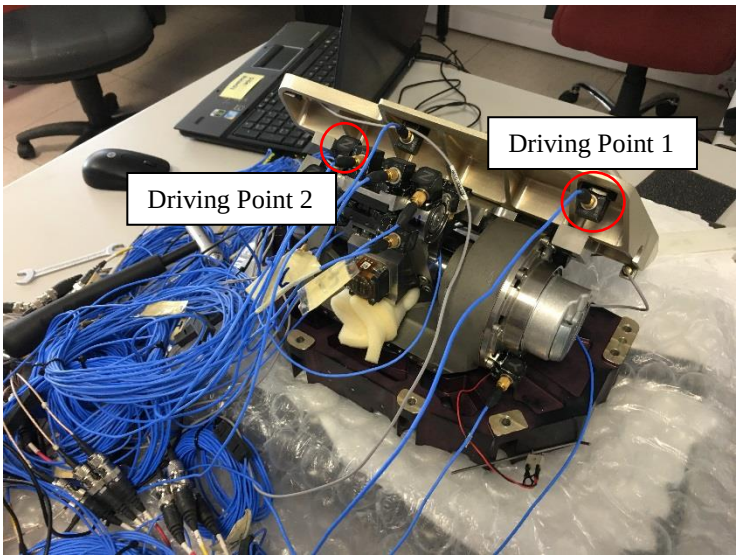

Figure 3.51. Modal Test Setup of the Complete Assembly

For all the measurement points, FRFs are obtained from measured forces and accelerations, and modal parameters are extracted from these functions by using LMS Test Lab software's Polymax algorithm. A typical measured direct FRF of the driving point 1 on the optical element (location is shown in Figure 3.51 and direction

is perpendicular to the surface), and natural frequencies and corresponding damping ratios identified are shown in Figure 3.52 and Table 3.37, respectively.

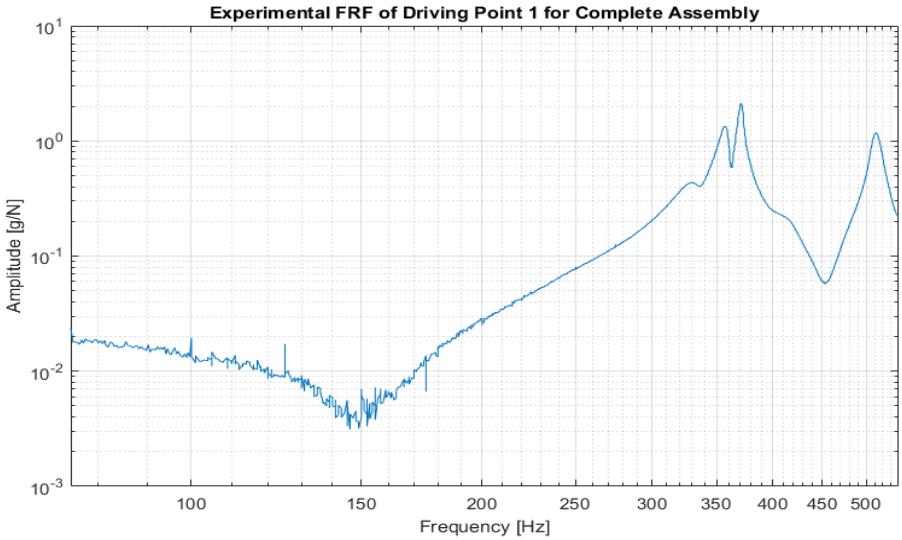

Figure 3.52. Experimental FRF of Driving Point 1 on Complete Assembly

Table 3.37 Modal Parameters of the Complete Assembly Obtained from Experimental Modal Analysis

Mode	Natural Frequency [Hz]	Damping Ratio [%]
1.	356.9	1.23
2.	370.4	0.58
3.	511.3	1.00

The FRFs obtained from the initial FE model (Figure 3.50) are compared with those measured experimentally (Figure 3.52), in Figure 3.53. Also, the natural frequencies found from initial FE model (Table 3.36) are compared with those measured experimentally (Table 3.37), in Table 3.38 and Figure 3.54. It can be observed that the FRFs are not in good agreement, and similarly the differences in natural

frequencies are very high. Therefore, the FE model of the Complete Assembly needs to be updated according to experimental results.

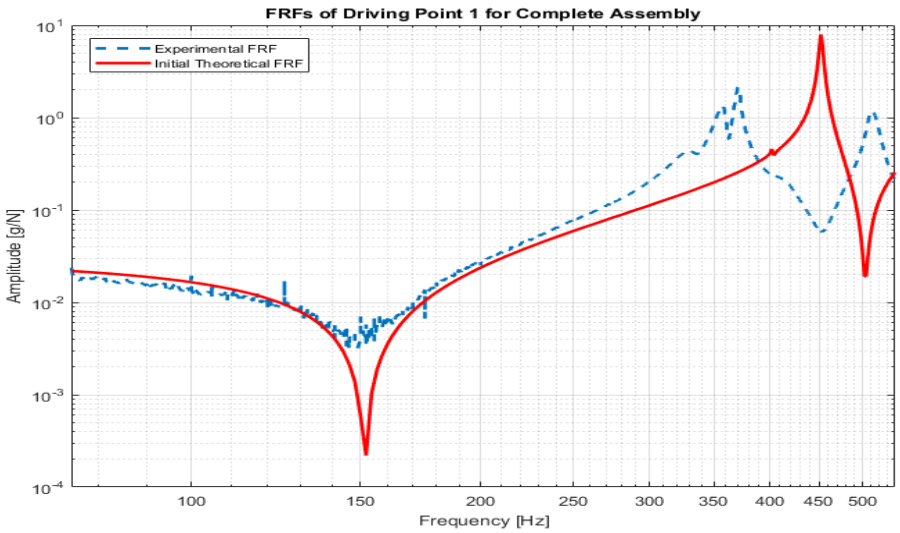

Figure 3.53. Comparison of Theoretically Calculated and Experimentally Measured FRFs of Driving Point 1 for Complete Assembly

Table 3.38 Comparison of Natural Frequencies of the Complete Assembly Calculated from Initial FE Model with Those Obtained from Experimental Modal Analysis

Mode	Natural Frequency (Initial FE Model) [Hz]	Natural Frequency (Experimental) [Hz]	% Error
1.	402.7	356.9	12.83
2.	452.43	370.4	22.15
3.	582.98	511.3	14.02

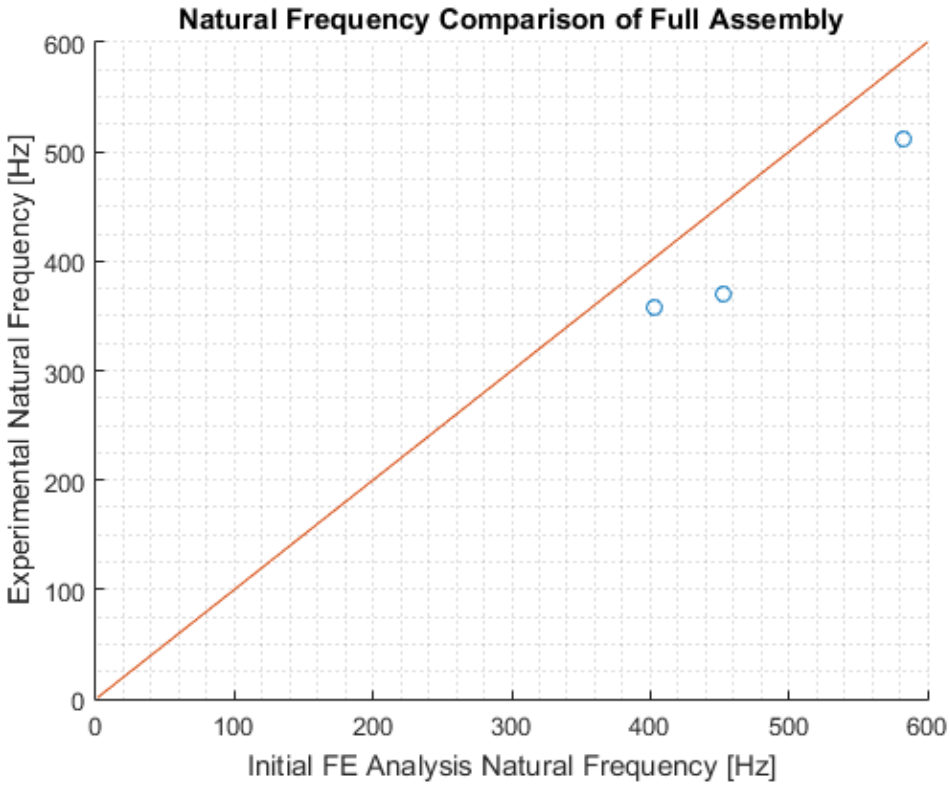

Figure 3.54. Comparison of the Natural Frequencies of the Complete Assembly Calculated from Initial FE Model with Those Obtained from the Experimental Modal Analysis

3.7.3 Updated Finite Element Model of the Complete Assembly

It can be observed in Table 3.38 that the initial FE model of the Complete Assembly does not match with the experimental model. Therefore, FE model is updated by improving modeling of the bearings and the linear motion guide and the material properties of the sensor arm and gimbal holder parts. The damping ratios of the sensor arm and gimbal holder parts are defined according to the modal test results.

Joints are defined as rigidly fixed in the initial FE model, but they are redefined in the updated FE model as beam-rigid to simulate the bolts used in the real model. The radii of the beams are defined identical to the real bolt radii in the real model.

Bearings are modelled with bushing type joints in the updated FE model, which define matrices between selected surfaces to simulate the stiffness and damping characteristics. Stiffness values are taken from the bearing producer and defined to the stiffness matrices in the bushing type joints. Modeling of the linear motion guide existing in the sensor arm is given in APPENDIX A. The densities of the new parts are not changed because they were already verified at the initial FE modeling stage. Young's modulus and Poisson's ratio values of the new parts are not changed, since after updating the joint definition, bearing and linear motion guide, a good correlation between FE and experimental model is obtained. The updated material properties of sensor arm and gimbal holder parts used in the analyses are shown in Table 3.39 and 3.40, respectively.

Table 3.39 Material Properties of Sensor Arm Parts Used in the Updated FE Model

Density	7850 kg/m^3
Modulus of Elasticity	200 GPa
Poisson's Ratio	0.3
Damping Ratio	1.0%

Table 3.40 Material Properties of Gimbal Holder Part Used in the Updated FE Model

Density	2770 kg/m^3
Modulus of Elasticity	71 GPa
Poisson's Ratio	0.33
Damping Ratio	0.6%

The geometry of the FE model is not changed in order not to diverge from the real structure. Since the assembly is tested in free-free conditions, the same boundary conditions are used in the FE model. The meshing of the assembly is done after these operations. The final FE model has 157278 nodes and 89556 tetrahedral elements.

The direct FRF of the driving point 1 and natural frequencies obtained from the updated FE model of the Complete Assembly are given in Figure 3.55 and Table 3.41, respectively.

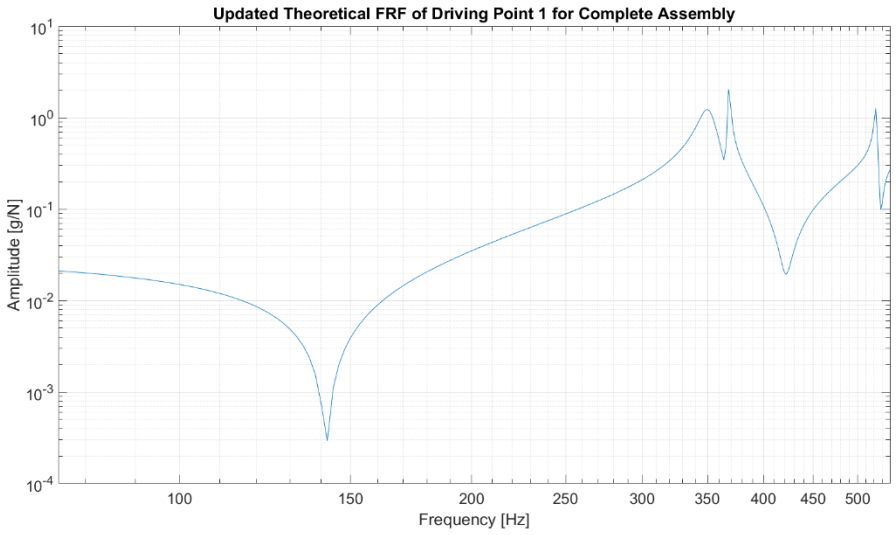

Figure 3.55. FRF of the Driving Point 1 for the Complete Assembly Obtained from the Updated FE Model

Table 3.41 Natural Frequencies of the Complete Assembly Obtained from the Updated FE Model

Mode	Natural Frequency [Hz]
1.	350.71
2.	368.41
3.	522.27

The FRFs of driving point 1 measured experimentally (Figure 3.52) are compared with those obtained from the updated FE model (Figure 3.55), in Figure 3.56. The FRFs of driving point 2 measured experimentally are also compared with those obtained from the updated FE model, in Figure 3.57. In addition, the natural frequencies measured experimentally (Table 3.37) are compared with those obtained from the updated FE model (Table 3.41), in Table 3.42 and Figure 3.58. It can be observed that the FRFs are in agreement, the natural frequency results are very close to each other, and percentage errors are very low. Therefore, the model updating process of the FE model of the Complete Assembly is completed at this point. FRFs of the driving point 1, found from the initial FE model, experimentally, and from the updated FE model are compared in Figure 3.59 to see the improvement in the FE model of the Complete Assembly.

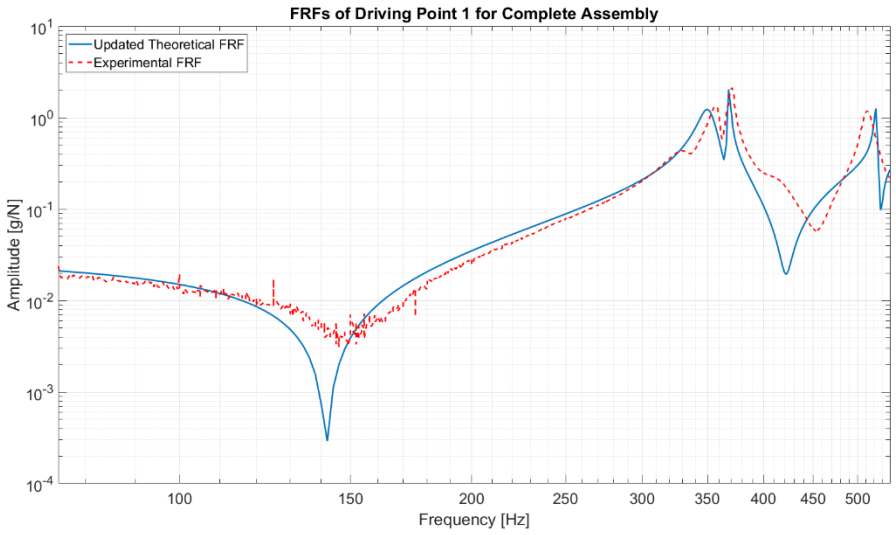

Figure 3.56. Comparison of Theoretically Calculated and Experimentally Measured FRFs of Driving Point 1 for the Complete Assembly

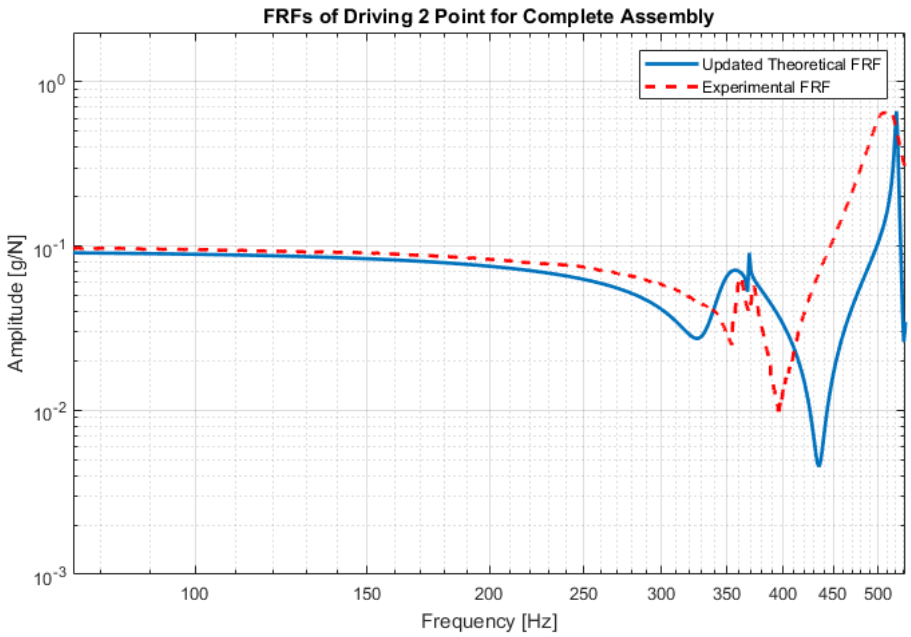

Figure 3.57. Comparison of Theoretically Calculated and Experimentally Measured FRFs of Driving Point 2 for the Complete Assembly

Table 3.42 Comparison of the Natural Frequencies of the Complete Assembly Calculated from the Updated FE Model with Those Obtained from the Experimental Modal Analysis

Mode	Natural Frequency (Updated FE Model) [Hz]	Natural Frequency (Experimental) [Hz]	Error (%)
1.	350.71	356.9	-1.73
2.	368.41	370.4	-0.54
3.	522.27	511.3	2.15

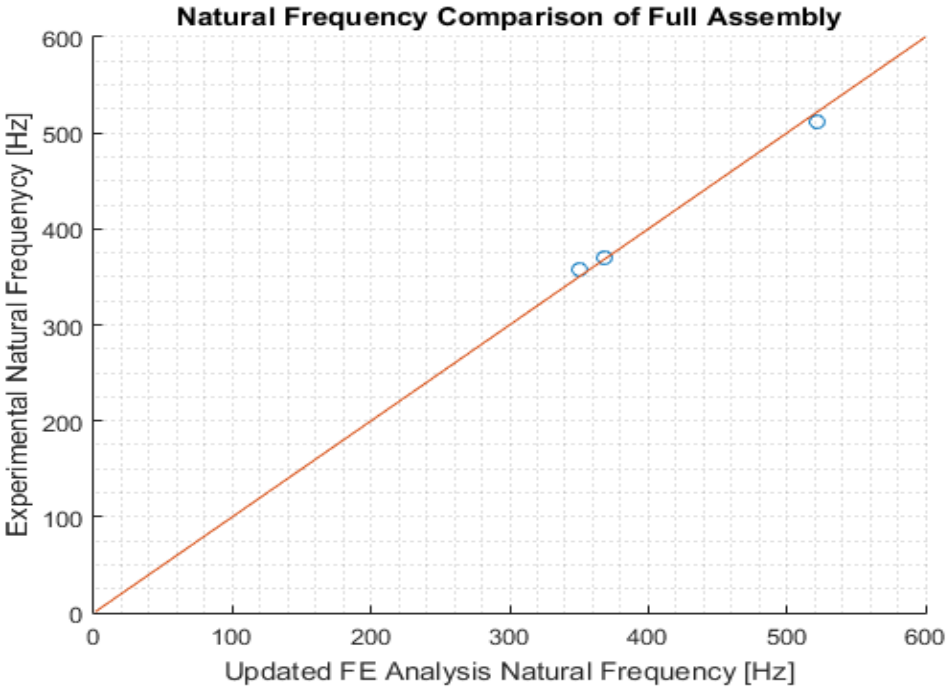

Figure 3.58. Comparison of the Natural Frequencies of the Complete Assembly Calculated from the Updated FE Model with Those Obtained from the Experimental Modal Analysis

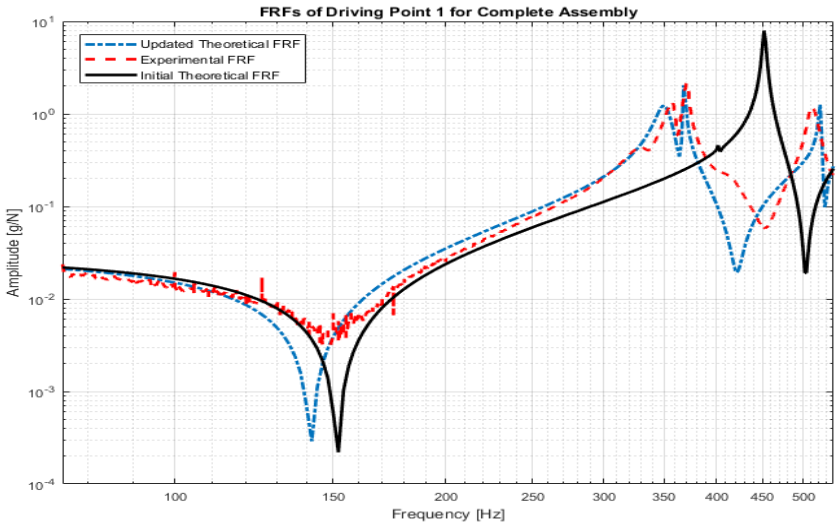

Figure 3.59. Comparison of Theoretically Calculated and Experimentally Measured FRFs of Driving Point 1 for the Complete Assembly

CHAPTER 4

DESIGN OPTIMIZATION BY USING UPDATED FINITE ELEMENT MODEL

In this chapter, structural modifications on the selected part of the optomechanical system is carried out in order to reduce the undesired vibration of the optical element. Firstly, design optimization is done on the selected part by using topology optimization method. After the optimization is completed, material of the optimized part is changed to have further improvements on the performance of the optomechanical system.

4.1 Introduction of the Optimization Procedure

In recent years, advances in technology provide engineers to create highly developed products in various fields. The engineers need to come up with optimal solutions to the problems, and make critical decisions while designing these products. Also, it is required for them to specify the best designs by using several optimization techniques, so that the cost of the production could be minimized, or the desired benefit could be maximized.

In mechanical engineering, several optimization methods are used to make the best design modifications on the parts of the electro-mechanical devices. By using suitable optimization methods, engineers can design lightweight components having maximum strength with minimum cost and effort in order to increase the overall performance of these technological devices.

In this thesis, it is required to make structural design optimization on critical parts in order to improve the image quality and performance of the optomechanical system. These modifications must shift natural frequencies of the system to avoid having resonances at frequencies where there are high excitations coming from the base vehicle. In this way, the vibration response of the optical part at these natural frequencies can be minimized.

There are several optimization methods used for structural design modifications of mechanical devices in the literature. Some of the optimization methods are described below [21]:

• Topological optimization – this method is based on mathematical techniques which determines the material distribution into a given volume. The aim of this method is to reduce the material weight and increase the rigidity of the optimized part;

• Topographical optimization – using this method, a new shape of the model is generated, which can contain the ribs and the reinforcement patterns;

• Free size optimizations – the optimized design is based on the mathematical method which generates thickness distributions of the part;

• Shape optimizations – this is an automatic geometry modification method based on the shape variable.

Since this optomechanical system has a complex design with many size, shape and mass limitations, it is not possible to increase the mass and volume of the parts freely, or change the geometry of them easily. Therefore, from the mentioned optimization techniques, topology optimization method is suitable for this study, so that the geometry of the selected parts could be modified with a given maximum mass and volume constraint in the optimization algorithm. Optimized components will have

high stiffness with minimum material usage by using this method. ANSYS Topology Optimization program is used for the optimization in this chapter.

Unlike the size and shape optimization methods, topology optimization method is used to have an optimal structural layout. The primary purpose of this method is reducing volume of the given structure and increasing the rigidity at the same time. The design domain, boundary and loading conditions of the structure must be defined before the optimization. In addition, the goal of the optimization, such as minimizing stress and weight, maximizing stiffness and natural frequency etc. is required to be specified. Once these are entered to the optimization algorithm, the conceptual optimal shape of the part will be formed according to the given design constraints. The shape of the optimized part is required to be improved to be manufacturable after the optimization is finished.

In this thesis, the procedure of the topology optimization is different from the general approach existing in literature. Since the aim of the topology optimization method is to reduce weight by determining the material distribution, the volume of the part is required to be maximized. Therefore, the design of the selected part to be optimized is improved, so that it has the maximum volume possible and suitable for the specified constraints of the optomechanical system. By this way, the initial design domain is given to the algorithm. After that, optimization region of the part is defined such that the boundary conditions and the regions which could not be changed are excluded from the design domain. In addition, objective function of the optimization, maximizing of the selected natural frequency in this case, is specified. Moreover, mass constraint is entered to the algorithm such that percentage of the mass of the part to be retained at the end of the process is defined. In this study, various percentage values are tried on the optimized part to see the effect on the optomechanical system.

At the end of each run, the design of the optimized part is improved to be manufacturable, and FE analysis results of the complete optomechanical system with the optimized part are analyzed to compare the natural frequency results and vibration response of the optical element, with those of the original system. Flowchart of the optimization procedure is presented in Figure 4.1.

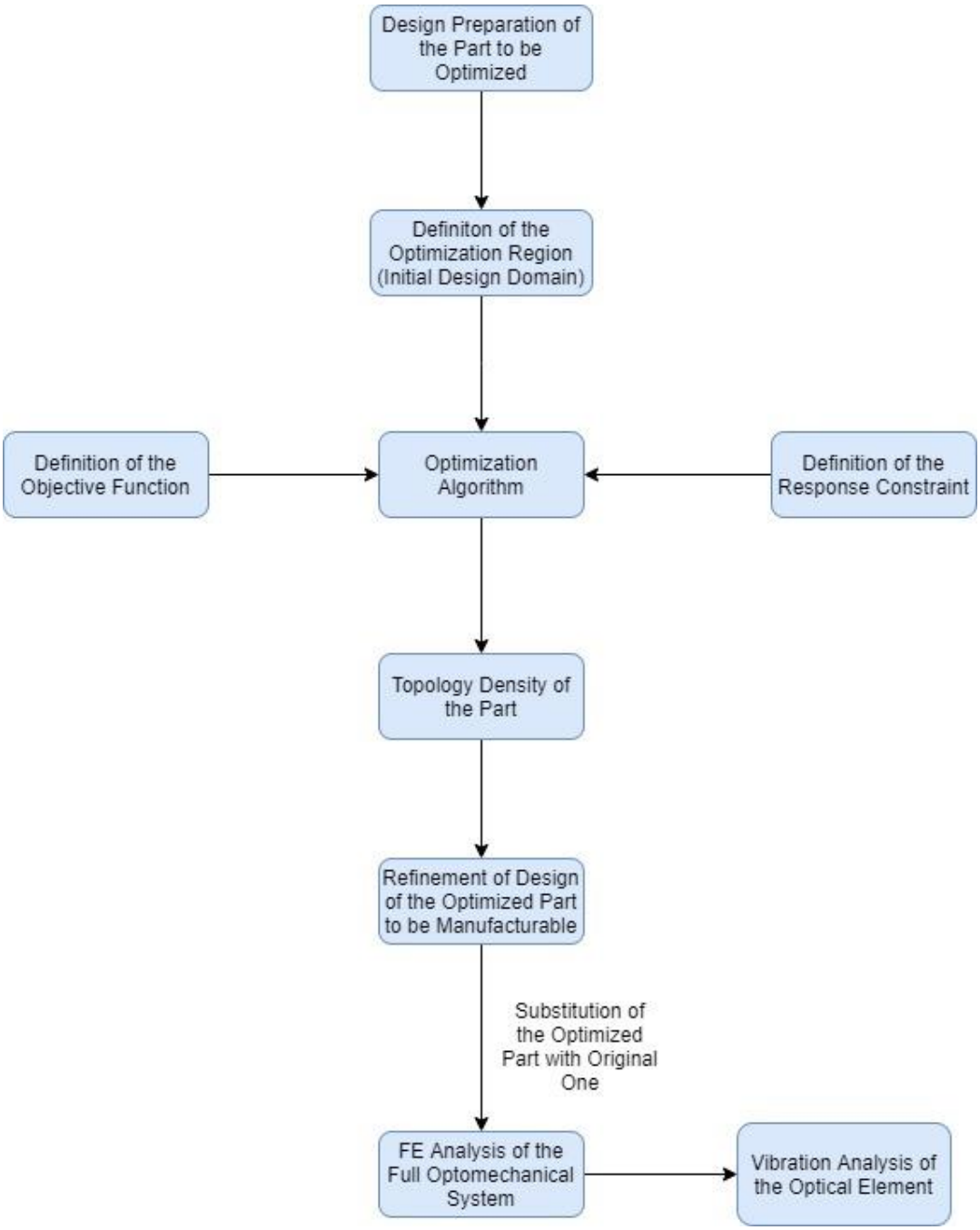

Figure 4.1. Flowchart of the Design Optimization Procedure Followed in this Thesis

4.2 Design Optimization of the Gimbal Holder Part

Optomechanical system used in this thesis has a unique mechanism to position and stabilize the optical element. The parts in this mechanism have very complex designs which could not be altered and optimized easily due to the nature of their configuration. For this reason, studies are started with the gimbal holder part, which is not involved in this moving mechanism. It has a critical role in the system, since it connects the stabilized gimbal mechanism to the housing of the optomechanical system and transfers the excitation generated by the base vehicle to the optical element. In addition, it is possible to change the geometry of this part easily to have a larger volume with a small number of constraints.

By optimizing the design of the gimbal holder part, which has a high importance in the system, it is aimed to increase the natural frequencies of the complete optomechanical system, so that the resonances of the system will be separated from the high excitation regions in the frequency spectrum. In addition, the gimbal holder part's deflection under any environmental load, including vibration, directly affects the image performance of the optical element, since it carries the stabilized mechanism, and transfers the excitation coming from the base vehicle to the optical element.

Firstly, the initial design of the gimbal holder part (3.5 kg), shown in Figure 4.2, is arranged such that all the unnecessary gaps, holes and features, which are created to reduce the unnecessary weights, are removed, but the boundary conditions, which provide connections of the other parts with the gimbal holder, are preserved. In addition, the part's volume is enlarged to its maximum limit according to the design constraints to define the design domain to the optimization program. The design domain of the gimbal holder part is shown in Figure 4.3. The increase in the mass of the part is 2.2 kg.

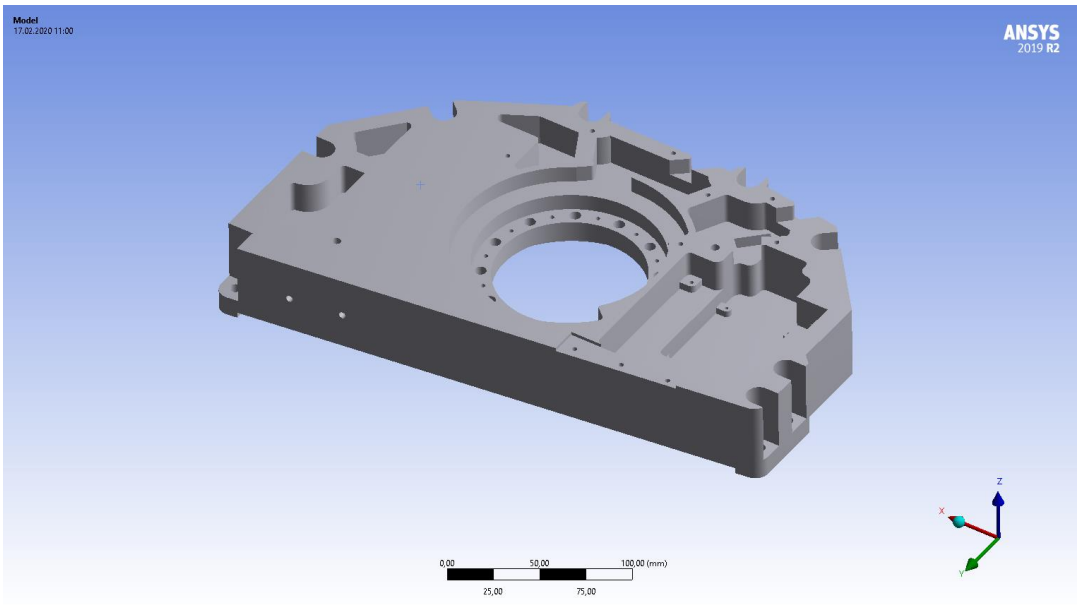

Figure 4.2. Initial Design of the Gimbal Holder Part

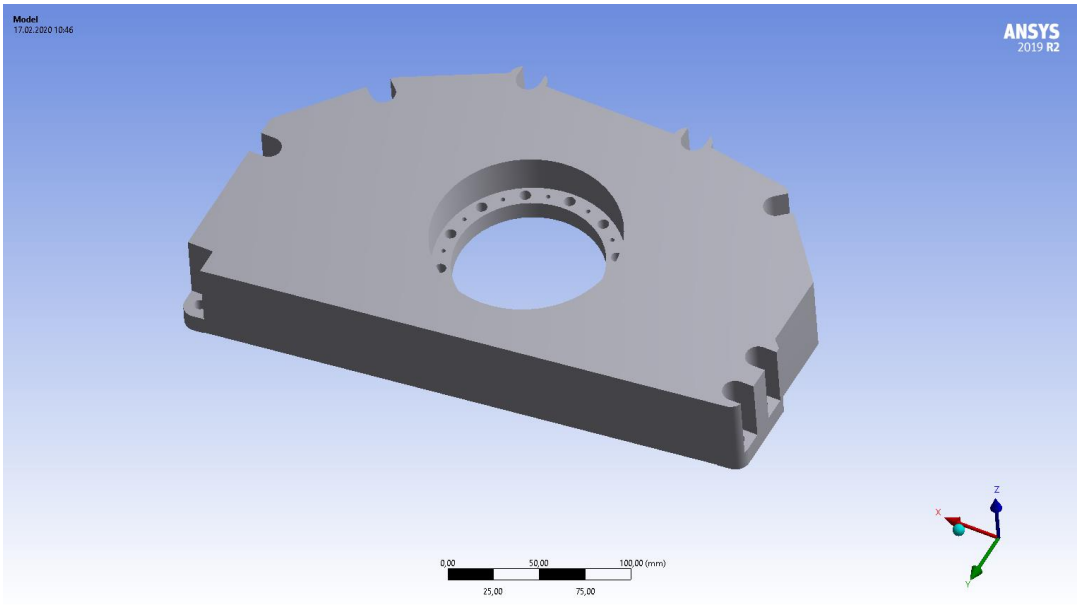

Figure 4.3. Design Domain of the Gimbal Holder Part before Optimization

The excluded regions of the part are selected and defined to the optimization program, so that these regions will not be affected from the topology optimization. Excluded regions of the gimbal holder part are shown in Figure 4.4.

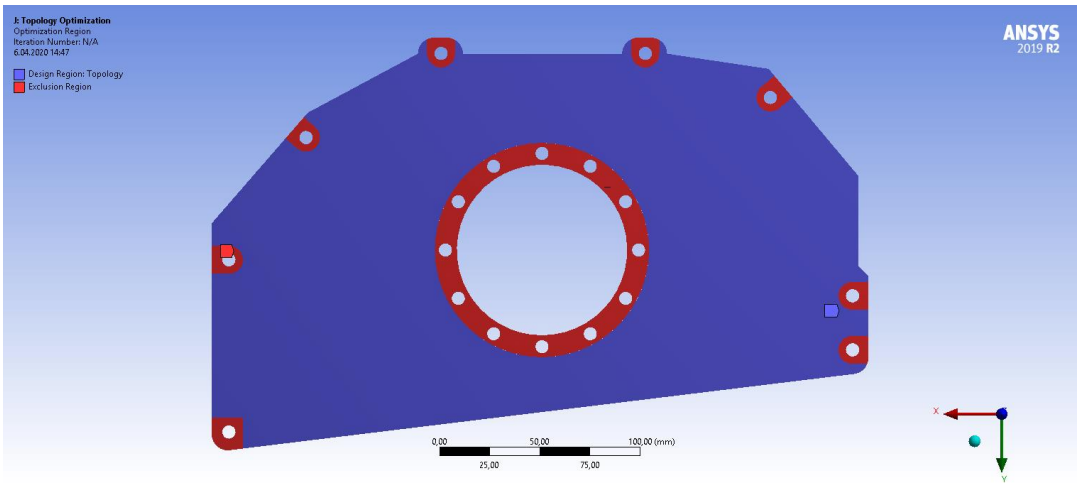

Figure 4.4. Excluded Regions of the Part

Objective function is defined to maximize the first six natural frequency of the gimbal holder part. In addition, mass constraint of the optimization program is arranged to retain the 60% and 80% of the mass in the first and second optimizations, respectively. Optimizations are carried out, and topology density results of the optimized part in the first (3.7 kg) and second (4.7 kg) optimizations are shown in Figure 4.5 and Figure 4.6, respectively. These structural layouts are conceptual shapes, and required to be improved, so that they can be manufactured. Final versions of the optimized part in the first (4.5 kg) and second (5.2 kg) optimizations are shown in Figure 4.7 and Figure 4.8, respectively.

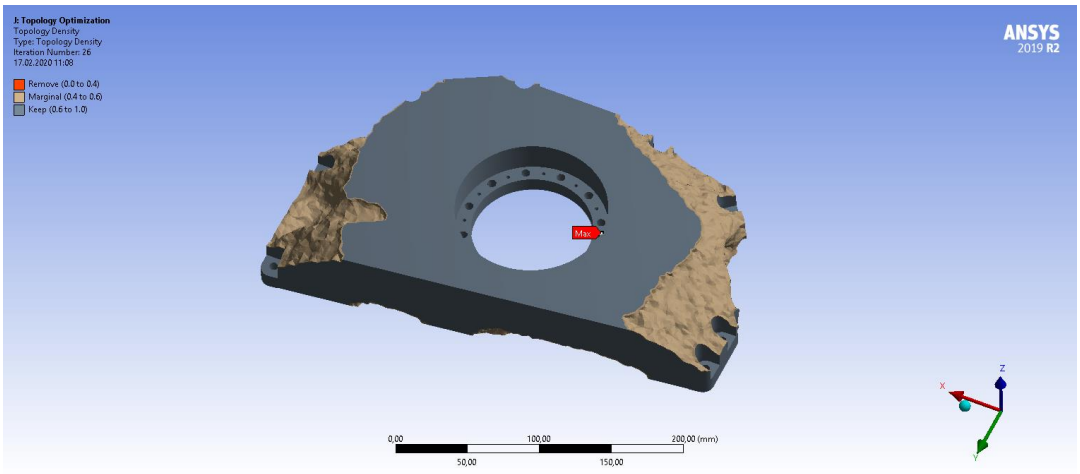

Figure 4.5. Topology Density Result in the 1st Optimization

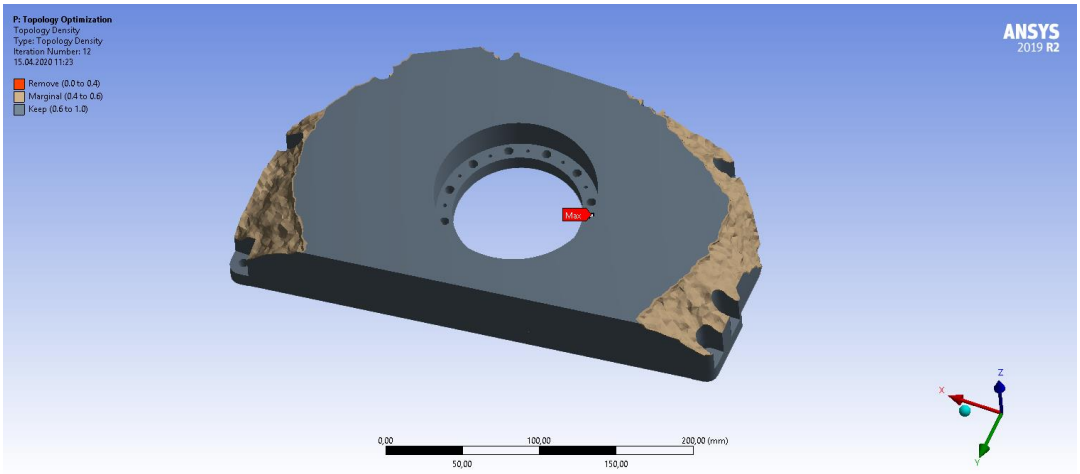

Figure 4.6. Topology Density Result in the 2nd Optimization

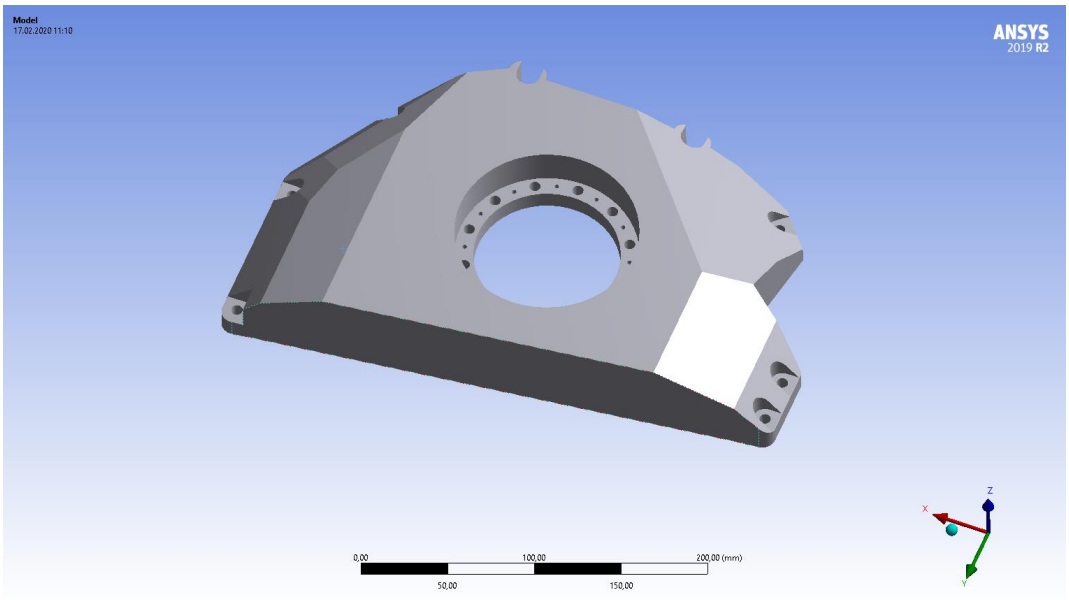

Figure 4.7. Final Optimized Design of the Gimbal Holder Part in the 1st Optimization

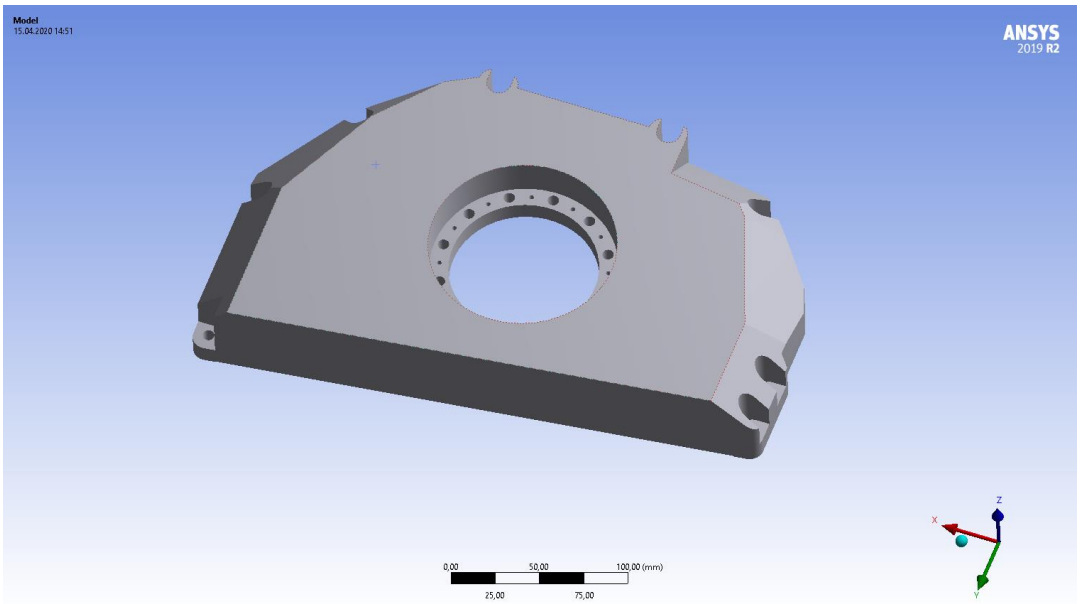

Figure 4.8. Final Optimized Design of the Gimbal Holder Part in the 2nd Optimization

After the optimizations, the updated FE model of the optomechanical system is re-arranged to perform analyses, and to see the effects of the optimized part on the

optomechanical system. All accelerometer models used in model updating procedure in Chapter 3 are removed from the FE model. In addition, fixed boundary condition is given to the model from the mounting locations used in the real system. In the analyses, the optimized part is substituted with the original one in the updated FE model. The objective of these analyses is to investigate the change in natural frequencies of the system, and observe the reduction in the vibration response of the optical element in the optomechanical system.

In order to investigate the dynamic behavior of the optical element when optimized part is used, harmonic analyses with the optimized part are carried out. Unit acceleration is given to the system from the fixed boundary conditions in 0 Hz – 600 Hz frequency range. These analyses are practiced in two directions; Y and Z separately to analyze the vibration response of the optical element, since these are the directions in which the system is affected due to high excitation coming from the base vehicle.

Optimized gimbal holder part with different mass constraints are replaced with the original one in the updated FE model of the complete optomechanical system. Firstly, modal analyses are carried out, and the natural frequencies obtained after the first and second optimizations are compared in Table 4.1 and Table 4.2, respectively. The analyses are also performed by using the design domain of the gimbal holder part before optimization, and natural frequency comparison is shown in Table 4.3.

Table 4.1 Natural Frequency Comparison of the Optomechanical System after 1st Optimization

Mode	Natural Frequency (Original Design) [Hz]	Natural Frequency (Optimized Gimbal Holder Part - First Optimization) [Hz]	Improvement (%)
1.	301.51	327.08	8.48
2.	320.22	336.76	5.17
3.	346.7	348.24	0.44
4.	402.76	454.74	12.91
5.	472.37	499.02	5.64
6.	509.77	553.88	8.65

Table 4.2 Natural Frequency Comparison of the Optomechanical System after 2nd Optimization

Mode	Natural Frequency (Original Design) [Hz]	Natural Frequency (Optimized Gimbal Holder Part - Second Optimization) [Hz]	Improvement (%)
1.	301.51	328.14	8.83
2.	320.22	337.57	5.42
3.	346.7	348.29	0.46
4.	402.76	459.23	14.02
5.	472.37	500.99	6.06
6.	509.77	556.52	9.17

Table 4.3 Natural Frequency Comparison of the Optomechanical System with Design Domain of Gimbal Holder

Mode	Natural Frequency (Original Design) [Hz]	Natural Frequency (Design Domain of Gimbal Holder) [Hz]	Improvement (%)
1.	301.51	328.37	8.91
2.	320.22	337.68	5.45
3.	346.7	348.3	0.46
4.	402.76	460.01	14.21
5.	472.37	501.37	6.14
6.	509.77	556.96	9.26

Natural frequency results, shown in Table 4.1 and Table 4.2, are very similar to each other in two cases, although different mass constraints are used for gimbal holder part in topology optimization. In addition, optimization of the gimbal holder part increased the natural frequencies up to 13% in both cases. Consequently, with 1 kg increase in mass of the gimbal holder part, natural frequencies of the complete optomechanical system are improved considerably by using topology optimization method. Normally, this much increase in the natural frequencies could be obtained with approximately 2.2 kg increase in mass without using any optimization method.

Reduction in the vibration response of the optical element is another important parameter affecting the performance of the optomechanical system, and is required to be investigated. Therefore, harmonic analyses are conducted to analyze the vibration response on the surface of the optical element in two directions. Comparisons of the displacement values in 0 Hz – 600 Hz frequency range are shown in Figure 4.9 and Figure 4.10.

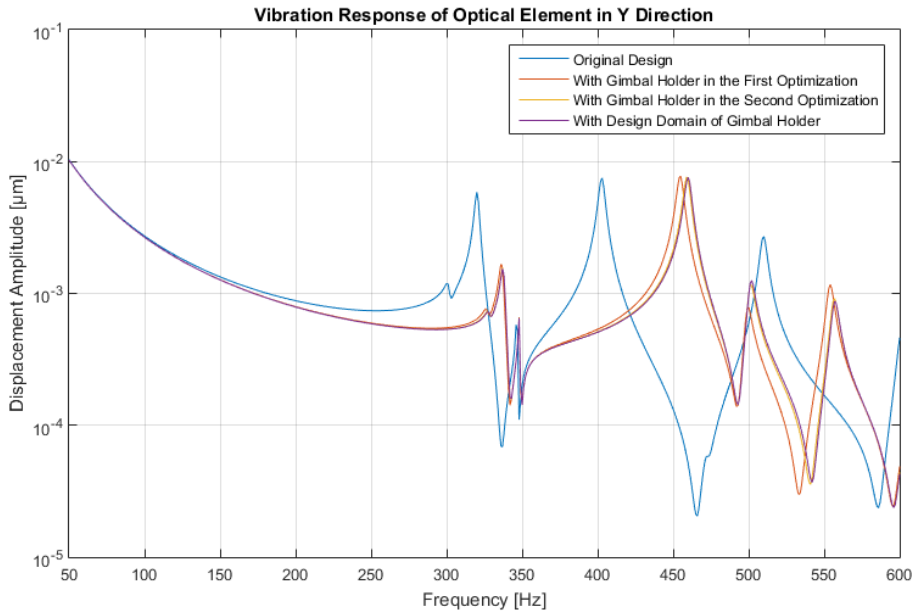

Figure 4.9. Vibration Response Comparison of Optical Element with Different Gimbal Holder Parts in Y Direction

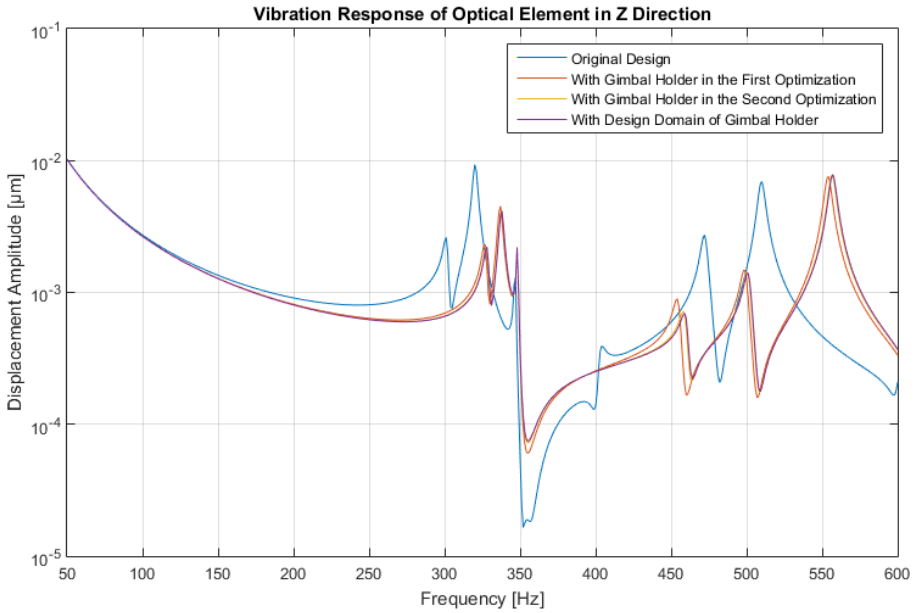

Figure 4.10. Vibration Response Comparison of Optical Element with Different Gimbal Holder Parts in Z Direction

The vibration of the optical element near the resonant frequencies of the complete optomechanical system, regardless of the mode shape, is an important problem for the optomechanical system. In Figure 4.9 and Figure 4.10, vibration response comparisons of the optical element in Y and Z directions show that optimization of the gimbal holder part by using topology optimization method reduced the vibration of the optical element effectively. Decrease in displacement amplitude is approximately 75% in Y direction and 50% in Z direction in the frequency range of 300-350 Hz with just 1 kg increase in the mass of the assembly (which corresponds to 7% increase in the total mass). A similar improvement could be achieved with 2.2 kg increase in mass without using any optimization method.

4.3 Material Change in the Gimbal Holder Part to Increase the Performance of the Optomechanical System

In Section 4.2, design optimization on the gimbal holder is done to increase the strength of the part. By using Topology Optimization method, convincing results are obtained in the analyses, and vibration response of the optical element is reduced. In this section, material of the part is changed to have further improvements on the performance of the optomechanical system by increasing strength and damping characteristics of the part at the same time.

Conventional monolithic materials (aluminum in this case) have limitations as a course of their nature. For this reason, composite materials are finding increasing use in many areas to meet the demands. Although composites have promising properties, machining of these materials is difficult, since conventional machining processes result in damage in both anisotropic and non-homogeneous structure of the composite material and cutting tool.

A specific type of metal matrix composite (MMC) is used in this thesis for the gimbal holder part, because MMCs have improved properties including high Young's modulus, damping ratio and low density. Also, these materials are more suitable for machining processes. MMCs combine the useful properties of the constituent materials to create superior structures. Although MMCs have excellent material properties, they have some disadvantages like higher cost, complex production methods and relatively immature technology.

MMCs are composed of at least two components; a metal having lower density (aluminum, magnesium, copper and titanium) and a reinforcing material (metal, ceramic or an organic compound). Metal creates the matrix and reinforcement is

embedded in this continuous structure. The reinforcement can be either continuous (embedded fibers or monofilament wires) and discontinuous (stirred reinforcement powder material). This difference affects the machining process of the material effectively. MMCs made by discontinuous reinforcing materials could be isotropic, and conventional machining techniques are applicable under appropriate conditions. MMCs are most widely used composite materials in the industrial scale, and these advantages extend the usage of MMCs further in various applications.

In this thesis, SiC particle reinforced aluminum matrix composite is used for the gimbal holder part in the analyses. "Aluminum-based MMCs are the most commonly used MMC in the automotive and aerospace applications. This is mainly due to its unique properties like greater strength, improved stiffness, reduced density, improved temperature properties, controlled thermal expansion and improved wear resistance." [22]

SiC particle reinforced aluminum matrix composites have continuous aluminum/aluminum alloy matrix, and SiC particle discontinuous reinforcements are embedded into the matrix. This type of MMC has isotropic mechanical properties so that conventional machining techniques could be applicable. Also, it has low-cost machining processes, and can be obtained for low prices.

Density, modulus of elasticity and Poisson's ratio values of the SiC particle reinforced aluminum matrix composite taken from [23] are given in Table 4.4.

Table 4.4 Material Properties of SiC Particle Reinforced Aluminum Matrix Composite Used in the Analyses

Density	2900 kg/m^3
Modulus of Elasticity	140 GPa
Poisson's Ratio	0.3
Damping Ratio	0.6%

The material properties of the optimized part in the first optimization are changed according to the values given in Table 4.4 in the FE model. The mass of the part reached to 5 kg with 0.5 kg increase. Modal analyses and harmonic analyses are repeated with the same configurations in Section 4.2 in order to see the effect of the material change on the natural frequencies of the system and vibration response of the optical element. Comparisons of the natural frequencies and the vibration response amplitudes of the optical element in Y and Z direction is given in Table 4.5, Figure 4.11 and Figure 4.12, respectively.

Table 4.5 Natural Frequency Comparison of the Optomechanical System by Using the Optimized Gimbal Holder Part in the First Optimization with MMC Material

Mode	Natural Frequency (Original Design) [Hz]	Natural Frequency (Optimized Gimbal Holder Part - First Optimization with MMC) [Hz]	Improvement (%)
1.	301.51	334.59	10.97
2.	320.22	344.56	7.60
3.	346.7	348.93	0.64
4.	402.76	482.85	19.89
5.	472.37	520.72	10.24
6.	509.77	577.23	13.23

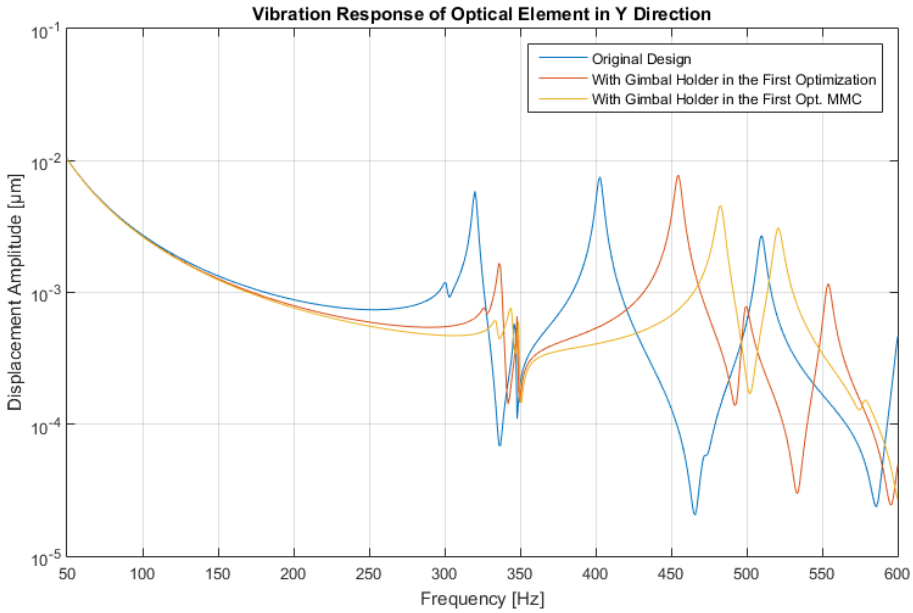

Figure 4.11. Vibration Response Comparison of Optical Element with Different Gimbal Holder Parts in Y Direction

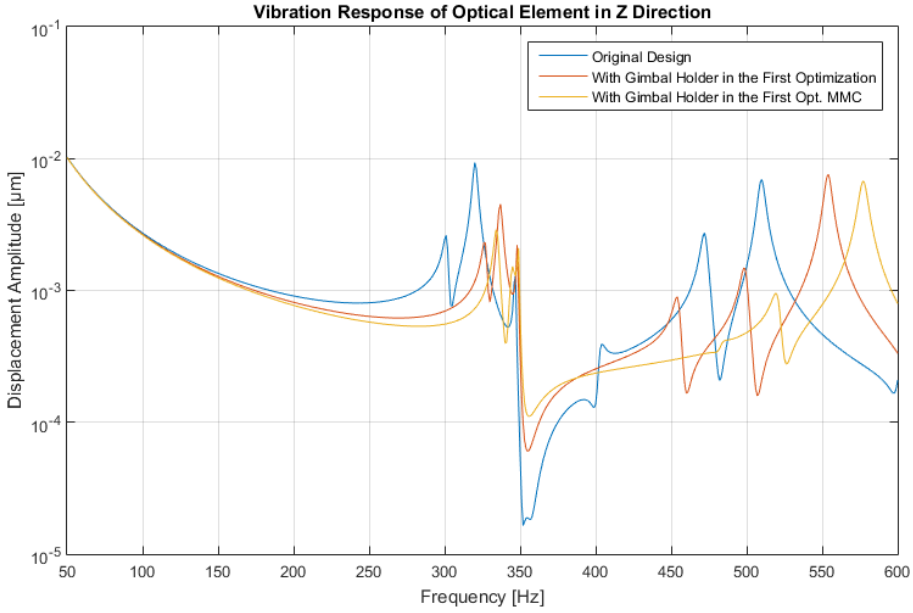

Figure 4.12. Vibration Response Comparison of Optical Element with Different Gimbal Holder Parts in Z Direction

Natural frequencies of the full optomechanical system are improved critically with just 1.5 kg increase in the total mass of the assembly by using SiC particle reinforced aluminum matrix composite (gimbal holder part in the first optimization). Natural frequencies are increased up to 20% and 11% in the most critical mode, with respect to original design (shown in Table 4.5).

Vibration response comparisons of the optical element in Y and Z directions (shown in Figure 4.11 and Figure 4.12, respectively) indicate that usage of the SiC particle MMC for gimbal holder part (gimbal holder part in the first optimization) reduced the vibration response of the optical element effectively. Decrease is approximately by 10 times in Y direction and 80% in Z direction in the frequency range of 300-350 Hz with just 1.5 kg increase in mass in total.

CHAPTER 5

SUMMARY AND CONCLUSION

In this thesis, studies are focused on solving the vibration-induced image problem of the optomechanical system integrated on an armored vehicle. Firstly, random vibration measurements and analyses are carried out to understand the energy level of the excessive random vibrations and the distribution of this energy in frequency spectrum, as the optomechanical system is exposed to these excitations transferred from the platform, which causes performance decrease in image processing. From the analyses, it is observed that there are high amplitude excitations in a specific frequency range, so it is aimed to shift the natural frequencies of the optomechanical system to higher values in order to avoid resonances at frequencies where there are high excitations, and to reduce the vibration response of the optical element.

Structural modifications on specified part of the system are required to eliminate the high excitation level coming from the vehicle to the optical element. In order to make structural modifications in the system, a reliable mathematical model of the complete system is required. In the beginning of modeling, the modal test and experimental modal analysis of the complete system are carried out, and thus the experimental model of the actual system is obtained. Then, the mathematical model of the system is formed by using FE method. It is observed from the comparison of the experimental and FE analysis results that these models do not match with each other. Since this complex system has many components, there are many parameters (material properties of the parts, bolted joint types, stiffness values of the bearings, damping values etc.) to define in model updating process, and updating of these parameters will cause uncertainties in the system. The computational time and effort of the FE analyses will also increase. In addition, the model updating methods

existing in the literature is inadequate for modeling of the complete optomechanical system. Correlating the response of the FE model of the whole assembly with that of the real model is not sufficient in order to make successful structural modifications. It is also required to have accurate FE models for all subsections of the system individually. However, updating all the variables of the FE model with the experimental results simultaneously, by using the existing methods in the literature, does not guarantee updated models for each component, since there are moving parts in the assembly.

A new approach, which is named Sequential Model Updating Method, is developed and used in this thesis for modeling and updating the FE model of each component sequentially, as the classical model updating approaches did not work for this complex system. In this method, the FE model of the complete system is obtained in several steps. Firstly, one component of the system is modeled and this model is updated. Afterwards, at each step a new subsystem is added and the resulting model is updated by using the experimental data for that assembly. At each step, the correlation between the FE model of that assembly with the experimental measurements is maximized by adjusting the values of the selected variables of the newly added subassembly only.

In this method, studies are started with the lowest level of the optomechanical system, which is the optical element. At each step, the initial FE model of the particular subassembly is formed in ANSYS, and FRFs of a particular point and natural frequencies of the subassembly are found from the FE analysis. These results are compared with the modal test results to check the correlation of the initial FE model with the experimental model of the real subassembly. The initial FE model is updated if it is not correlated with the experimental model. In model updating, the global (density, Young's modulus, Poisson's ratio values of the parts) or local (joint definitions, stiffness of the bearings etc.) parameters are updated by using ANSYS

Response Surface and Response Surface Optimization features in the first few steps. In the following steps, model updating is carried out iteratively with the knowledge obtained from initial steps. After obtaining a reliable FE model for the particular subassembly, another subassembly or part is mounted and new subassembly is obtained. The studies are repeated until the complete optomechanical system is modeled.

After having the updated FE model of the complete optomechanical system at the end of the model updating procedure by using Sequential Model Updating method, it is observed that the method developed in this thesis can successfully be used to update the mathematical models of the complex systems with many components, in order to obtain reliable models, which are compatible with the real systems. The maximum error of the natural frequencies of the updated FE model of the complete optomechanical system, compared with the experimental model, does not exceed 2.15%. In addition, comparison of the FRFs, measured experimentally and obtained from the updated FE model, for the complete assembly shows that the updated FE model is in good agreement with the experimental model.

After having the accurate FE model of the optomechanical system, studies are continued with the structural modifications on a selected part of the system to eliminate the undesired vibration of the optical element which reduces the image performance. The part that will be optimized is selected as the gimbal holder part, considering the critical role of the part in the system, since it connects stabilized gimbal mechanism to the housing, and it is possible to change its geometry with a small number of constraints. Firstly, design optimization is done on that selected part (the gimbal holder part) by using topology optimization method. With this method, it is aimed to increase the natural frequencies of the selected part by redesigning the geometry of the part considering the given constraints, so that the natural frequencies of the system will be shifted from the resonant frequencies, and vibration response

of the optical element will be reduced. Since the purpose of the topology optimization method is reducing volume and strengthening the part at the same time, the original design of the gimbal holder part is modified according to the design constraints, and initial geometry for the optimization algorithm is obtained. Excluded regions are defined to the algorithm to preserve the boundary conditions of the part. The objective function for the topology optimization is specified as maximizing the selected natural frequency. Moreover, the mass constraint is entered to the algorithm as the percentage of the mass of the initial geometry to be retained at the end of the process.

Topology density results of the part for two different mass constraints are obtained after the optimizations are carried out. These structural layouts are improved, so that the optimized part can be manufactured. At the end, the part obtained in the first optimization has 1 kg mass increase, and the part obtained in the second optimization has 1.7 kg mass increase with respect to original design. Although the goal of the optimization algorithm used in this thesis is to maximize the natural frequency by reducing the weight of the part, the weight of the optimized part is higher than the original design, because the weight of the initial geometry defined to the optimization algorithm is much higher than the original one.

In order to see the effect of the optimized part on the dynamic behavior of the optical element, modal and harmonic response analyses are performed. Final optimized design of the gimbal holder part is substituted with the original one in the updated FE model of the system. In addition, necessary arrangements are performed on the FE model of the system to perform the analyses with real boundary conditions (fixed boundary condition is given, all accelerometer models are removed from the model etc.). The harmonic response analyses are performed in two directions in which the system is affected mostly due to high excitation coming from the vehicle in the frequency range of 0 Hz – 600 Hz.

Although different mass constraints are used in the first and second optimizations, natural frequency results comparisons of the complete optomechanical system showed similar improvements. Optimization of the gimbal holder part raised the natural frequencies up to 13% in both cases. In addition, from the vibration response comparison of the optical element, it is seen that the design optimization reduced the vibration of the optical element up to 75% in the interested frequency range. Consequently, with just 1 kg increase (in the first optimization) in the mass of the complete assembly (which corresponds to 7% increase in the total mass), considerable improvement is obtained by using topology design optimization.

The material of the first optimized part is also changed to have further improvements on the image performance of the optomechanical system. A specific type of metal matrix composites, which is SiC particle reinforced aluminum matrix composite, is used in this study. It has improved the stiffness and gave higher damping ratio with respect to aluminum alloys. Also, this type of MMC has isotropic mechanical properties, so it has low-cost conventional machining processes. The material properties of the first optimized part are changed, and modal and harmonic response analyses are repeated in order to see the effect of the material change on the system. The mass of the optimized part has 0.5 kg increase with the new material.

At the end, with just 1.5 kg increase (which corresponds to 10% increase in the total mass) in the mass of the complete assembly (by using SiC particle reinforced aluminum matrix composite with first optimized gimbal holder part), natural frequencies are increased up to 20% and 11% in the most critical modes, and the vibration responses of the optical element are reduced 10 times in Y direction and 80% in Z direction in the interested frequency range with respect to original design.

These improvements will increase the image performance effectively and solve the vibration-induced image problem of the optomechanical system.

Consequently, the new model updating method developed in this thesis provides a very useful tool in obtaining reliable mathematical models for complex systems with moving parts. Its successful application in solving an important problem experienced in the optomechanical system provides a very good example for the performance of the method developed.

REFERENCES

[1] Baruch, M., & Itzhack, I. Y. B. (1978). Optimal weighted orthogonalization of measured modes. AIAA Journal, 16(4), 346–351. https://doi.org/10.2514/3.60896

[2] Baruch, M. (1978). Optimization procedure to correct stiffness and flexibility matrices using vibration tests. AIAA Journal, 16(11), 1208–1210. https://doi.org/10.2514/3.61032

[3] Bucher, I., & Braun, S. (1993). The structural modification inverse problem: An exact solution. Mechanical Systems and Signal Processing, 7(3), 217–238. https://doi.org/10.1006/mssp.1993.1010

[4] Friswell, M. I., Inman, D. J., & Pilkey, D. F. (1998). Direct updating of damping and stiffness matrices. AIAA Journal, 36(3), 491–493. https://doi.org/10.2514/2.396

[5] Lin, R. M., & Zhu, J. (2006). Model updating of damped structures using FRF data. Mechanical Systems and Signal Processing, 20(8), 2200–2218. https://doi.org/10.1016/j.ymssp.2006.05.008

[6] Li, W. L. (2002). A new method for structural model updating and joint stiffness identification. Mechanical Systems and Signal Processing, 16(1), 155–167. https://doi.org/10.1006/mssp.2000.1339

[7] Kwon, K. S., & Rong-Ming, L. (2005). Robust finite element model updating using Taguchi method. Journal of Sound and Vibration, 280(1–2), 77–99. https://doi.org/10.1016/j.jsv.2003.12.013

[8] Giagopulos, D., & Natsiavas, S. (2007). Hybrid (numerical-experimental) modeling of complex structures with linear and nonlinear components. Nonlinear Dynamics, 47(1–3), 193–217. https://doi.org/10.1007/s11071-006-9067-3

[9] Sadeghi, M. H., Soleimanian, P., & Samandari, H. (2012). Model updating of complex assembly structures based on substructures-joint parameters. In Conference Proceedings of the Society for Experimental Mechanics Series (Vol. 4, pp. 175–190). https://doi.org/10.1007/978-1-4614-2431-4_18

[10] Grafe, H. (1998). Model Updating of Large Structural Dynamics Models Using Measured Response Functions. Vibration University Technology Centre. Retrieved from http://vibration.ex.ac.uk/doc/1183.pdf

[11] Belotti, R., Caracciolo, R., Palomba, I., Richiedei, D., & Trevisani, A. (2018). An Updating Method for Finite Element Models of Flexible-Link Mechanisms Based on an Equivalent Rigid-Link System. Shock and Vibration, 2018. https://doi.org/10.1155/2018/1797506

[12] Goller, B., Broggi, M., Calvi, A., & Schuëller, G. I. (2011). A stochastic model updating technique for complex aerospace structures. Finite Elements in Analysis and Design, 47(7), 739–752. https://doi.org/10.1016/j.finel.2011.02.005

[13] Atalla, M. J., & Inman, D. J. (1998). On model updating using neural networks. Mechanical Systems and Signal Processing, 12(1), 135–161. https://doi.org/10.1006/mssp.1997.0138

[14] Cao, Z., Fei, Q., Jiang, D., & Wu, S. (2017). Substructure-based model updating using residual flexibility mixed-boundary method. Journal of Mechanical Science and Technology, 31(2), 759–769. https://doi.org/10.1007/s12206-017-0127-z

[15] Arailopoulos, A., & Giagopoulos, D. (2016). Finite element model updating techniques of complex assemblies with linear and nonlinear components. In Conference Proceedings of the Society for Experimental Mechanics Series (Vol. 3, pp. 293–306). Springer New York LLC. https://doi.org/10.1007/978-3-319-29754-5_29

[16] Soleimanian, P., Sadeghi, M. H., & Tizfahm, A. (2012). Substructure-joint based approach to damped FE model updating of complex assembly structure. In Advanced Materials Research (Vol. 463–464, pp. 1169–1174). https://doi.org/10.4028/www.scientific.net/AMR.463-464.1169

[17] Power-spectral-density analysis - Technical Knowledge Base. (2014, April 03). Retrieved June 27, 2020, from https://wiki.csiamerica.com/display/kb/Power-spectral-density analysis/

[18] T. I. (2020, April 06). Vibrationdata Matlab Signal Analysis & Structural Dynamics Package. Retrieved June 27, 2020, from https://vibrationdata.wordpress.com/2013/05/29/vibrationdata-matlab-signal-analysis-package/

[19] Visser, W. J., Ewins, Prof. D. J., & Imregun, Dr. M. (1992). Updating Structural Dynamics Models Using Frequency Response Data. Department of Mechanical Engineering, PhD(September), 238.

[20] Blair, M., Stevens, T. and Linskey, B., 1995. Steel Castings Handbook, Sixth Edition. Materials Park, Ohio: ASM International.

[21] Liviu, S. I., Mariana, B. S., & Nadia, J. A. (2016). DESIGN OPTIMIZATION METHOD USED IN MECHANICAL ENGINEERING. Journal of Industrial Design and Engineering Graphics, 11(2), 13-17. Retrieved from http://sorging.ro/jideg/index.php/jid/article/view/304

[22] Haghshenas, M. (2016). Metal–Matrix Composites. In Reference Module in Materials Science and Materials Engineering. Elsevier. https://doi.org/10.1016/b978-0-12-803581-8.03950-3

[23] (n.d.). Materion - A Global Leader in Advanced Materials. Retrieved June 27, 2020, from https://materion.com/-/media/files/aerospace-metal-composites/supremex/supremex-640xa-data-sheet.pdf

[24] Hung, J. P. (2009). Load effect on the vibration characteristics of a stage with rolling guides. Journal of Mechanical Science and Technology, 23(1), 89–99. https://doi.org/10.1007/s12206-008-0925-4

[25] Chang, J. C., & Hung, J. P. (2014). Analytical and finite element modeling of the dynamic characteristics of a linear feeding stage with different arrangements of rolling guides. Mathematical Problems in Engineering, 2014. https://doi.org/10.1155/2014/454156

[26] Jackson, R. L., Ghaednia, H., Lee, H., Rostami, A., & Wang, X. (2013). Contact mechanics. In Tribology for Scientists and Engineers: From Basics to Advanced Concepts (Vol. 9781461419457, pp. 93–140). Springer New York. https://doi.org/10.1007/978-1-4614-1945-7_3

[27] Norden, B. N. (1973). On the compression of a cylinder in contact with a plane surface. Interagency Report, 73--243.

APPENDICES

A. Modeling of Linear Motion Guide in FE

Linear motion guide is a type of bearing which makes straight-line motion. It is generally used for high-precision positioning of machinery components, and provides low friction under normal loading conditions. These guides basically consist of slide carriage, rail and rolling elements. Rolling elements can be balls or cylindrical rollers, which can circulate between slide carriage and rail, and provide the motion of the guide.

The linear motion guide used in this thesis has cylindrical elements instead of balls, which is different from the general usage and studies in the literature. In literature, several studies are carried out in order to analyze dynamical characteristics of linear motion guides having balls for rolling elements. This study will have a different approach than other studies by investigating a linear motion guide with cylindrical rolling elements, and modeling it in FE.

Linear motion guides have rolling interfaces between rollers and other components, and rolling elements' contact status and material properties affect the dynamical characteristics of linear guides effectively [24]. As a result of these rolling interfaces, contact stiffness forms between the surfaces of rolling elements and rail (or slide carriage), and it is dependent on the applied load on the rolling element. To model the linear motion guide more realistically in FE, spring elements can be used between the railways to simulate the rolling elements, and stiffness values of these elements can be defined by using Hertzian contact theory [25].

In literature, Hertzian spherical contact theory is used for linear motion guides having balls. In this study, linear motion guide has cylindrical rolling elements and Hertzian line contact theory (elastic cylindrical contact) will be used for the calculations.

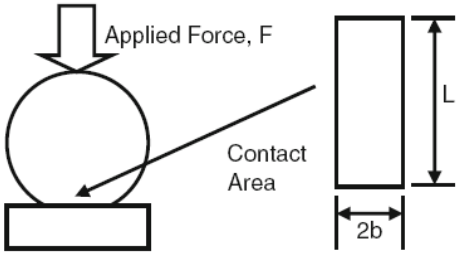

Figure A.1. Schematic of Contact Area between a Cylinder and a Flat Surface [26]

According to [27] solution to the compression of a cylinder in contact with a plane surface by using Hertzian contact theory:

$$\delta = \frac{F}{L}(\lambda_1 + \lambda_2)\left[\ln\left(\frac{L^3}{FR(\lambda_1 + \lambda_2)}\right) + 1\right] \qquad (A.1)$$

where F is applied force, L is contact length between cylinder and flat plane, R is radius of cylinder, and λ_i can be expressed as:

$$\lambda_i = \frac{1 - \nu_i^2}{\pi E_i} \qquad (A.2)$$

Here, ν_i is Poisson's ratio, and E_i is modulus of elasticity of the cylinder and the flat plane. The force acting on the rolling elements is constant and known from the preload value taken from the information provided by the producer. By using the force and deflection values calculated from equation (A.1), the contact stiffness at the surface between rolling element and rail (or slide carriage) could be expressed as:

$$k = \frac{F}{\delta} \qquad (A.3)$$

There are two contact surfaces between a rolling element and other components, and the contact stiffness is equal at each side of the rolling element (rolling elements are assumed as rigid and all parameters are equal in each side):

$$k_{eqv} = \frac{1}{\frac{1}{k} + \frac{1}{k}} = \frac{k}{2} \qquad (A.4)$$

CAD model of the linear motion guide is imported from PTC Creo software to ANSYS Workbench interface (shown in Figure A.2).

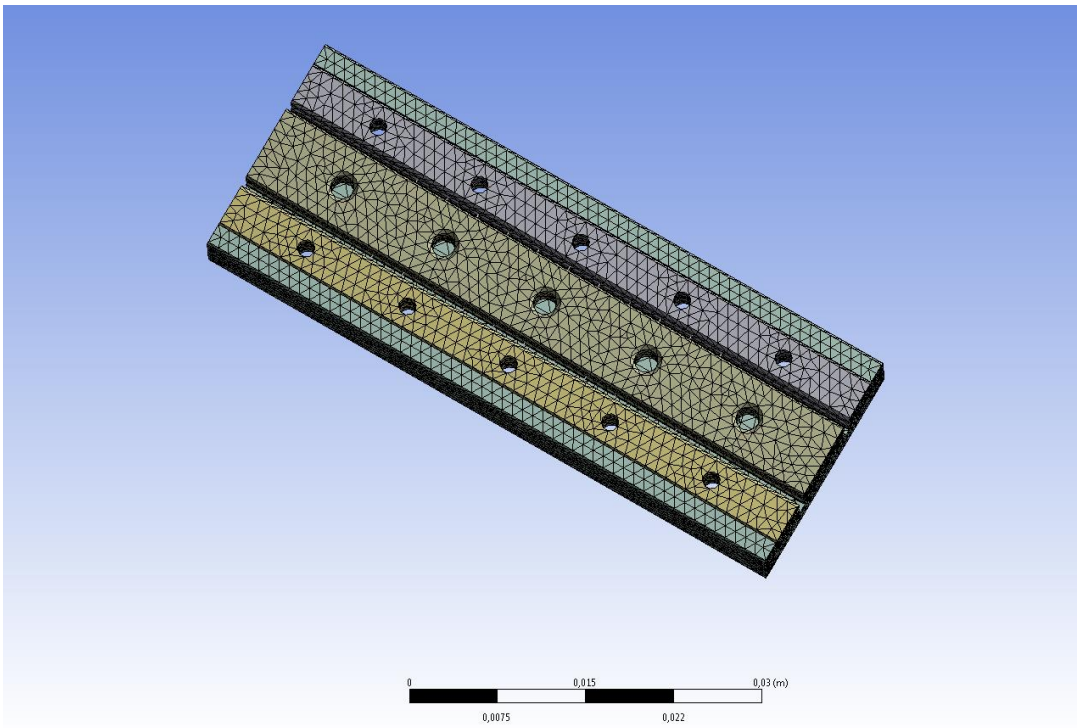

Figure A.2. Finite Element Model of the Linear Motion Guide

In FE modeling of linear motion guide used in this thesis, the main components (slide carriage and rail) are modeled as solid bodies. Material properties of these bodies are defined to ANSYS Library, and meshing of the solid parts are done. FE model has 138605 nodes and 85671 tetrahedral elements. Slide carriage and rail parts are connected with linear spring elements to represent the cylindrical rollers, and the masses of the rollers are neglected, since they are much lower than those of the other components. In real system, cylindrical rollers and other components have line contacts in between, so spring elements are defined by using line contacts between the springs and rail (or slide carriage) at the locations where they are placed in real system. Stiffness values of the springs are taken as the calculated k_{eqv} value calculated from equation (A.4).